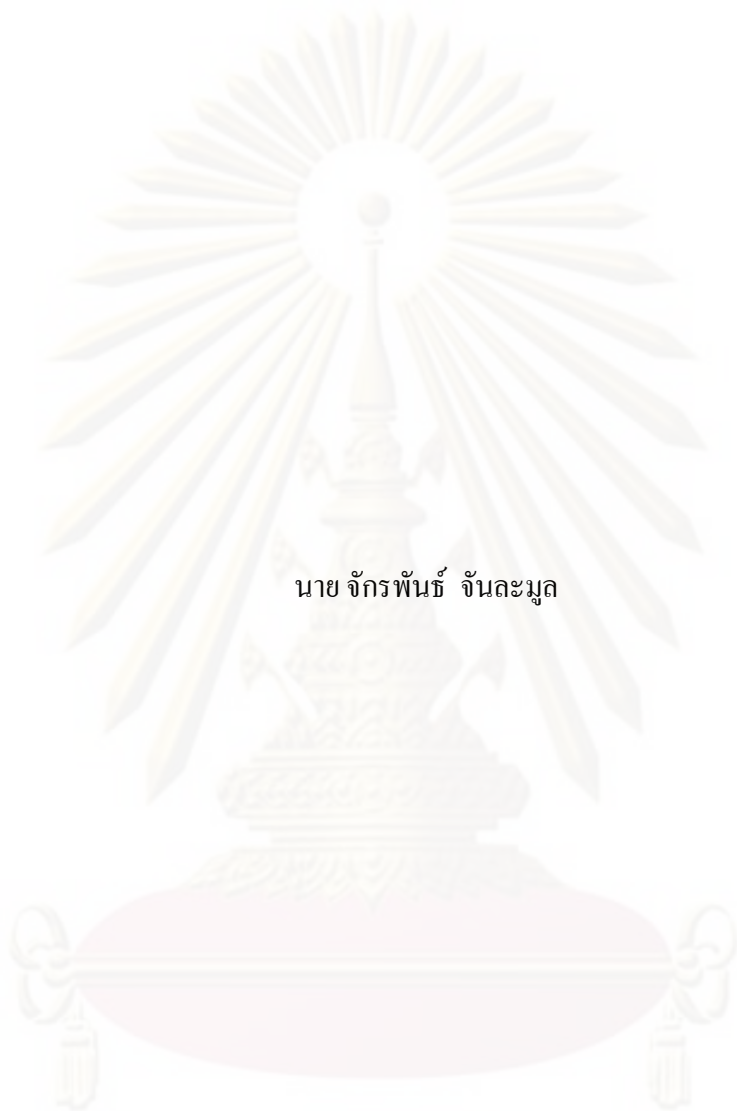ไฮโดรจิเนชันของคาร์บอนไดออกไซด์โดยตัวเร่งปฏิกิริยาโคบอลต์ และ นิกเกิล บน
วัสดุเชิงประกอบไทเทเนียกับซิลิกา

นาย จักรพันธ์ จันละมูล

CARBON DIOXIDE HYDROGENATION OVER TITANIA-SILICA COMPOSITES SUPPORTED COBALT AND NICKEL CATALYSTS

Mr. Jakrapan Janlamool

A Thesis Submitted in Partial Fulfillment of the Requirements
for the Degree of Master of Engineering Program in Chemical Engineering
Department of Chemical Engineering
Faculty of Engineering
Chulalongkorn University
Academic Year 2009
Copyright of Chulalongkorn University
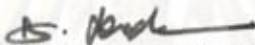
Thesis Title   CARBON DIOXIDE HYDROGENATION OVER TITANIA-SILICA
                    COMPOSITES SUPPORTED COBALT AND NICKEL CATALYSTS
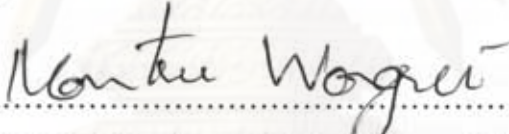
By   Mr. Jakrapan Janlamool
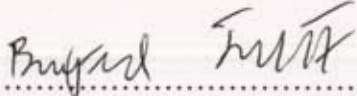
Field of Study   Chemical Engineering

Thesis Advisor   Associate Professor Bunjerd Jongsomjit, Ph.D.

Accepted by the Faculty of Engineering, Chulalongkorn University in Partial
Fulfillment of the Requirements for the Master's Degree
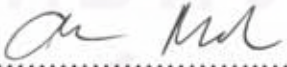
....Dean of the Faculty of Engineering

(Associate Professor Boonsom Lerdhirunwong, Dr.Ing.)

THESIS COMMITTEE

.... Chairman

(Assistant Professor Montree Wongsri, D.Sc.)

.... Thesis Advisor

(Associate Professor Bunjerd Jongsomjit, Ph.D.)

.... Examiner

(Assistant Professor Joongjai Panpranot, Ph.D.)

....External Examiner

(Assistant Professor Okorn Mekasuwandamrong, D.Eng.)

จักรพันธ์ จันละมูล : ไฮโดรจิเนชันของคาร์บอนไดออกไซด์โดยตัวเร่งปฏิกิริยาโคบอลต์ และ นิกเกิล บนวัสดุเชิงประกอบไทเทเนียกับซิลิกา (CARBON DIOXIDE HYDRO GENATION OVER TITANIA-SILICA COMPOSITES SUPPORTED COBALT AND NICKEL CATALYSTS) อ. ที่ปรึกษาวิทยานิพนธ์หลัก : รศ. ดร. บรรเจิด จงสมจิตร, 123 หน้า

งานวิจัยนี้ได้ศึกษาคุณลักษณะและสมบัติของตัวรองรับซิลิกา 2 ชนิด คือ ซิลิกาทรงกลม (SSP) และ MCM41 ที่ถูกปรับปรุงด้วยการเคลือบฝังของอนุภาคไทเทเนียบนพื้นผิวของซิลิกาทั้งสองชนิดโดยใช้ปฏิกิริยาไฮโดรลิซิสของไทเทเนียมไอโซโพรพรอกไซด์ ผลการศึกษาพบว่า วัสดุเชิงประกอบไทเทเนียกับซิลิกาชนิด MCM41 หรือ TiMCM มีความเสถียรภาพทางความร้อนดีกว่าวัสดุเชิงประกอบไทเทเนียกับซิลิกาชนิดทรงกลม หรือ TiSSP ยิ่งกว่านั้นยังพบว่า การกระจายตัวของอนุภาคไทเทเนียบนพื้นผิวของซิลิกามีลักษณะดี นอกจากนี้ การศึกษาคุณลักษณะของตัวเร่งปฏิกิริยาโคบอลต์และนิกเกิลบนซิลิกาและวัสดุเชิงประกอบไทเทเนียกับซิลิกาทั้งสองชนิด พบว่าความสามารถในการรีดิวซ์ของตัวเร่งปฏิกิริยาโคบอลต์และนิกเกิลเพิ่มขึ้นเมื่อใช้ตัวรองรับชนิดวัสดุเชิงประกอบไทเทเนียกับซิลิกาทั้งสองชนิด จากผลการศึกษาความว่องไวและค่าการเลือกเกิดผลิตภัณฑ์ของตัวเร่งปฏิกิริยาโคบอลต์สำหรับปฏิกิริยาคาร์บอนไดออกไซด์ไฮโดรจิเนชันพบว่าโคบอลต์บนตัวรองรับชนิด MCM41 มีค่าร้อยละการเปลี่ยนแปลงของสารตั้งต้นสูงสุดคือ 82.77 เปอร์เซ็นต์ และค่าการเลือกเกิดมีเทน คือ 92.74 เปอร์เซ็นต์ที่อุณหภูมิของปฏิกิริยา 270 องศา นอกจากนี้ยังพบว่าตัวเร่งปฏิกิริยานิกเกิลบนวัสดุเชิงประกอบไทเทเนียกับซิลิกายังคงมีค่าการเลือกเกิดมีเทน 100 เปอร์เซ็นต์ในปฏิกิริยาคาร์บอนไดออกไซด์ไฮโดรจิเนชันที่อุณหภูมิ 270 องศาเซลเซียส โดยตัวเร่งปฏิกิริยานิกเกิลบนตัวรองรับชนิด TiSSP650 มีค่าร้อยละการเปลี่ยนแปลงของสารตั้งต้นสูงสุดคือ 82.77 เปอร์เซ็นต์ที่อุณหภูมิของปฏิกิริยา 270 องศา

ภาควิชา..............วิศวกรรมเคมี.......... ลายมือชื่อนิสิต...................................

สาขาวิชา..............วิศวกรรมเคมี.......... ลายมือชื่อ อ.ที่ปรึกษาวิทยานิพนธ์หลัก...................

ปีการศึกษา..........2552....................

##5070237321: MAJOR CHEMICAL ENGINEERING

KEYWORDS: TITANIA SILICA COMPOSITES/ COBALT CATALYST/ NICKEL CATALYST/ CARBON DIOXIDE HYDROGENATION

JAKRAPAN JANLAMOOL: CARBON DIOXIDE HYDROGENATION OVER TITANIA-SILICA COMPOSITES SUPPORTED COBALT AND NICKEL CATALYSTS. THESIS ADVISOR: ASSOC. PROF. BUNJERD JONGSOMJIT, Ph.D., 123 pp.

This research focused on investigation of characteristics and properties of two types of silica i) spherical silica ii) MCM41 with and without impregnation of titania by hydrolysis of titanium isopropoxide. It was found that The TiO_2-MCM microparticle composites (TiMCM) had better thermal stability than The TiO_2-spherical silica microparticle composites (TiSSP). Moreover, the titania distribution on the silica surface was good. Furthermore, the investigation in the characteristics of cobalt and nickel supported on the both of silica and TiO_2-SiO_2 microparticle composites. It was found that the reducibilities of cobalt and nickel supported on TiO_2-SiO_2 microparticle composites catalysts were increasing. In addition, the catalystic activity and selectivities of cobalt for CO_2 hydrogenation showed that the catalystic activity and selectivities to methane of cobalt supported MCM41 are 82.77 and 92.74% in reaction temperature at $270^{\circ}C$. Furthermore, selectivities to methane of nickel supported on TiO_2-SiO_2 microparticle composites are 100% in the CO_2 hydrogenation at $270^{\circ}C$. It has been found that nickel supported on TiSSP650 has the highest conversion about 82.77% in reaction temperature at $270^{\circ}C$.

Department : ......Chemical Engineering....   Student's Signature...Jakrapan Janlamool

Field of Study : ...Chemical Engineering....   Advisor's Signature...

Academic Year : .....2009.....................

ACKNOWLEDGEMENTS

CONTENTS

Page

LIST OF TABLES

LIST OF FIGURES

Figure   **Page**

CHAPTER I

INTRODUCTION

Carbon dioxide is a trace gas being only 0.038% of the atmosphere. Carbon dioxide is an end product in organisms that obtain energy from breaking down sugars, fats and amino acids with oxygen as part of their metabolism, in a process known as cellular respiration. In recently, human activities, such as the combustion of fossil fuels and deforestation have caused the atmospheric concentration of carbon dioxide to increase by about 35% since the beginning of the age of industrialization. This reason exhibits the noticeable problem in the life, such as global warming, acid rain and the lost of oxygen-carrying molecule in red blood cells. The natural mechanism to maintain the level of carbon dioxide that plant photosynthesis CO_2 gains entry into the carbon backbone of glucose by a dark reaction. Six molecules of CO_2 can ultimately be converted into glucose by cyclic operation of the Culvin cycle. [Lehninger, 1970] In contrast catalytic hydrogenation of CO_2 has been recently attracting considerable attention as one of the chemical fixation and recycling technologies for emitted CO_2 [Kusama et al., 2001]. The catalytic hydrogenation of carbon monoxide and carbon dioxide produces a large variety of products ranging from methane and methanol (C1 products) to higher molecular weight alkanes, alkenes and alcohols, a process that requires C–C bond formation as well (oligomerization or polymerization) [Somorjai et al., 1994; Dry, 1996; Adesina, 1996; Iglesia, 1997]. The activation energies for the two hydrogenation process increase steeply with oxygen content. It is 86 kJ/mol for CO and 158 kJ/mol for CO_2 hydrogenation [Lahtinen et al., 1994], however carbon monoxide occurs in small amout about 0.1 ppm in the atmosphere. Then, carbon dioxide is the most abundant carbon source in the atmosphere for catalytic hydrogenation.

CO_2 hydrogenation on metal catalysts occurred through a consecutive mechanism in which CO_2 was first converted to CO by the reverse water gas shift (RWGS) reaction, and then CO was hydrogenated to hydrocarbon. Furthermore, carbon dioxide is the key process for the organic synthesis of chemicals like methanol (MeOH) [Lackner, 2003 ; Song, 2006]. Formate was identified as the first

intermediate of the MeOH synthesis reaction on Cu [Rasmussen et al., 1994; Nerlov, 1998]. Several reaction mechanisms for the CO_2 hydrogenation have been proposed including direct hydrogenation of CO_2, dissociation to CO and O [Mills and Steffgren, 1973], or to C and 2O [Peebles et al., 1983; Fujitani et al., 1997] prior to the methane formation. CO_2 is known to dissociate to CO and O on rhodium surfaces [Castner et al., 1980]. On Ni surfaces the reaction is reported to proceed via dissociation to C and 2O and subsequent hydrogenation of surface carbon to methane [Peebles et al., 1983; Fujitani et al., 1997]. Some process is also invoked on copper as one of the elementary step sleading to the water-gas shift reaction [Ernst et al., 1992; Yoshihara et al., 1995] ($CO+H_2O \leftrightarrow CO_2 +H_2$).

The previous research exhibited that the supports, such as Al_2O_3, SiO_2, ZrO_2, TiO_2 and CeO_2 can necessarily affect activity/selectivity properties of the active phase for surface reaction [Ruiz and Ramos,1985; Sou et al.,1997; Storsaeter et al., 2005; Zhao et al, 2008]. In recently, the composites of TiO_2-SiO_2 supported active phase for catalytic reaction were studied. New synthesis methods of TiO_2-SiO_2 mixed oxides are needed for overcoming the present disadvantages of pure titania powder. Grzechowiak et al. [2008], suggested that the catalytic activity of TiO_2-SiO_2 supported nickel in aromatic hydrogenation depended on the preparation method and titania content. The results indicate that the deposition of TiO_2 on the silica surface via hydrolysis of titanium isopropoxide improves the hydrogenation activity of nickel catalysts. Furthermore, the addition of small amount of TiO_2 to silica-supported cobalt catalysts significantly increasing the dispersion of cobalt and Co metallic surface area and enhance slurry phase catalytic activity of Fisher-Tropsch synthesis [Hinchiranan et al., 2008].

The proposed research will focus on titania-silica composites supported cobalt and nickel catalysts for CO_2 hydrogenation. The catalyst samples were prepared and characterized by several techniques, such as BET, XRD, SEM/EDX, TEM, TPR, TGA, ICP, H_2 chemisorption, and XPS. The reaction study of CO_2 hydrogenation was carried out in order to measure activity and product selectivity under methanation condition.

Motivation

The TiO_2-SiO_2 composites supports can exhibit the novel properties that are not finding in a single oxide supports, with combination, the benefit of TiO_2 support provided the thermal stability and SiO_2 has a sufficiently high surface area. In this work, in order to improve activities and properties of the obtained product (selectivity) of cobalt and nickel based TiO_2-SiO_2 composites catalysts, it can be achieved by using cobalt and nickel based TiO_2-SiO_2 composites catalyst over CO_2 hydrogenation.

Objective

The research objective is to investigate the effects of different TiO_2-SiO_2 composites supports on their characteristics. Cobalt and nickel supported on TiO_2-SiO_2 composites catalysts for CO_2 hydrogenation is further investigated.

Research scopes

- Preparation of MCM-41 and submicroshere silica support.

- Characterization of silica support samples by BET surface area and scanning electron microscopy (SEM)

- Preparation of TiO_2- SiO_2 composites supports with 25 wt% of TiO_2 on the composites support using hydrolysis of titanium isopropoxide method.

- Characterization of the TiO_2- SiO_2 composites supports by BET surface area, X-ray diffraction (XRD) scanning electron microscopy (SEM), energy dispersive X-ray spectroscopy (EDX), differential thermal analysis and thermogravimetric (DTA/TG)

- Preparation of supported Co and Ni catalyst on the TiO_2- SiO_2 composites supports, which was calcined at various temperature, using the incipient wetness impregnation method.

- Characterization of the catalyst samples using X-ray diffraction (XRD), temperature programmed reduction (TPR), hydrogen chemisorptions, energy dispersive X-ray spectroscopy (EDX), X-ray photoelectron spectroscopy (XPS) and transmission electron spectroscopy (TEM).

- Investigation of the catalytic activity of Co/ TiO_2- SiO_2 and Ni/ TiO_2- SiO_2 catalyst in the hydrogenation of carbon dioxide (CO_2) at $220^{o}C$ and 1 atm and a H_2/CO_2 ratio of 10 under methanation condition.

Benefits

      - Develop the cobalt abd nickel base titania-silica composites catalyst for CO_2 hydrogenation.

      - Enhance CO_2 fixation system.

      - Produce international research article based on the results obtained.

CHAPTER II

LITERATURE REVIEWS

Heterogeneous catalysts are those, which act in a different phases than the reactants. Most heterogeneous catalysts are solids that act on substrates in a liquid or gaseous reaction mixture. Diverse mechanisms for reactions on surfaces are known, depending on how the adsorption takes place. Many industrial catalysts are metals and the structurally simple single crystals provide an introduction to the more typical metal structures used in industrial catalysts. Typical supports are robust porous solids, including metal oxides, such as alumina, silica, titania and carbon.

This chapter reviews the work about titania-silica composites supported Co and Ni catalyst that is also of great interest in the field of heterogeneous catalysis, while it has been used for catalytic application. The last section of this review shows a few research investigations about the titania-silica composites supported metal catalyst.

2.1 The titania-silica composites supported metals

The study of hybrid particles can provide important fundamental insights for new functional materials, such as photonic catalyst [Fu et al., 2005], high-performance electronic materials [Chung et al., 2005] and so on. Nowadays, the titania-silica composites supported metal catalysts have attracted the scientists attention in the catalysis field. Recently, it was reported that titania-silica composites particles exhibited better catalytic properties than classical oxides such as titania and silica [Fu et al., 2001]. The inclusion of titania in silica structures is reported in several works. Eidenmeyer et al. [2001] grafted metaloorganic titanium reagents on to dehydrated MCM-48 samples in dry hexane. Xiao et al. [2002] produced mesoporous titanosilicates with high catalytic activity. Ogawa [2003] produced nanoporous silica films containing titanium. Mrowiec-Bialon [2000] synthesized titania–silica aerogels.

Titania-silica mesosized particles were obtained by TiCl$_4$ hydrolysis in Aerosol OT / water / n-hexane microemulsion. These particles were incorporated insurfactant templated silica mesoporous materials of MCM-41 and MCM-50 structures. Results depended on the surfactant : hexadecyltrimethyl ammonium bromide templated materials retained the honeycomb structure with small modifications in their characteristics. The dodecyltrimethyl ammonium bromide templated material changed from honeycomb to lamellar structure when the titania particles were included, with dramatic changes in the structure characteristics. The didodecyldimethyl ammoniumbromide templated lamellar structure was retained after TiO$_2$ inclusion, with as light increase in the specific area, pore diameter and pore walls thickness [Messinal et al., 2006].

Ohno et al. [2009] describes the effect of drying process on the preparation of TiO$_2$-SiO$_2$ nano-hybrid particles. The hybrid sol was prepared by sol–gel process with controlled chemical modification (CCM) to attain the TiO$_2$ nano-coating on the SiO$_2$ nano-sphere. The hydrolysis reaction of titanium alkoxide was controlled by R$_A$ ([CH$_3$COOH]/[Ti]) and R$_W$ ([H$_2$O]/[Ti]). The hybrid particles were dried by under the super critical drying to suppress the hard agglomeration of the as-prepared nano-hybrid sol. As a result, the hard agglomeration of the primary particles was successfully suppressed to obtain TiO$_2$-SiO$_2$ nano-hybrid particles with controlled chemical modification of titanium alkoxide. The quantum size effect of nano-hybrid particles was confirmed by the band gap energy shift, using ultraviolet–visible spectroscopy (UV–vis).

Zhao et al. [2005] prepared TiO$_2$-SiO$_2$ composite microspheres with microporous SiO$_2$ core and mesoporous TiO$_2$ shell structures by hydrolysis of titanium tetrabutylorthotitanate in the presence of microporous silica microspheres using hydroxypropyl cellulose as a surface esterification agent and porous template, and then dried and calcined at different temperatures. It shows that composite particles were about 1.8 μm in diameter, and had a spherical morphology and a narrow size distribution. The anatase and rutile phase in the TiO$_2$-SiO$_2$ composite microspheres began to form at 700 and 900 $^{\circ}$C, respectively. At 700 $^{\circ}$C, the specific surface area and pore volume of the TiO$_2$-SiO$_2$ composite microspheres were 552 and

0.652 mLg^{-1} respectively. However, at 900 ^{o}C, the specific surface area and pore volume significantly decreased due to the phase transformation from anatase to rutile.

Previous scientists reported that titania-silica composites materials have been used as catalysts and supports for various catalytic reaction in recent years. It was previously reported that the catalytic activity of TiO$_2$-SiO$_2$ is 3-fold higher than corresponding TiO$_2$ (Anderson and Bard, 1995; Ruetten and Thomas, 2003; Chun et al., 2001). Grezechowiak et al. [2008] prepared titania-silica composites particles by deposition of titania on the silica surface via hydrolysis of titania isopropoxide or via hydrolysis of titanium tetrachloride and by sol-gel method. They found that the titania content influences the nature of oxidic nickel species on titania-silica supports. Titania distribution in the titania-silica support depends on the method of support preparation and influences the reducibility and distribution of nickel oxide, as the quantity of titanium increases, so does the quantity of nickel. The results indicate that the deposition of titania on the silica surface via hydrolysis of titanium isopropoxide improves the toluene hydrogenation activity of nickel catalysts. The use of TiPOT for the preparation of titania-silica increases the reducibility of nickel oxide, as well as the acidity and specific surface area of the catalyst.

In present, the photo-assisted deposition (PAD) and impregnation synthesis of nano-sized Pt metal on titania-silica are reported. Photocatalytic activity using Pt-TiO$_2$-SiO$_2$ catalysts under visible-light condition for the oxidation of 2-propanol was evaluated. The results showed a notable photocatalytic activity of PAD-Pt-TiO$_2$-SiO$_2$, which was 1.5 and 4.7 times higher than that of imp-Pt-TiO$_2$-SiO$_2$ and TiO$_2$-SiO$_2$, respectively. In summary, using the PAD method, nano-sized Pt metal particles with a well-controlled size and a well-dispersed state can be deposited on tetrahedrally coordinated Ti-oxide of the support. The direct interaction between nano-sized Pt metal and the photo-excited tetrahedrally coordinated Ti-oxiderealized by the PAD method under UV-light irradiation have the possibility to design the unique and active nano-sized metal catalyst [Mohamed, 2009].

Sukamon Hinchiranan et al. [2008] proposed the addition of small amount of TiO$_2$ to silica-supported cobalt catalysts significantly increased the dispersion of cobalt and Co metallic surface area resulting in there markable enhancement of the

Fisher–Tropsch synthesis (FTS) activity in the slurry-phase reaction. The addition of TiO_2 adjusted the interaction between cobalt and silica support quite well to realize the favorite dispersion and reduction degree of supported cobalt, leading to high catalytic activity in FTS. The high activity of titania promoted catalysts could be attributed to the increase in bridge-type adsorbed CO, which was easily dissociated to carbon and oxygen, contributing to the higher reaction rate of FTS.

Bunjerd Jongsomjit et al. [2006] investigated the catalytic behaviors of mixed TiO_2-SiO_2 with various weight ratio of TiO_2/SiO_2, supported cobalt in Fisher–Tropsch synthesis. The initial and steady state rates decreased with the amounts of titania present in mixed supports that had the less number of reduced cobalt metal. The selectivity of long chain hydrocarbons (C_2-C_5) was increased with the presence of titania in the mixed supports. Furthermore, Jongsomjit et al. [2005] investigated influence of various titania/silica mixed-oxides supported MAO on the catalytic activity copolymerization of ethylene and 1-hexane with zirconocene catalyst. The activity, that had titania range between 20 and 40 % in the mixed oxide supports, increased up to 30% compared with pure silica.

2.2 The supported metal catalysts in CO and CO_2 hydrogenation system

Development of catalyst for CO and CO_2 hydrogenation is the key technology of gas to liquid (GTL) process. The catalytic hydrogenation of carbon monoxide and carbon dioxide produces a large variety of products ranging from methane and methanol to higher molecular weight alkanes, alkenes and alcohols. [Somorjai, 1994 ; Dry, 1996 ; Adesina, 1996 ; Iglesia, 1997] Aksoylu et al. [1997] prepared a group of Ni/Al_2O_3 catalysts having metal contents in the 0-16.5 wt % range using coprecipitation and impregnation methods. The CO and CO_2 methanation activities of the catalyst were studied in order to compare the effect of preparation method on structure properties as well as on catalyst activity and selectivity. The comparison of Co hydrogenation results in catalyst with similar nickel loading indicates that coprecitated catalysts have higher productivity and C_2-C_4 hydrocarbon selectivity, whereas impregnated catalysts yield better olefin/paraffin ratios for the C_2-C_4 hydrocarbons. In CO_2 methanation, coprecipitation shows higher methanation activity for all nickel loadings. Furthermore, Chang et al. [2003] prepared nickel catalysts

supported on rice husk ash-alumina (Ni/RHA-Al$_2$O$_3$) using the incipient wetness impregnation method. The catalytic activities of nickel catalysts were tested by CO$_2$ hydrogenation with H$_2$/CO$_2$ ratio of 4 : 1 for temperatures between 400 and 800 ^{o}C. The TPR analysis indicated that the interaction between nickel and support was strong and difficult to reduce with more than one nickel oxide compound. The CO$_2$ conversion and CH$_4$ yield for CO$_2$ hydrogenation were found to depend on the nickel loading. The reaction temperature of 500 ^{o}C might be the optimum temperature for CO$_2$ hydrogenation to give the maximum yield and selectivity of CH$_4$. Furthermore, the hydrogenation tests showed that the performance of Ni/RHA-Al$_2$O$_3$ is better than that of Ni/SiO$_2$-Al$_2$O$_3$. Previously, Chang et al. [2001] investigated the nickel catalysts supported on rice husk ash prepared by the ion exchange technique. The catalytic acitivities of nickel catalysts were tested by CO$_2$ hydrogenation with H$_2$/CO$_2$ ratio of 4 : 1 for temperatures between 400 and 800 ^{o}C. The results show that catalysts prepared by ion exchange yield finely dispersed and evenly distributed nickel crystallites. The metal dispersion increases with a decrease in nickel loading. The conversion of CO$_2$ and the yield of CH$_4$ are found to be independent of the calcination time and temperature. Furthermore, the conversion and yield increase with an increasing reaction temperature up to 500 ^{o}C, but decrease with a further increase in the reaction temperature. Moreover, rice husk ash supported nickel catalysts display higher nickel surface area and acitivity than silica gel as revealed by the H$_2$-TPD and the hydrogenation tests.

Panagiotopoulou et al. [2008] investigated that the catalytic performance of Al$_2$O$_3$ supported noble metal catalysts for the methanation of CO, CO$_2$ and their mixture with respect to the nature of the dispersed metallic phase (Ru, Rh, Pt, Pd). It has been found that, for all experimental conditions investigated, Ru and Rh are significantly more active than Pt and Pd. Selectivity towards hydrogenation products depends strongly on the noble metal catalyst employed as well as on whether solo- or co-methanation of Co/ CO$_2$ is occurring. In present of water in the feed, catalytic activity of Ru is not affected, while that of Rh is reduced. On the other hand, the performance of Pt and Pd is poor since they promote the undesired water-gas shift reaction.

Iron catalyzed CO_2 hydrogenation is proposed as a mechanism that occurs during natural gas formation in coalbeds. The percentage of methane in the produced gas was typically greater than 90%, resembling natural gas composition. Fe_2O_3 was reduced at 200 ^{o}C under a hydrogen atmosphere. The results show that under those conditions ca. 6% of iron oxide is reduced to metal, which is believed to be the catalytically active species. Addition of water to the reactor increased the generation of methane [Medina et al., 2000].

Okabe et al. [2004] investigated the Fischer-Tropsch synthesis that was carried out in slurry phase over uniformly dispersed Co/ SiO_2 catalysts prepared by sol-gel method. When 0.01-1 wt.% of noble metals were added to the Co/ SiO_2 catalysts, a high and stable catalytic activity was obtained over 60 h of the reaction at 503 K and 1 MPa. The addition of noble metals increased the reducibility of surface Co on the catalysts, without changing the particle size of Co metal. The uniform pore size of the catalysts was enlarged by varying the preparation conditions. Increased pore size resulted in decreased CO conversion and selectivity for CO_2 and increased olefin/paraffin ratio of the products.

Takenaka et al. [2004] show that complete removal of CO by methanation in H_2-rich gas stream was performed over different metal catalysts. Ni/ ZrO_2 and Ru/ TiO_2 were the most effective catalysts for complete removal of CO through the methanation. These catalysts can decrease a concentration of CO from 0.5% to 20 ppm by the steam reforming of methane with a significantly low conversion of CO_2 into methane. Catalytic activities of supported Ni and Ru strongly depended on the type of supports.

Takanabe et al.[2005] prepared titania supported cobalt and nickel bimetallic catalysts for CO_2 reforming of methane to synthesis gas at 1023 K under ambient pressure. Bimetallic Co-Ni/TiO_2 catalysts with an appropriate Co/Ni ratio show highly stable activities without carbon deposition. Whereas the monometallic Co/TiO_2 catalyst deactivated rapidly because of the oxidation of metal, 10% mol substitution of nickel for cobalt suppressed the oxidation of metal, providing a high catalytic stability. The advantages of the bimetallic catalysts are high resistance to undesirable metal oxidation and coaking through the control of reactions between CH_4 and CO_2.

CHAPTER III

THEORY

3.1 CO$_2$ Hydrogenation Reactions

In recently, several reaction mechanisms for the CO$_2$ hydrogenation have been proposed. First, The catalytic hydrogenation over promoted Cu-ZnO catalysts under pressurized conditions produces mainly CH$_3$OH, CO and H$_2$O. A small amount of CH$_4$ was produced. At higher temperature, a very small amount of CH$_3$OCH$_3$ was also produced. Therefore, main reactions are shown in the following equations [Arakawa et al., 1992].

$$CO_2 + 3H_2 \rightleftharpoons CH_3OH + H_2O$$
$$CO_2 + H_2 \rightleftharpoons CO + H_2O$$
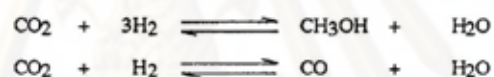
An in situ FT-IR observation of surface species over 5 wt% Cu-ZnO/SiO$_2$ as model catalyst showed the presence of bidentate carbonate species on both Cu and ZnO at the condition of 3 MPa, 30 $^{\circ}$C and 100 ml/min. Also a small amount of adsorbed CO on Cu site was observed. These bidentate carbonate species were rapidly transformed to the bidentate formate species with the increase of reaction temperature up to 150 $^{\circ}$C under 3 MPa. However, a small amount of adsorbed CO species has diminished at 100 $^{\circ}$C and it was never observed under the reaction condition. The experimental dynamic in situ FT-IR spectra of adsorbed species over the catalyst at various reaction conditions. This observation also suggests the direct formation of CH$_3$OH from CO$_2$ via bidentate carbonate species, formate species and methoxy species as shown in Figure.
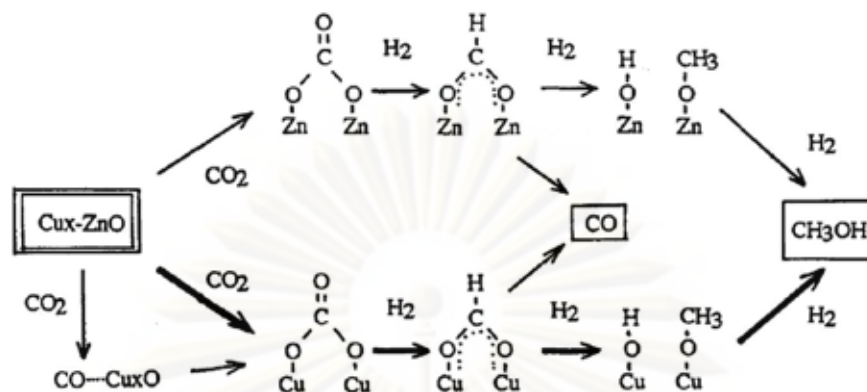
A proposed reaction mechanism for CH_3OH formation from H_2/CO_2 over Cu-ZnO/SiO$_2$ catalyst. [Arakawa et al., 1992]

The fibrous Cu/Zn/Al/Zr catalyst showed high activity for producing methanol from CO_2 hydrogenation [Xin et al., 2009]. Thus, there are three independent reac tions present in methanol synthesis from CO_2, namely, Methanol synthesis from CO:

$$CO + 2H_2 \rightleftharpoons CH_3OH \qquad \Delta H = -90.4 \text{ kJ/mol}$$

Reverse water gas shift:

$$CO_2 + H_2 \rightleftharpoons CO + H_2O \qquad \Delta H = +41.0 \text{ kJ/mol}$$

Methanol synthesis from CO_2:

$$CO_2 + 3H_2 \rightleftharpoons CH_3OH + H_2O \qquad \Delta H = -49.3 \text{ kJ/mol}$$
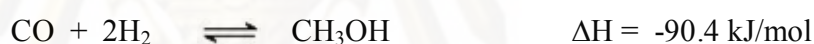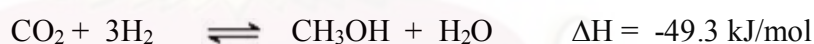
Second, Chen et al. [2009] used a commercially available Ni/Al$_2$O$_3$ sample containing K additive to enable carbon deposition from CO_2 exposure by means of catalytic hydrogenation. The experimental results suggest that K additives induce the formation of carbon nanofibers (CNFs) or carbon deposition on Ni/Al$_2$O$_3$ during the CO_2 hydrogenation reaction. We propose that the rate of carbon deposition depends on the reaction temperature, on H_2 and CO_2 partial pressures, and on the reactant residence time.

$$(1) \quad CO_2 + 2S \rightleftharpoons CO_2\text{-}2S$$
$$(2) \quad H_2 + CO_2\text{-}2S \rightleftharpoons H_2O + CO\text{-}S + S$$
$$(3) \quad H_2 + CO\text{-}S \rightleftharpoons H_2O + C\text{-}S$$

Third, Lahtinen et al. [1994] investigated C, CO and CO_2 hydrogenation on cobalt foil model catalysts. It was found that the reactions produce mainly methane, but with selectivities of 98, 80, and 99 wt% at 525 K for C, CO, and CO_2, respectively. The rate of methane formation on cobalt foil shows zero order partial pressure dependence on CO_2 and first order partial pressure dependence on H_2. The reaction proceeds via dissociation of C-O bonds and formation of CoO on the surface. The reduction of CoO is the rate limiting step in the CO and CO_2 hydrogenation reaction. These authors also proposed the reaction mechanisms for C, CO and CO_2 hydrogenation.

The reaction mechanisms proposed for C, CO and CO_2 hydrogenation.

C Hydrogenation	CO Hydrogenation	CO_2 Hydrogenation		
	$CO+* \Leftrightarrow CO*$	$CO2 + * \Leftrightarrow CO2*$		
$H_2+2* \Leftrightarrow 2H*$	$H_2+2* \Leftrightarrow 2H*$	$H_2+2* \Leftrightarrow 2H*$		
		$CO_2*+Co \Leftrightarrow CO*+CoO$		
	$CO*+Co \Leftrightarrow C*+CoO$	$CO*+Co \Leftrightarrow C*+CoO$		$CO*+H* \Leftrightarrow COH*+*$
$C*+H* \Leftrightarrow CH*+*$	$C*+H* \Leftrightarrow CH*+*$	$C*+H* \Leftrightarrow CH*+*$	or	$COH*+H* \Leftrightarrow H_2CO*+*$
$CH*+H* \Leftrightarrow CH_2*+*$		$CH*+H* \Leftrightarrow CH_2*+*$		$HCO*+Co \Leftrightarrow CH_2*+CoO$
$CH_2*+H* \Leftrightarrow CH_3*$	$CH_2*+H* \Leftrightarrow CH_3*$	$CH_2*+H* \Leftrightarrow CH_3*$		
$CH_3*+H* \Leftrightarrow CH_4+2*$	$CH_3*+H* \Leftrightarrow CH_4+2*$	$CH_3*+H* \Leftrightarrow CH_4+2*$		
	$CoO+H* \longrightarrow OH*+Co$	$CoO+H* \longrightarrow OH*+Co$		
	$OH*+H* \Leftrightarrow H_2O+2*$	$OH*+H* \Leftrightarrow H_2O+2*$		
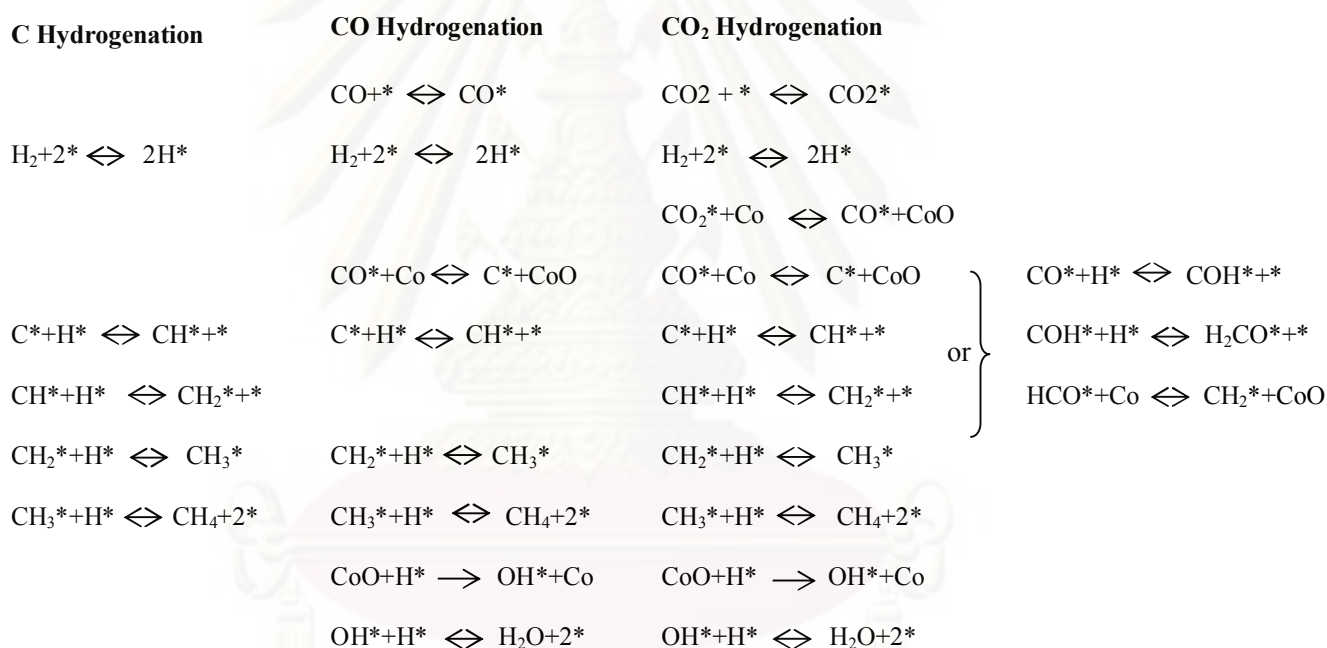
CO and CO_2 methanation is investigated as an alternative purification step [Xu et al., 2006 ; Choudhury et al., 2006 ; Dagle et al., 2007]

$$CO + 3H_2 \rightleftharpoons CH_4 + H_2O \qquad \Delta H = -206 \text{ kJ/mol}$$

$$CO_2 + 4H_2 \rightleftharpoons CH_4 + H_2O \qquad \Delta H = -165 \text{ kJ/mol}$$
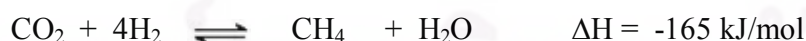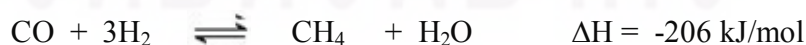
3.2 Silicon dioxide

General feature of silica

Table 3.1 Physical properties of silica

Other names	Silica
Molecular formula	SiO_2
Molar mass	60.1 g/mol
Appearance	white or colourless solid (when pure)
Density and phase	2.6 g/cm^3, solid
Solubility in water	insoluble
Melting point	1610 °C
Boiling point	2230 °C

In its many forms, silica has been used in all stages of civilization, from the ancient flints of the Stone Age to the modern silica laboratory ware. Because of its many uses, and of the many varied forms in which it occurs, silica has been called by more names than any other mineral. Many of the older names of flint are now so obsolete that repetition is needless, but many of the present-day names for quartz gems are unknown save to a few jewellers. Then, too, the exact research of the modern laboratory has shown several distinct crystallographic varieties of silica; some of which are closely connected with the temperatures experienced in their life-history.

The many different names, and their different connotations, which are now in use for silica minerals, call for a classification and arrangement in a more ample, yet more concise manner than is to be found in the usual discussion of the varieties of silica. This article is written with the hope of making a scientific classification of these names, so that

the use of the different terms will no longer be a cause for tedious searching for definitions.

These varieties are named in the order formed with descending temperatures. Recrystallization changes occur at the temperatures noted when ample time is allowed for the action, often in the laboratory only in the presence of catalysts. Besides the changes at these critical temperatures, there are probably similar changes from unstable forms towards quartz at atmospheric temperatures, especially after long time intervals. With fairly rapid cooling or heating intermediate forms may not occur in their stable zone, but a direct change from one to another without the intermediate product may take place. Most of the recrystallization changes noted are found to occur at oth ascending and descending temperatures.

(A) SILICA GLASS - amorphous, a true non-crystalline glass, stable below the melting point and above the "gc" temperature. Quartz Glass, Fused Silica, Fused Quartz, are other names for this supercooled liquid. In most forms at atmospheric temperatures there are traces of cristobalite.

(B) CRISTOBALITE - isometric, or pseudo-isometric, "gc" range is at 1710° where Cristobalite changes to glass as temperatures rise, or glass to cristobalite as they fall. Christobalite, an alternate spelling. Beta Cristobalite, also called High Cristobalite, is the high temperature product, forming in the "gc" range in cooling. It is isometric, and in cooling recrystallizes to Alpha Cristobalite, or Low Cristobalite, at 200-275°, providing cooling through the "ct" and "tq" ranges has been too rapid for recrystallization. It is tetragonal.

(C) TRIDYMITE - hexagonal, bipyramidal. "ct" range is at 1470°, where cristobalite changes to tridymite on cooling. Glass may crystallize as tridymite at 1670° if the cooling was too rapid through the "gc" range. Beta Second Tridymite, or Upper High Tridymite, is the high temperature product, forming in the "ct" range in cooling, and which recrystallizes to Beta First Tridymite, also called Lower High Tridymite, at 163° if

cooling was too rapid for the "tq" transformation. This in turn alters to Alpha Tridymite, or Low Tridymite, at 117°, which is the usual tridymite of nature.

Asmanite	-	a meteoric tridymite, related to the above series.
Vestan	-	a doubtful silica mineral, probably to be ascribed to tridymite.
Granuline	-	a doubtful pulverescent mineral which seems allied to tridymite on optical grounds.

(D) QUARTZ - hexagonal, forms from tridymite in the "tq" range at 870° in cooling. Glass may change to crystalline quartz at about 1400° providing cooling was too rapid for the "gc", "gt" and "ct" transformations. Beta Quartz, or High Quartz, is the high temperature product, forming at the "tq" point. It is hemihedral. On cooling it recrystallizes to Alpha Quartz, also called Low Quartz, at 573°, yielding the stable low temperature mineral. It is tetartohedral, showing polarity along the c axis and is divisable into Right Hand Quartz and Left Hand Quartz

(E) CHALCEDONY - a cryptocrystalline, or very finely fibrous mineral, which has not been successfully located in the thermal equilibrium diagram. Heating to 725-850° usually results in an alteration to tridymite, which thereafter acts as normal tridymite. Chalcedony is usually found as a deposit from solutions, and may be a mixture of glass and quartz, or more probably an intermediate product in the dehydration of the opal colloid. Various subdivisions of chalcedony have been made on optical grounds.

Chalcedony	-	biaxial,positive,elongationpositive.
Chalcedonite	-	biaxial,negative.
Lussatite	-	biaxial, positive, parallel, elongation.
Quartzine	-	biaxial, positive, negative elongation pseudochalcedonite,Lutecite.
Jenzschite	-	differently soluble, but of same S. G. as chalcedony.

Melanophlogite -   possibly impure chalcedony.

Sulfuricin   -   probably a chalcedony rich in sulphur.

(F) COLLOIDAL SILICA - is usually hydrous, and is commonly described under opal. Silicon occurs in nature combined with oxygen in various forms of silica and silicates. Silicates have complex structures consisting of SiO_4 tetrahedral structural units incorporated to a number of metals. Silicon is never found in nature in free elemental form. Among all elements silicon forms the third largest number of compounds after hydrogen and carbon. There are well over 1000 natural silicates including clay, mica, feldspar, granite, asbestos, and hornblende. Such natural silicates have structural units containing orthosilicates, SiO_4^{4-}, pyrosilicates $Si_2O_7^{6-}$, and other complex structural units, such as, $(SiO_3)_n^{2n-}$ that have hexagonal rings arranged in chains or pyroxene $(SiO_3^{2-})^n$ and amphiboles, $(Si_4O_{11}^{6-})^n$ in infinite chains. Such natural silicates include common minerals such as tremolite, $Ca_2Mg_5(OH)_2Si_8O_{22}$; diopside, $CaMg(SiO_3)_2$; kaolin, $H_8Al_4Si_4O_{18}$; montmorillonite, $H_2Al_2Si_4O_{12}$; tale, $Mg_3[(OH)_2 SiO_{10}]$; muscovite (a colorless form of mica), $H_2KAl_3(SiO_4)_3$; hemimorphite, $Zn_4(OH)_2Si_2O_7.H_2O$; beryl, $Be_3Al_2Si_6O_{18}$; zircon, $ZrSiO_4$; benitoite, $BaTiSi_3O_9$; feldspars, $KAlSi_3O_8$; zeolites, $Na_2O.2Al_2O_3.5SiO_2.5H_2O$; nephrite, $Ca(Mg,Fe)_3(SiO_3)_4$; enstatite, $(MgSiO_3)_n$; serpentine, $H_4Mg_3Si_2O$, jadeite, $NaAl(SiO3)_2$; topaz, $Al_2SiO_4F_2$; and tourmaline, $(H,Li,K,Na).Al_3(BOH)_2SiO_{19}$. silica, the other most important class of silicon compounds, exists as sand, quartz, flint, amethyst, agate, opal, jasper, and rock crystal.

3.3 Titanium (IV) Oxide (Fujishima et al., 1999)

Titanium (IV) oxide occurs naturally in three crystalline forms:

1. Rutile, which tends to more stable at high temperatures. The application of almost rutile type is used in industrial products such as paints, cosmetics foodstuffs and sometimes found in igneous rocks.

2. Anatase, which tends to be more stable at lower temperatures. This type generally shows a higher photoactivity than other types of titanium dioxide.

3. Brookite, which is usually found only in minerals and has a structure belonging to orthorhombic crystal system.

Both of rutile and anatase type have a structure belonging to tetragonal crystal system but they are not isomorphous (Figure 1). The two tetragonal crystal types are more common because they are easy to make. Anatase occurs usually in near-regular octahedral, and rutile forms slender prismatic crystal, which are frequently twinned. Rutile is the thermally stable form and is one of the two most important ores of titanium.

The three allotropic forms of titanium dioxide have been prepared artificially but only rutile, the thermally stable form, has been obtained in the form of transparent large single crystal. The transformation form anatase to rutile is accompanied by the evolution of ca. 12.6 kJ/mol (3.01 kcal/mol), but the rate of transformation is greatly affected by temperature and by the presence of other substance which may either catalyze of inhibit the reaction. The lowest temperature at which conversion of anatase to rutile takes place at a measurable rate is ca. 700°C, but this is not a transition temperature. The change is not reversible; ΔG for the change from anatase to rutile is always negative.
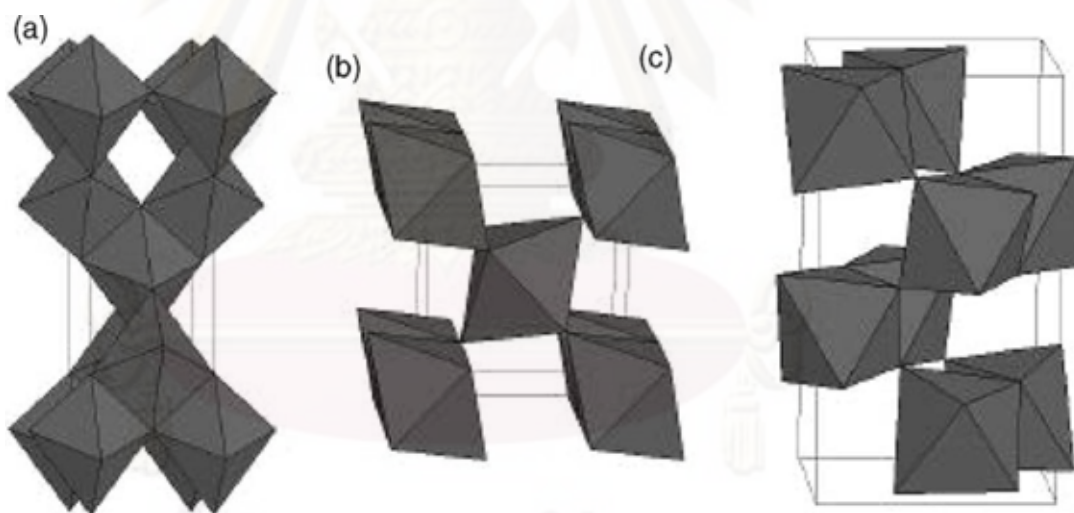
Figure. 3.1 Crystal structures of anatase (a), rutile (b), and brookite (c) TiO_2. (Carp et al., 2004)

Table. 3.2 Crystallographic properties of anatase, brookite, and rutile.

Properties	Anatase	Brookite	Rutile
Crystal structure	Tetragonal	Orthorhombic	Tetragonal
Optical	Uniaxial, negative	Biaxial, positive	Uniaxial, negative
Density, g/cm^3	3.9	4.0	4.23
Harness, Mohs scale	$5^1/_2 - 6$	$5^1/_2 - 6$	$7 - 7^1/_2$
Unit cell	$D_4a^{19}.4TiO_2$	$D_2h^{15}.8TiO_2$	$D_4h^{12}.3TiO_2$
Dimension, nm			
a	0.3758	0.9166	0.4584
b		0.5436	
c	0.9514	0.5135	2.953

Brookite has been produced by heating amorphous titanium (IV) oxide, prepared from alkyl titanates of sodium titanate with sodium or potassium hydroxide in an autoclave at 200 to 600 ^{o}C for several days. The important commercial forms of titanium (IV) oxide are anatase and rutile, and these can readily be distinguished by X-ray diffraction spectrometry.

Since both anatase and rutile are tetragonal, they are both anisotropic, and their physical properties, e.g. refractive index, vary according to the direction relative to the crystal axes. In most applications of these substances, the distinction between crystallographic directions is lost because of the random orientation of large numbers of small particles, and it is mean value of the property that is significant.

Measurement of physical properties, in which the crystallographic directions are taken into account, may be made of both natural and synthetic rutile, natural anatase crystals, and natural brookite crystals. Measurements of the refractive index of titanium dioxide must be made by using a crystal that is suitably orientated with respect to the crystallographic axis as a prism in a spectrometer. Crystals of suitable size of all three

modifications occur naturally and have been studied. However, rutile is the only form that can be obtained in large artificial crystals from melts. The refractive index of rutile is 2.75. The dielectric constant of rutile varies with direction in the crystal and with any variation from the stoichiometric formula, TiO_2; an average value for rutile in powder from is 114. The dielectric constant of anatase powder is 48.

Titanium dioxide is thermally stable (mp 1855˚C) and very resistant to chemical attack. When it is heated strongly under vacuum, there is a slight loss of oxygen corresponding to a change in composition to $TiO_{1.97}$. The product is dark blue but reverts to the original white color when it is heated in air.

3.4 Cobalt

3.4.1 General

Cobalt, a transition series metallic element having atomic number 27, is similar to silver in appearance. Cobalt and cobalt compounds have expended from use colorants in glasses and ground coat frits for pottery to drying agents in paints and lacquers, animal and human nutrients, electroplating materials, high temperature alloys, hard facing alloys, high speed tools, magnetic alloys, alloys used for prosthetics, and used in radiology. Cobalt is also as a catalyst for hydrocarbon refining from crude oil for the synthesis of heating fuel.

3.4.2 Physical Properties

The electronic structure of cobalt is [Ar] $3d^7 4s^2$. At room temperature the crystalline structure of the α (or ε) form, is close-packed hexagonal (cph) and lattice parameters are a = 0.2501 nm and c = 0.4066 nm. Above approximately 417˚C, a face-centered cubic (fcc) allotrope, the γ (or β) form, having a lattice parameter a = 0.3544 nm, becomes the stable crystalline form. Physical properties of cobalt are listed in Table 3.3.

Table 3.3 Physical properties of cobalt

Property	Value
atomic number	27
atomic weight	58.93
transformation temperature, ^{o}C	417
heat of transformation, J/ga	251
melting point, ^{o}C	1493
latent heat of fusion, ΔHfus J/ga	395
boiling point, , ^{o}C	3100
latent heat of vaporization at bp, ΔHvap kJ/ga	6276
specific heat, J/(g.^{o}C)[a]	
15-100°C	0.442
molten metal	0.560
coefficient of thermalexpansion, $^{o}C^{-1}$	
cph at room temperature	12.5
fcc at 417°C	14.2
thermal conductivity at 25 ^{o}C, W/(m.K)	69.16
thermal neutron absorption, Bohr atom	34.8
resistivity, at 20 ^{o}C[b], 10^{-8} Ω.m	6.24
Curie temperature, ^{o}C	1121
saturation induction, 4πIs, T[c]	1.870

Table 3.3 Physical properties of cobalt (cons.)

Property	Value
permeability, μ	
initial	68
max	245
residual induction, T^e	0.490
coercive force, A/m	708
Young's modulus, Gpac	211

The scale formed on unalloyed cobalt during exposure to air or oxygen at high temperature is double-layered. In the range of 300 to 900°C, the scale consists of a thin layer of mixed cobalt oxide, Co_3O_4, on the outside and cobalt (II) oxide, CoO, layer next to metal. Cobalt (III) oxide, Co_2O_3, may be formed at temperatures below 300°C. Above 900°C, Co_3O_4 decomposes and both layers, although of different appearance, are composed of CoO only. Scales formed below 600°C and above 750°C appear to be stable to cracking on cooling, whereas those produced at $600\text{-}750^{\circ}$C crack and flake off the surface.

Cobalt forms numerous compounds and complexes of industrial importance. Cobalt, atomic weight 58.933, is one of the three members of the first transition series of Group 9 (VIIIB). There are thirteen know isotopes, but only three are significant, Co is the only stable and naturally occurring isotope, Co has a half-life of 5.3 years and is a common source of γ-radioactivity; and [57]Co has a 270-d half-life and provides the γ-source for Mᴄssbauer spectroscopy.

Cobalt exists in the +2 or +3 valance states for the major of its compounds and complexes. A multitude of complexes of the cobalt (III) ion exists, but few stable simple salt are known. Octahedral stereochemistries are the most common for cobalt (II) ion as

well as for cobalt (III). Cobalt (II) forms numerous simple compounds and complexes, most of which are octahedral or tetrahedral in nature; cobalt (II) forms more tetrahedral complex than other transition-metal ions. Because of the small stability difference between octahedral and tetrahedral complexes of cobalt (II), both can be found equilibrium for a number of complexes. Typically, octahedral cobalt (II) salts and complexes are pink to brownish red; most of the tetrahedral Co (II) species are blue.

3.5 Nickel

3.5.1 General

Nickel, a transition series metallic element having atomic number 28, is is a silvery-white lustrous metal with a slight golden tinge.

Nickel is used in many industrial and consumer products, including stainless steel, magnets, coinage, rechargeable batteries, electric guitar strings and special alloys. It is also used for plating and as a green tint in glass. Nickel is pre-eminently an alloy metal, and its chief use is in the nickel steels and nickel cast irons, of which there are many varieties. It is also widely used in many other alloys, such as nickel brasses and bronzes, and alloys with copper, chromium, aluminium, lead, cobalt, silver, and gold

3.5.2 Physical Properties

The electronic structure of nickel is [Ar] $3d^8 4s^2$. Physical properties of nickel are listed in Table 3.4.

Table 3.4 Physical properties of nickel

Property	Value
atomic number	28
atomic weight	58.69
melting point, ^{o}C	1453
latent heat of fusion, ΔH_{fus} kJ/mol[a]	17.48
boiling point, , ^{o}C	2732
latent heat of vaporization at bp, ΔH_{vap} kJ/mol[a]	377.5
specific heat, kJ/(mol^{o}K)[a]	
25°C	26.07
coefficient of thermal expansion, ^{o}C^{-1}	13.4 μm·m^{-1}·K^{-1}
thermal conductivity at 27 ^{o}C, W/(m·K)	90.9
Curie temperature, ^{o}C	355
Young's modulus, Gpac	200

3.5.3 Nickel oxide

NiO adopts the NaCl structure, with octahedral Ni(II) and O^{2-} sites. The conceptually simple structure is commonly known as the rock salt structure. Like many other binary metal oxides, NiO is often non-stoichiometric, meaning that the Ni:O ratio deviates from 1:1. In nickel oxide this non-stoichiometry is accompanied by a color change, with the stoichiometrically correct NiO being green and the non-stoichiometric NiO being black. NiO can be prepared by multiple methods. Upon heating above 400 °C, nickel powder reacts with oxygen to give NiO. In some commercial processes, green nickel oxide is made by heating a mixture of nickel powder and water at 1000 °C, the rate for this reaction can be increased by the addition of NiO

Ni_2O_3 has been referred to in the literature but is not a well characterised compound.[1] The substance black nickel oxide is sometimes described as being Ni_2O_3 however the composition quoted by suppliers has a nickel content of around 77% by weight whereas Ni_2O_3 would have 70.98% Ni by weight, and may be non-stoichiometric NiO

CHAPTER IV

METHODOLOGY

4.1 Research Methodology

Preparation SiO$_2$ supports $\dashrightarrow$ - submicrosphere / - MCM41

SiO$_2$ support Characterization $\dashrightarrow$ - BET surface area / - SEM, TEM

Titanium isopropoxide $\dashrightarrow$ Preparation TiO$_2$- SiO$_2$ composites supports

TiO$_2$- SiO$_2$ composites supports characterization $\dashrightarrow$ - XRD / - BET surface area / - SEM/EDX / - TEM / - TGA
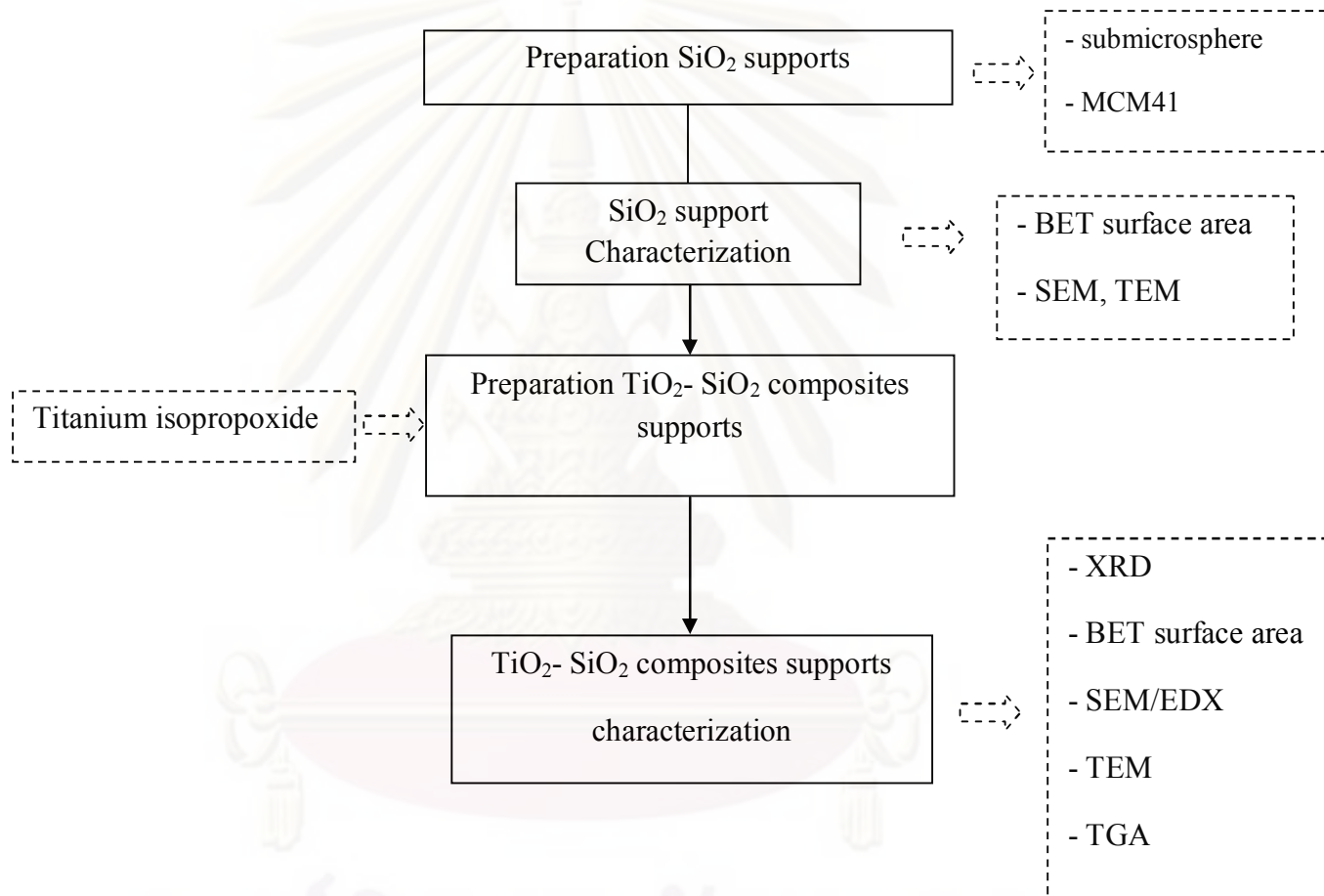
Scheme.4.1 Flow diagram of research methodology for supports preparation
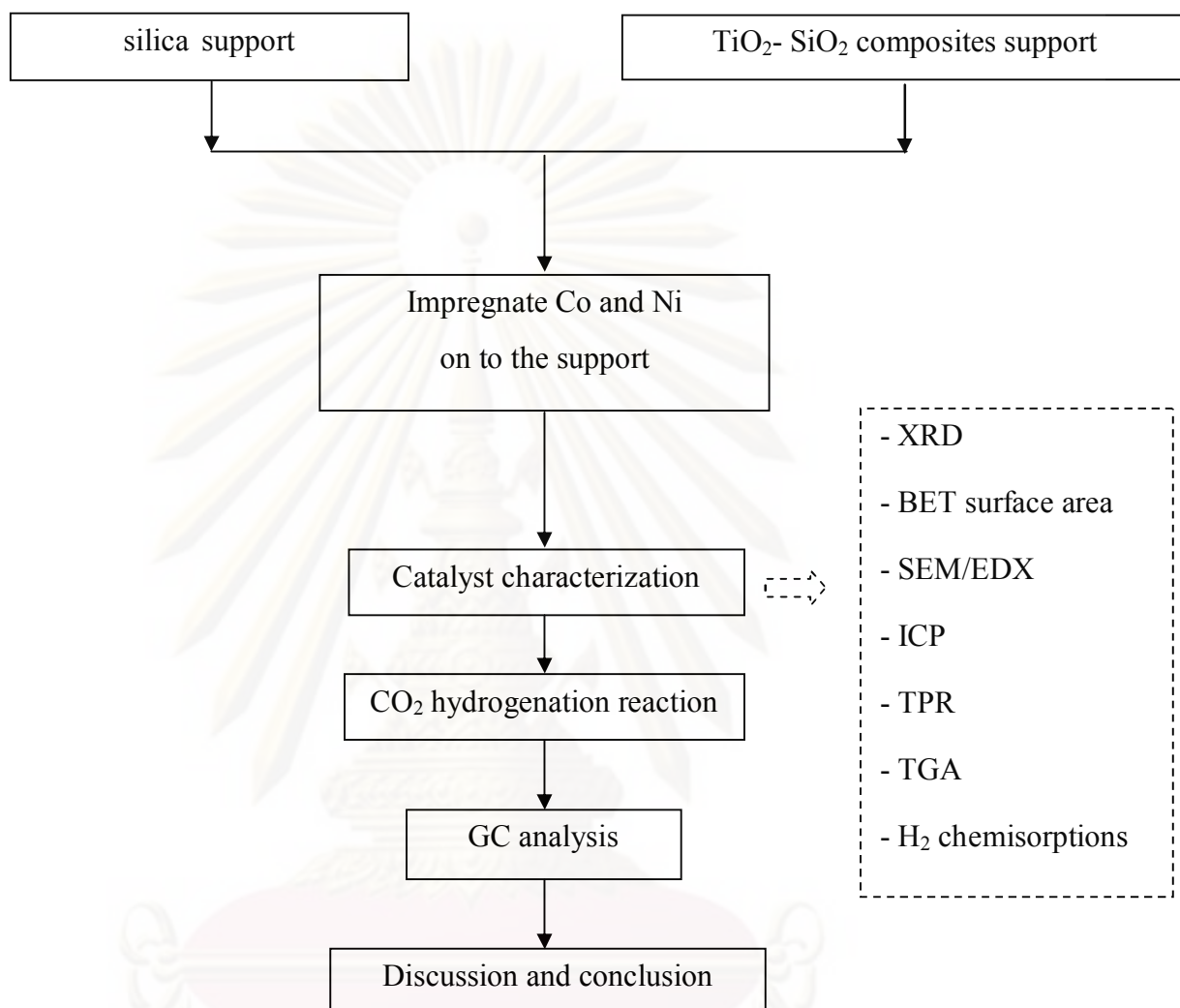
Scheme.4.2 Flow diagram of research methodology for catalysts preparation and characterization.

4.2 Catalyst preparation

    4.2.1 Chemicals

    1. Titanium isopropoxide 97% (TiPOT) available from Aldrich

    2. Tetraethyl othosilicate 98% (TEOS) available from Aldrich

    3. Cobalt (II) nitrate hexahydrate 98% [$Co(NO_3)_2 \cdot 6H_2O$] available from Aldrich

    4. Nickel (II) nitrate hexahydrate 98% [$Ni(NO_3)_2 \cdot 6H_2O$] available from Aldrich

    5. Ammonia 30% available from Panreac

    6. Ethanol 99.99% available from J.T. Baker

    7. Isopropanol available from QReC

    8. De-ionized water

    4.2.2 Preparation of the spherical silica particle (SSP) and MCM41 [Liu et al., 2004]

    1. The composition of the synthesis gel has following molar ratio: 1 TEOS : 0.3 C_{16}TMABr : 11NH_3 : x Ethanol : 144 H_2O. Molar ratios of ethanol addition is 0 and 58 for the preparation MCM41 and SSP, respectively.

    2. The solution will be further stirred for 2 h at room temperature.

    3. The white precipitate will be then collected by filtration and washed with distilled water.

    4. Dried samples will be calcined at 550 °C for 6 h with a heating rate of 10 ^{O}C min^{-1} in air.

    4.2.3 Preparation of the TiO$_2$- SiO$_2$ composites supports modified from Grzechowaik [2008]

    1. The desired amount of titanium isopropoxide (equivalent to the desired TiO$_2$ loading percentage) will be dissolved in isopropanol (using 1:3 w/w of support : isopropanol)

    2. The silica from 4.2.2 will be added to the solution and stirred for 1 h.

    3. Hydrolysis will be performed by addition of ammonia (H_2O : TiPOT = 4:1). The sol will be further stirred for 20 h at room temperature. Then, the sample will be dried at 110 °C for 24 h.

4.2.4 Cobalt and Nickel Loading

In this experiment, incipient wetness impregnation is the one methods used for loading cobalt. Cobalt (II) nitrate hexahydrate [$Co(NO_3)_2 \cdot 6H_2O$] and Nickel (II) nitrate hexahydrate [$Ni(NO_3)_2 \cdot 6H_2O$]is used as precursor in this method

The incipient wetness impregnation procedure is as follow:

1. The certain amount of cobalt (20 wt% loading) will be introduced into the de-ionized water which its volume equals to pore volume of catalyst.

2. titania-silica composites support will be impregnated with aqueous solution of cobalt and nickel. The cobalt and nickel solution is dropped slowly to the titania-silica composites support

3. The catalyst is dried in the oven at 383 K for 12 h.

4. The catalyst is calcined in air at 773 K for 4 h.

4.2.5 Catalysts Nomenclature

The nomenclature used for the catalyst samples in this study is as follows :

- **CoTiSSPXXX**
- **CoTiMCMXXX**
- **NiTiSSPXXX**
- **NiTiMCMXXX**

CoTiSSPXXX refers to cobalt supported on titania-spherical silica composites (TiSSP) calcined at XXX ^{o}C

CoTiMCMXXX refers to cobalt supported on titania-MCM-41 composites (TiMCM) calcined at XXX ^{o}C

NiTiSSPXXX refers to nickel supported on titania-spherical silica composites (TiSSP) calcined at XXX ^{o}C

NiTiMCMXXX refers to nickel supported on titania-MCM-41 composites (TiMCM) calcined at XXX ^{o}C

4.3 Catalyst characterization

4.3.1 X- ray diffraction (XRD)

XRD will be performed to determine the bulk phase of catalysts by SIEMENS D 5000 X-ray diffractometer connected with a computer with Diffract ZT version 3.3 programs for fully control of the XRD analyzer. The experiments will be carried out by using CuK_α radiation with Ni filter in the 2θ range of 20-80 degrees resolution 0.04^{o}. The crystallite size will be estimated from line broadening according to the Scherrer equation and α-Al_2O_3 will be used as standard.

4.3.2 N_2 physisorption

BET apparatus for the single point method, the reaction apparatus of BET surface area measurement consisted of two feed lines for helium and nitrogen. The flow rate of the gas will be adjusted by means of fine-metering valve on the gas chromatograph. The sample cell made from pyrex glass. The mixture gases of helium and nitrogen will flow through the system at the nitrogen relative of 0.3. The catalyst sample (ca. 0.1 g) will be placed in the sample cell, which will be then heated up to 160 ^{o}C and will hold at this temperature for 2 h. After the catalyst sample will be cooled down to room temperature, nitrogen uptakes will be measure as follows.

1. Adsorption step: The sample that set in the sample cell will be dipped into liquid nitrogen. Nitrogen gas that will flow through the system will be adsorbed on the surface of the sample until equilibrium will be reached.

2. Desorption step: The sample cell with nitrogen gas-adsorption catalyst sample will dip into the water at room temperature. The adsorbed nitrogen gas will be desorbed from the surface of the sample. This step will be completed when the indicator line will be in the position of base line.

3. Calibration step: 1 ml of nitrogen gas at atmospheric pressure will be injected through the calibration port of the gas chromatograph and the area will be measured. The area will be the calibration peak.

4.3.3 Scanning Electron Microscopy: SEM and Energy Dispersive X-ray Spectroscopy (EDX)

Scanning electron microscopy (SEM) and Energy dispersive X-ray spectroscopy (EDX) will be used to determine the morphology and elemental distribution of the catalyst particles. Model of SEM: JEOL mode JSM-5800LV and EDX will be performed using Link Isis Series 300 program at the Scienctific and Technological Research Equipment Center, Chulalongkorn University (STREC).

4.3.4 Temperature programmed reduction (TPR)

TPR will be used to determine the reducibility of catalysts. The catalyst sample 0.1 g will use in the operation and temperature ramping from 35 ^{o}C to 800 ^{o}C at 10 ^{o}C/min. The carrier gas will be 5 % H_2 in Ar. During reduction, a cold trap will be placed to before the detector to remove water produced. A thermal conductivity detector (TCD) will be measure the amount of hydrogen consumption. The calibration of hydrogen consumption will be performed with bulk cobalt oxide (Co_3O_4) at the same conditions.

4.3.5 Thermogravimetry analysis (TGA)

TGA will be used to determine the weight loss pattern and the reducibility of catalysts by Shimadzu TGA model 50. The catalyst sample of ca. 10-20 mg and temperature ramping from 35 ^{o}C to 1000 ^{o}C at 10 ^{o}C/min will be used in the operation. The carrier gas will be H_2 UHP.

4.3.6 Carbon monoxide Chemisorption

Static CO chemisorption at room temperature on the reduce catalysts will be used to determine the number of reduce surface nickel metal atoms. The total CO chemisorption will be calculated from the number of injection of a known volume. CO chemisorption will be carried out following the procedure using a Micrometritics Pulse Chemisorb 2750 instrument at the Analysis Center of Department of Chemical Engineering, Faculty of Engineering, Chulalongkorn University. In an experiment, about 0.10 g of the catalyst sample was placed in a glass tube. Prior to chemisorption, the catalysts will be reduced at 350 ^{o}C for 3 hour after ramping up at a rate of 10 ^{o}C/min. After, carbon monoxide 30 microlite was inject to catalyst and repeat until desorption peak constant. Amount of carbon monoxide adsorption on catalyst was relative amount of active site.

.

4.4 Reaction study in CO_2 hydrogenation

4.4.1 Materials

CO_2 hydrogenation will be performed using 0.1 g of catalyst packed in the middle of the stainless steel microrector, which is located in the electrical furnace. The total flow rate will be 30 ml/min with the H_2/CO_2 ratio of 10/1. The catalyst sample will be re-reduced *in situ* in flowing H_2 at 350^oC for 3 h prior to CO_2 hydrogenation. CO_2 hydrogenation will be carried out at 220^oC and 1 atm total pressure. The effluent will be analyzed using gas chromatography technique [Thermal conductivity detector (TCD), molecular sieve 5 A^o will be used for separation of carbon dioxide (CO_2) and methane (CH_4) and flame ionization detector (FID),VZ-10 will be used for separation of light hydrocarbon such as methane (CH_4), ethane (C_2H_6), propane (C_3H_8), etc.]

4.4.2 Apparatus

Flow diagram of CO_2 hydrogenation system is shown in Figure 4.1. The system consists of a reactor, an automatic temperature controller, an electrical furnace and a gas controlling system.

4.4.2.1 Reactor

The reactor was made from a stainless steel tube (O.D. 3/8"). Two sampling points were provided above and below the catalyst bed. Catalyst was placed between two quartz wool layers

4.4.2.2 Automation Temperature Controller

This unit consisted of a magnetic switch connected to a variable voltage transformer and a solid-state relay temperature controller model no. SS2425DZ connected to a thermocouple. Reactor temperature was measured at the bottom of the catalyst bed in the reactor. The temperature control set point is adjustable within the range of $0-800^oC$ at the maximum voltage output of 220 volt.

4.3.2.3 Electrical Furnace

The furnace supplied heat to the reactor for CO hydrogenation. The reactor could be operated from temperature up to $800^{\circ}C$ at the maximum voltage of 220 volt.

4.3.2.4 Gas Controlling System

Reactant for the system was each equipped with a pressure regulator and an on-off valve and the gas flow rates were adjusted by using metering valves.

4.3.2.5 Gas Chromatography

The composition of hydrocarbons in the product stream was analyzed by a Shimadzu GC14B (VZ10) gas chromatograph equipped with a flame ionization detector. A Shimadzu GC8A (molecular sieve 5A) gas chromatography equipped with a thermal conductivity detector was used to analyze CO and H_2 in the feed and product streams. The operating conditions for each instrument are shown in the Table 4.2.

Table 4.1 Operating condition for gas chromatograph.

Gas Chromagraph	SHIMADZU GC-8A	SHIMADZU GC-14B
Detector	TCD	FID
Column	Molecular sieve 5A	VZ10
- Column material	SUS	-
- Length	2 m	-
- Outer diameter	4 mm	-
- Inner diameter	3 mm	-
- Mesh range	60/80	60/80
- Maximum temperature	350 ^{o}C	80 ^{o}C
Carrier gas	He (99.999%)	H_2 (99.999%)
Carrier gas flow	40 cc/min	-
Column gas	He (99.999%)	Air, H_2
Column gas flow	40 cc/min	-
Column temperature		
- initial (^{o}C)	60	70
- final (^{o}C)	60	70
Injector temperature (^{o}C)	100	100
Detector temperature (^{o}C)	100	150
Current (mA)	80	-
Analysed gas	Ar, CO, H_2	Hydrocarbon C_1-C_4

4.4.3 Procedures

1. Using 0.05 g of catalyst packed in the middle of the stainless steel microrector, which is located in the electrical furnace.

2. A flow rate of Ar = 8 CC/min, 8.8% CO_2 in H_2 = 22 CC/min and H_2 = 50 CC/min in a fixed-bed flow reactor. A relatively high H_2/CO_2 ratio was used to minimize deactivation due to carbon deposition during reaction.

3. The catalyst sample was re-reduce *in situ* in flowing H_2 at 350 ^{o}C for 3 h prior to CO_2 hydrogenation.

4. CO_2 hydrogenation was carried out at 220 ^{o}C and 1 atm total pressure in flowing 8.8% CO_2 in H_2.

5. The effluent was analyzed using gas chromatography technique. [Thermal conductivity detector (TDC) was used for separation of carbon dioxide (CO_2) and methane (CH_4) and flame ionization detector (FID) were used for separation of light hydrocarbon such as methane (CH_4), ethane (C_2H_6), propane (C_3H_8), etc.] In all cases, steady-state was reached within 6 h.
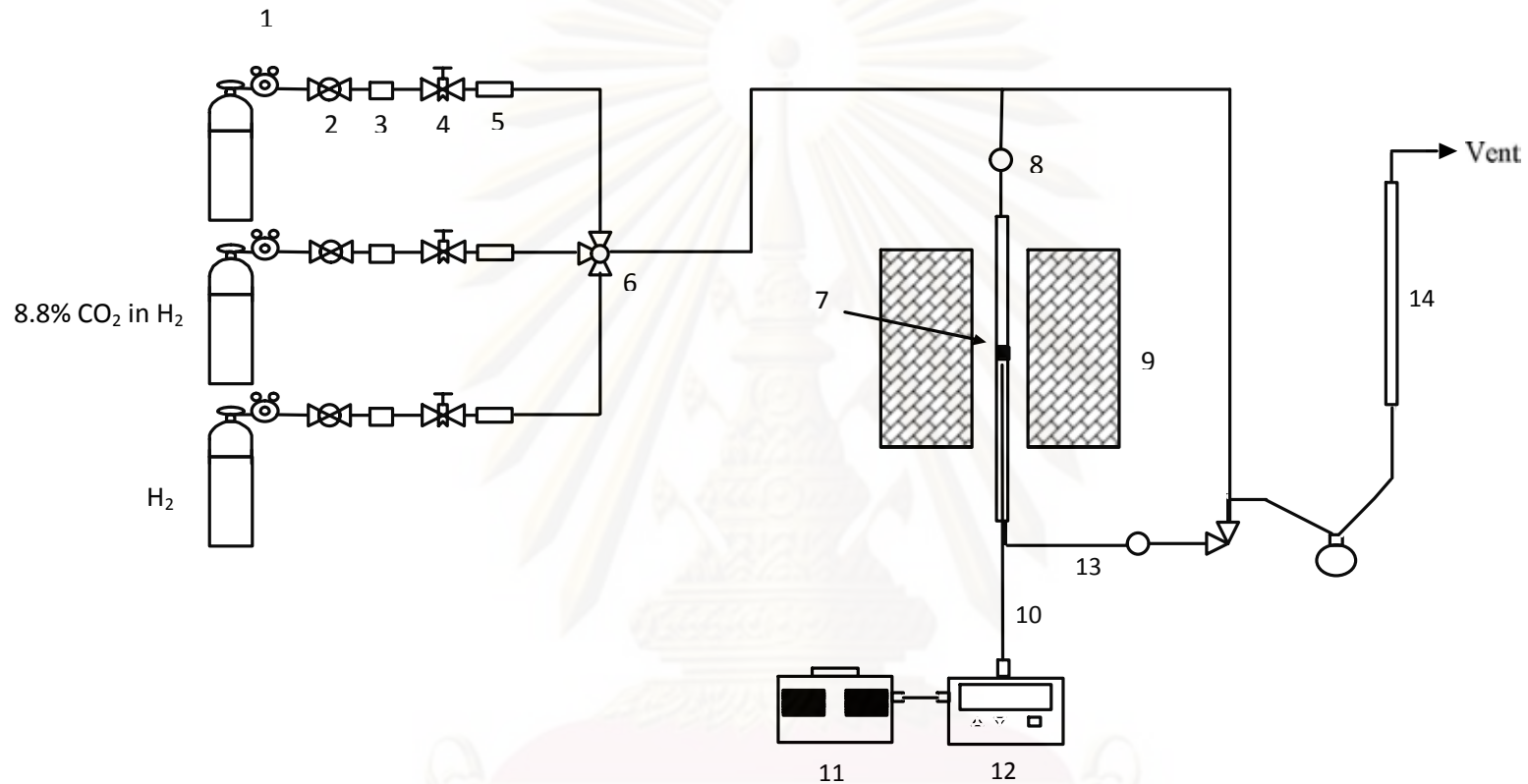
1. Pressure Regulator   2. On-Off Value   3. Gas Filter   4. Metering Valve   5. Back Pressure   6. 3-way Valve

7. Catalyst Bed   8. Sampling point   9. Furnace   10. Thermocouple   11. Variable Voltage Transformer

12. Temperature Controller   13. Heating Line   14. Bubble Flow Meter

Figure 4.3 Flow diagram of CO_2 hydrogenation system.

CHAPTER V

RESULTS AND DISCUSSIONS

This chapter was conducted in order to investigate the characteristic and catalytic properties of titania-silica composites supported Co and Ni catalysts for carbon dioxide hydrogenation. This chapter is divided into three sections. The first section contains the preparation and characterization of titania-silica composites microparticles. The second section shows characteristic and catalytic activity of titania-silica composites supported cobalt catalyst. The last section presents characteristic and catalytic activity of titania-silica composites supported nickel catalyst.

5.1 Support preparation and characterization

This section describes the preparation and characterization of silica and titania-silica composites microparticle by deposition of TiO_2 particles on the spherical silica particle (SSP) and MCM41 surface using hydrolysis of titanium isopropoxide to obtain TiSSP and TiMCM, respectively.

5.1.1 Preparation of spherical silica particle (SSP) and MCM-41

The morphology of spherical silica particle and MCM-41 characterized by scanning electron microscopy (SEM). Figure 5.1 (a). shows the SEM images of spherical silica particle with a size ranging from 0.1 to 0.8 μm. The SEM image of the silica sample prepared with the largest amount of ethanol reveals small, regular, spherical particles, with anaverage size about 0.6 μm. Figure 5.1 (b). shows the SEM images of MCM-41 synthesized without alcohol.
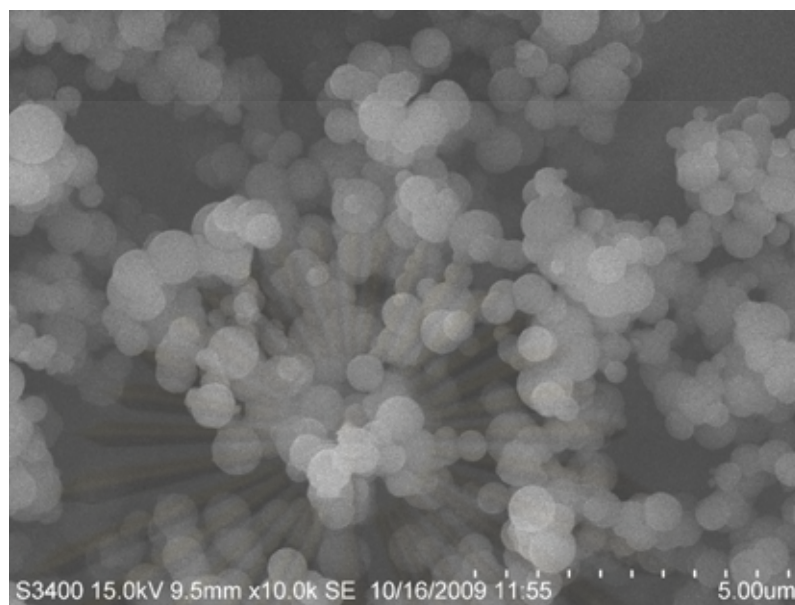
Figure 5.1 (a) The SEM images of the spherical silica particle.
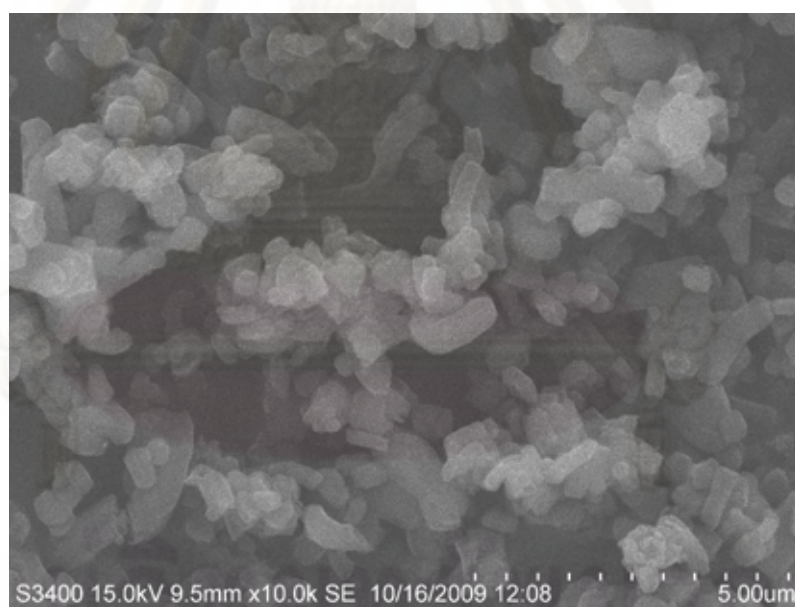
Figure 5.1 (b) The SEM images of the MCM-41.

The specific surface area , pore size and pore volume of spherical silica particle and MCM-41 were measured by nitrogen physisorption technique. The results are summarized in Table 5.1.

Table 5. 1 BET surface areas, pore volume and pore diameter of spherical silica particle and MCM41

Support samples	A_{BET} m^2/g	V_p cm^3/g	D_{BJH} nm
SSP	927	0.8135	2.04
MCM41	1187	1.0287	2.13

Nitrogen physisorption of the silica samples confirms the clear mesoporous structure are shown in Table 5.1. All samples have similar pore diameters (BJH calculation model). In contrast, the BET surface area and pore volumes of MCM-41 were higher than those of the spherical silica particle.

5.1.2 Preparation and characterization of titania-spherical silica particle composites supports (TiSSP)

This section presents the characterization of of silica and titania-silica composites microparticle by deposition of TiO_2 particles on the spherical silica particle (SSP). The structure and crystallinity of the titania-silica composites microparticle (TiSSP) were measured by X-ray diffraction. Scanning electron microscopy and energy dispersive X ray spectroscopy (EDX) were used to study the morphology of the titania-silica composites microparticle. The thermal properties of the titania-silica composites microparticle were characterized by differential thermal analysis and thermogravimetric (DTA/TG).

5.1.2.1 X-Ray Diffraction

Bulk crystal structure and chemical phase composition of a crystalline material having crystal domain of greater than 3-5 nm can be determined by X-ray diffraction. The measurements were carried out at the diffraction angles (2θ) between 20° and 80°.
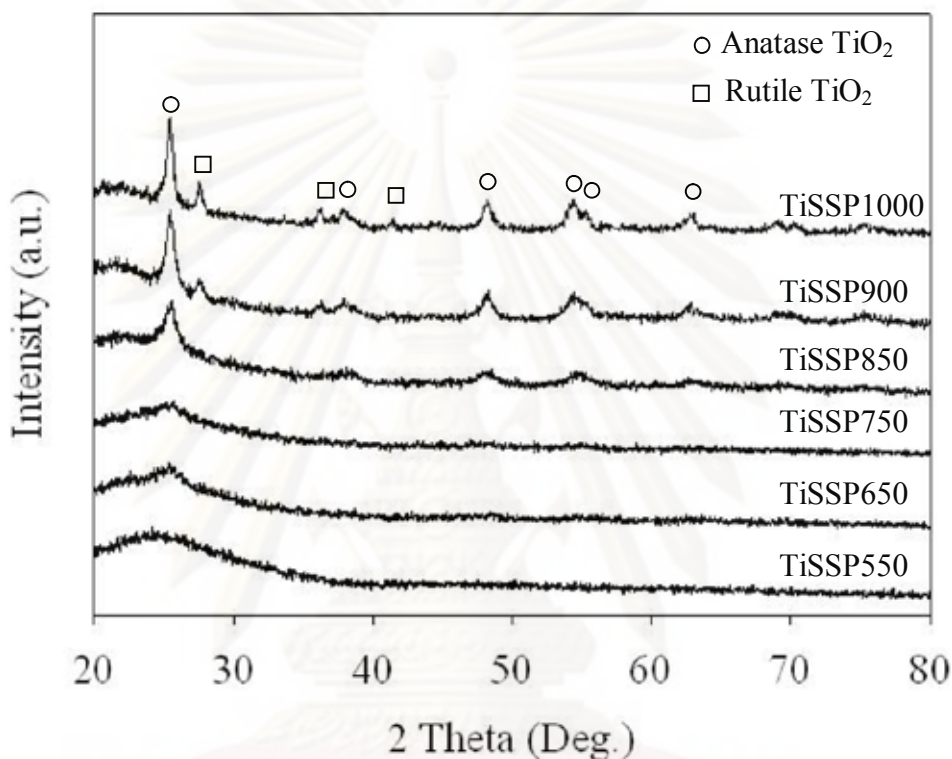
Figure 5.2 XRD patterns of the TiSSP microparicle composites calcined at various temperatures for 2 h.

Figure 5.2 shows XRD patterns of titania-spherical silica particle microparicle composites (TiSSP) calcined at various temperatures for 2 h. After calcined at 550°C for 2 h, the XRD patterns of TiSSP exhibited only amorphous silica and titania resulting in broad peak observation. At 650 and 750°C, the slight diffraction peak of TiO_2 crystalline can be observed at 25.3°. This demonstrates that TiO_2 had a small crystallite size of anatase form. Anatase TiO_2 crystalline form exhibited XRD peaks at 2θ of 25.3, 37.8, 48, 54, 55 and 75° displayed distinctly at 850°C. The XRD patterns for two TiO_2 crystalline forms displayed at temperature above 900°C. A portion of TiO_2 having the form of rutile exhibited XRD peaks at 2θ of 27.5, 36, 41, 54.5 and 56.5°.

5.1.2.2 Nitrogen physisorption

The BET surface area, pore volume and average pore diameter analysis of titania-spherical silica particle microparicle composites (TiSSP) calcined at various temperatures between 450 and 900°C, which are measured by nitrogen physisorption technique are given in Table 5.2.

Table 5.2 BET surface areas, pore volume and pore diameter of composite titania-spherical silica microparticle.

Support samples	A_{BET} m^2/g	V_p cm^3/g	D_{BJH} nm
Pure SSP	927	0.8135	2.04
TiSSP450	747	0.6383	2.55
TiSSP550	755	0.6476	2.40
TiSSP650	716	0.5671	2.59
TiSSP750	632	0.3425	2.71
TiSSP850	385	0.1587	3.23
TiSSP900	11	0.0235	12.59

From the result, it can be observed that the surface areas of all TiSSP microparicle were less than pure spherical silica particle. This was in accordance with the larger pore sizes of TiSSP microparticle than those of pure spherical silica particle. This is probably due to the increase of titania amount in the silica particle. The optimum BET surface area of TiSSP is 755 m^2/g with calcined at 550°C. At 650 ^{o}C, the BET surface area and pore volume apparently decreased. This was in accordance with grain growth from phase transformation of amorphous to anatase. At 750°C, the BET surface area and pore volume apparently decreased. This is probably due to the particle agglomeration. However, at 900°C, the BET surface area and pore volume of TiSSP was remarkably low at 11 m^2/g. This can be attributed to grain growth from phase transformation of anatase to rutile and the particles sintering. The smaller anatase crystallites grow into bigger rutile crystallites through the phase transformation, leading to the decrease of the voids among anatase crystallites.

5.1.2.3 Differential thermal analysis and thermogravimetric (DTA/TG)

The thermal properties was characterized by thermogravimetric and differential thermal analysis (TG-DTA). Figure 5.3 shows the DTA curve of TiSSP that displays several endothermic peaks below 450°C. This is due to the evaporation of physicsorbed water and isopropanol solvent. Two noticeable exothermal peaks at 612 and 948°C were related to the XRD patterns as mentioned before. The DTA curve indicated the exothermic peak that was due to the phase transformation of amorphous to anatase at 612°C. Furthermore, the exothermal peak is caused by the phase transition from anatase to rutile at 948°C. The TG curve shows a largest weight loss about 15.84% in TiSSP.
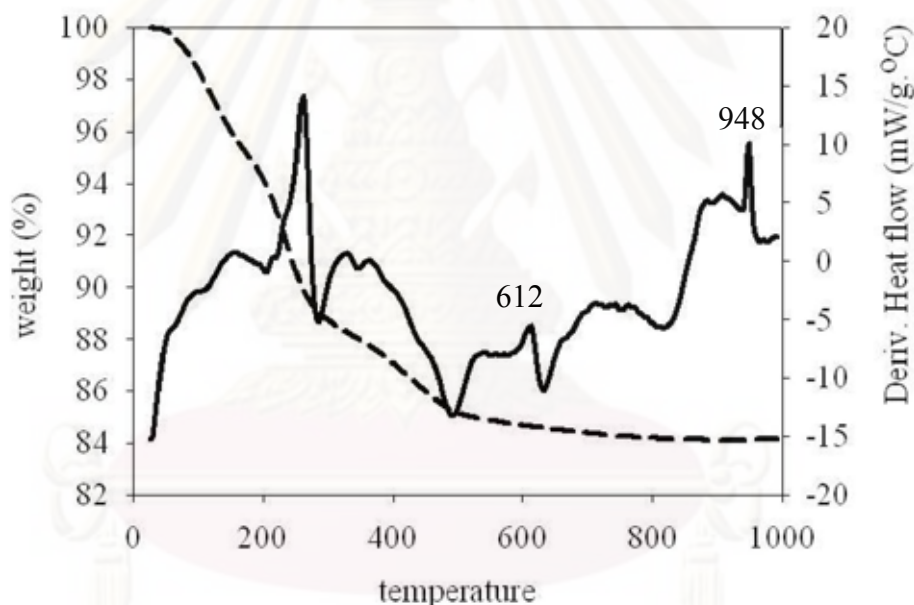
Figure 5.3 DTA/TG curve of the TiSSP microparicle composites.

5.1.2.4 Scanning electron microscopy (SEM) and energy dispersive X-ray spectroscopy (EDX)
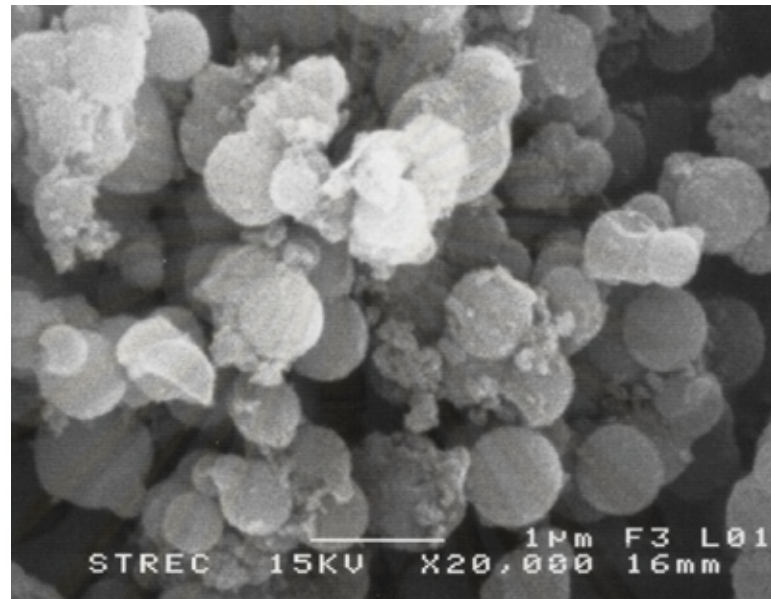
Figure 5.4 SEM micrograph for the TiSSP750 microparicle composites.

Scanning electron microscopy (SEM) is a powerful tool for direct observing surface texture and morphology of materials. In the backscattering scanning mode, the electron beam focused on the sample is scanned by a set of deflction coils. Backscattered electrons or secondary electrons emitted from the sample are detected. Figure 5.4 shows the SEM micrographs of the titania/silica microparticle composites. It reveals the titania colloid deposition on the surface of spherical silica core in TiSSP. As a result, the slight portion of TiSSP microparticle was coagulated. Figure 5.5 presents a typical spectrum and element quantity of the TiSSP surface from EDX analysis. Figure 5.6 shows that the EDX mapping of titania, silica and oxygen distribution on TiSSP suface. It indicates that the titania distribution on the spherical silica surface is uniform.
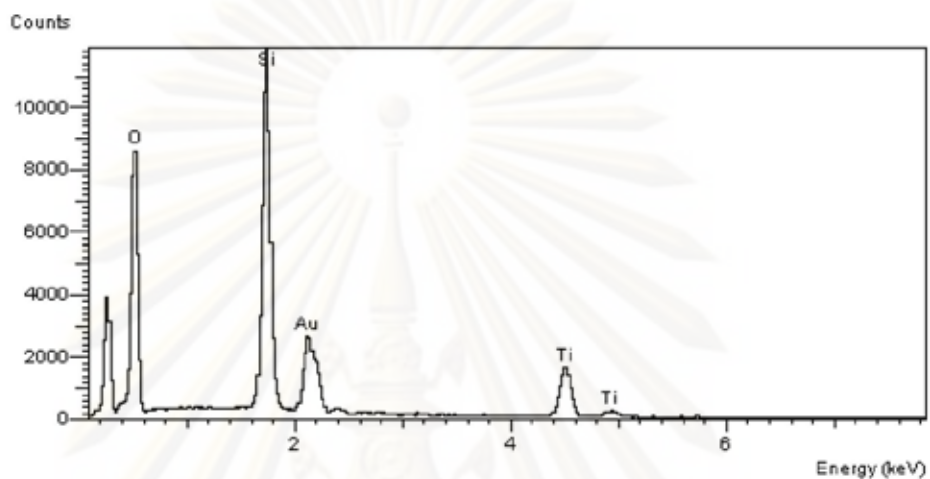
Element	Element(%)	Atomic(%)
O	66.03	79.05
Si	26.10	17.80
Ti	7.86	3.14

Figure 5.5 A typical spectrum of the TiSSP750 microparicle composites from EDX analysis.
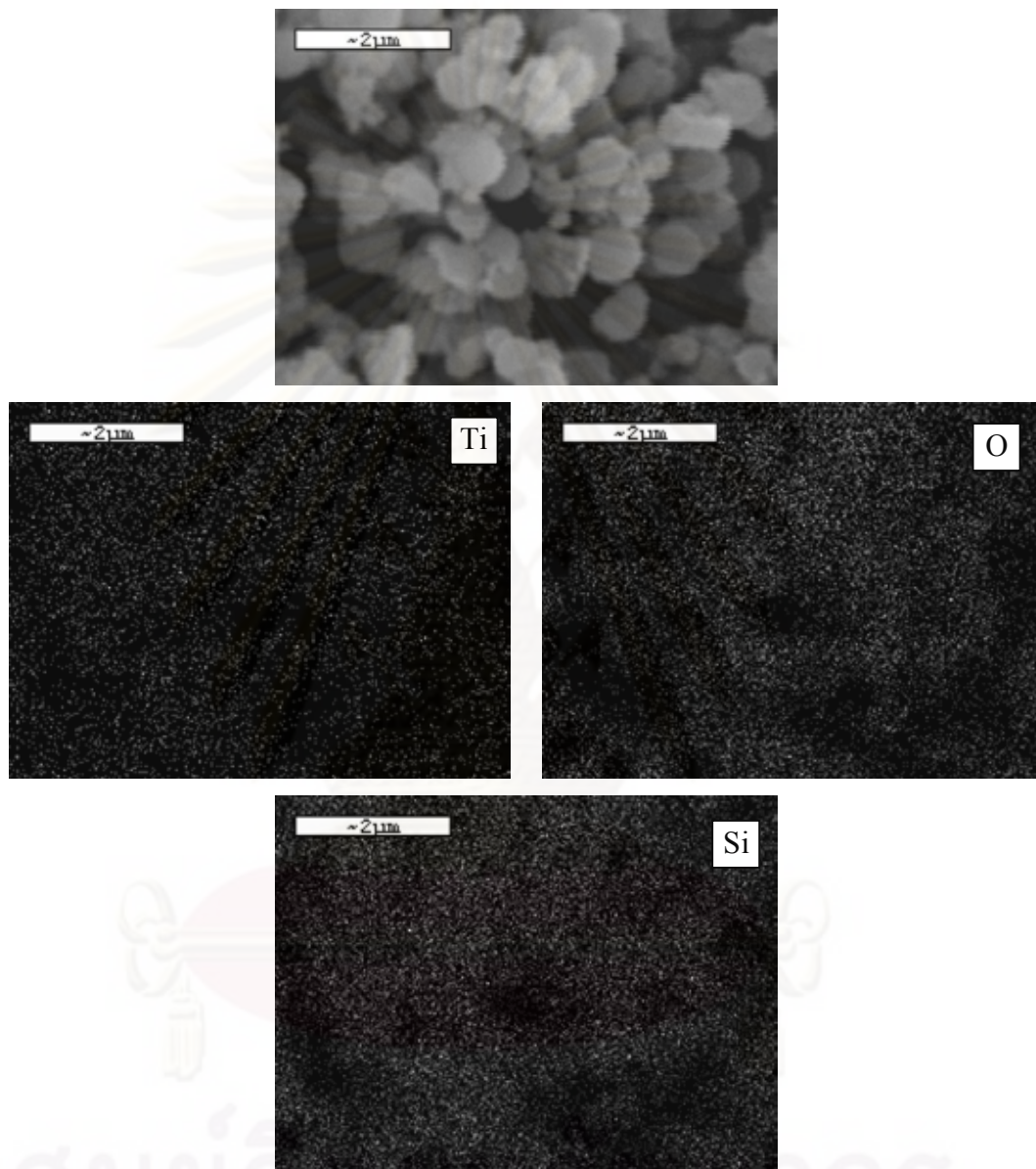
Figure 5.6 EDX mapping of the TiSSP750 microparicle composites.

5.1.3 Preparation and characterization of titania-MCM41 composites supports (TiMCM)

This section presents the characterization of of silica and titania-silica composites microparticle by deposition of TiO_2 particles on the MCM-41. The structure and crystallinity of the titania-silica composites microparticle (TiMCM) were measured by X-ray diffraction. Scanning electron microscopy and energy dispersive X ray spectroscopy (EDX) were used to study the morphology of the titania-silica composites microparticle. The thermal properties of the titania-silica composites microparticle were characterized by differential thermal analysis and thermo gravimetric (DTA/TG).

5.1.3.1 X-Ray Diffraction

Bulk crystal phases of sample were determined using X-Ray Diffraction. The measurements were carried out at the diffraction angles (2θ) between 20° and 80°.
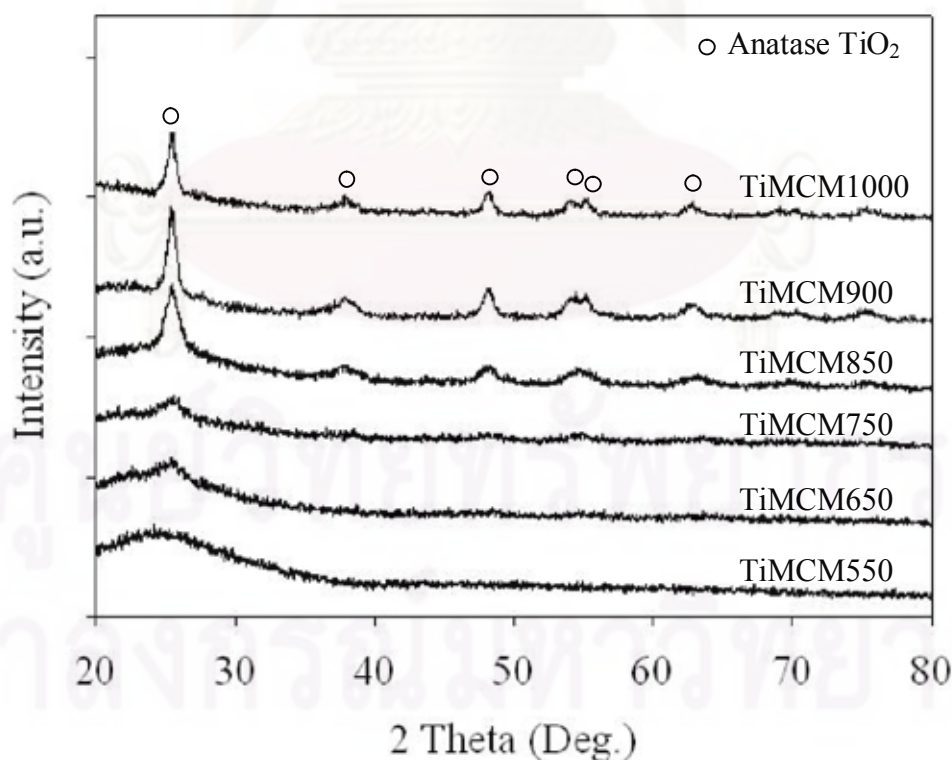
Figure 5.7 XRD patterns of the TiMCM microparicle composites calcined at various temperatures for 2 h.

XRD patterns of titania-MCM-41 microparicle composites (TiMCM) calcined at various temperatures between 550 and 1000°C are shown in Figure 5.7. After calcined at 550°C for 2 h, the XRD patterns of TiMCM exhibited only amorphous silica and titania resulting in broad peak observation. At 650 and 750°C, the slight diffraction peak of TiO_2 crystalline can be observed at 25.3°. This demonstrates that TiO_2 had a small crystalline size of anatase form. Anatase TiO_2 crystalline form exhibited XRD peak at 2θ of 25.3, 37.8, 48, 54, 55 and 75° displayed distinctly at the temperature above 850°C.

5.1.3.2 Nitrogen physisorption

The BET surface area, pore volume and average pore diameter analysis of titania-MCM-41 microparicle composites (TiMCM) calcined at various temperature between 450 and 900°C which were measured by nitrogen physisorption technique are shown in Table 5.3.

Table 5.3 BET surface areas, pore volume and pore diameter of composite titania-MCM41 microparticle.

Support samples	A_{BET} m^2/g	V_p cm^3/g	D_{BJH} nm
Pure MCM41	1187	1.0287	2.13
TiMCM450	801	0.6278	2.98
TiMCM550	837	0.6219	2.64
TiMCM650	607	0.3486	3.01
TiMCM750	351	0.2167	3.92
TiMCM850	137	0.1371	4.57
TiMCM900	97	0.0593	5.43

From the result, it can be observed that the surface areas of all TiMCM microparicle were less than pure MCM-41. This was in accordance with the larger pore sizes of TiMCM microparicle than those of pure MCM-41 and this is probably due to the increase of titania amount in the silica particle. The optimum BET surface area of TiMCM is 837 m^2/g with calcined at 550°C. At 650°C, the BET surface area

and pore volume apparently decreased. This was in accordance with grain growth from phase transformation of amorphous to anatase. At $750^{\circ}C$, the BET surface area and pore volume apparently decreased. This is probably due to the particle substantial coagulation. However, at $900^{\circ}C$, the BET surface area and pore volume of TiMCM was remarkably low at 97 m^2/g.

5.1.3.3 Differential thermal analysis and thermogravimetric (DTA/TG)

The thermal properties characterized by thermogravimetric and differential thermal analysis (TG-DTA) was shown in Figure 5.8. The DTA curve of TiMCM displays several endothermic peaks below $450^{\circ}C$. This result is similar to that of TiSSP. This is due to the evaporation of physicsorbed water and isopropanol solvent. The only exothermal peaks at $645^{\circ}C$ were related to the XRD patterns as mentioned before. The DTA curve indicated the exothermic peak that was due to the phase transformation of amorphous to anatase at $645^{\circ}C$. The TG curve shows a largest weight loss about 14.93% in TiMCM.
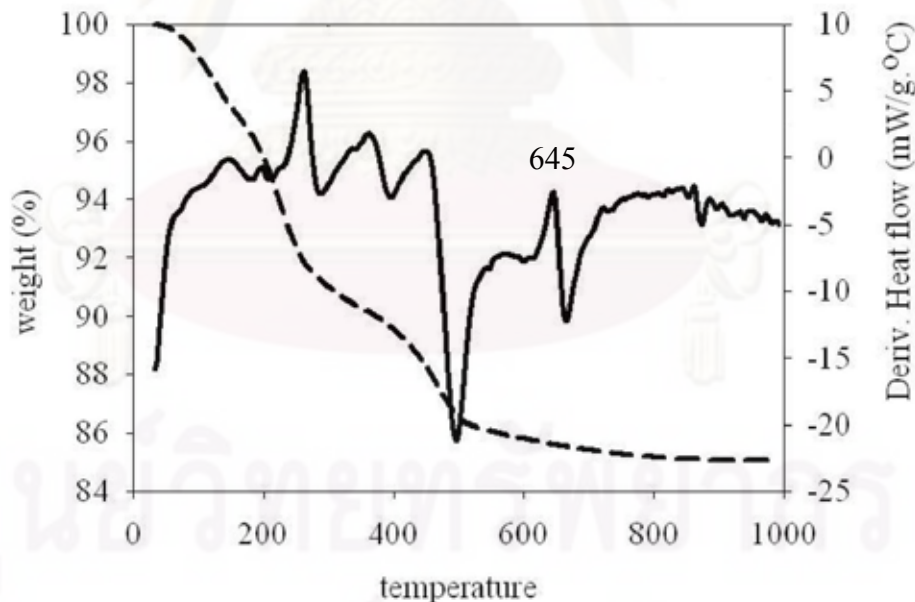
Figure 5.8 DTA/TG curve of of the TiMCM microparicle composites.

5.1.3.4 Scanning electron microscopy (SEM) and energy dispersive X-ray spectroscopy (EDX)
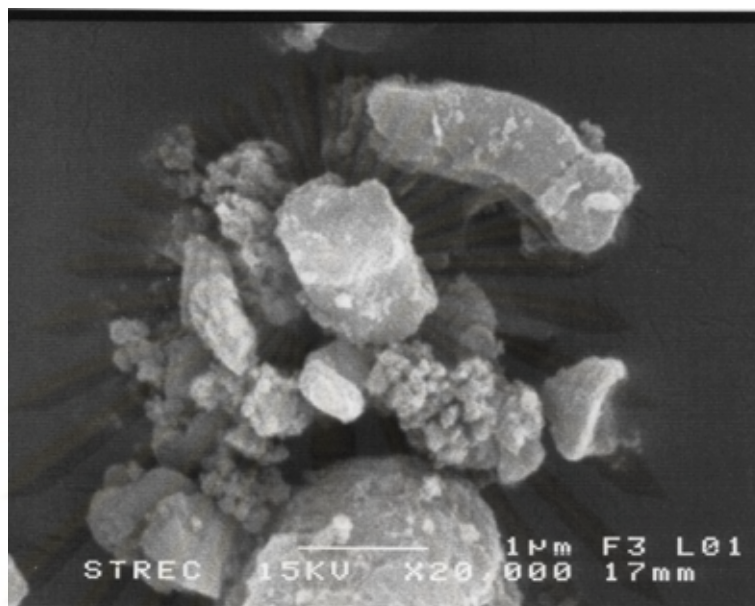
Figure 5.9 SEM micrograph for the TiMCM750 microparicle composites.

Scanning electron microscopy (SEM) and energy dispersive X-ray spectroscopy (EDX) were also conducted in order to study the morphologies and elemental distribution of the samples, respectively. The SEM micrographs of the titania/silica microparticle composites was shown in Figure 5.9. It reveals the titania colloid deposition on the surface of MCM-41 core in TiMCM that was also substantial coagulation. Figure 5.10 presents a typical spectrum and element quantity of the TiMCM surface from EDX analysis. Figure 5.11 shows that the EDX mapping of titania, silica and oxygen distribution on TiMCM suface. It indicates that the titania distribution on the MCM-41 surface is uniform.
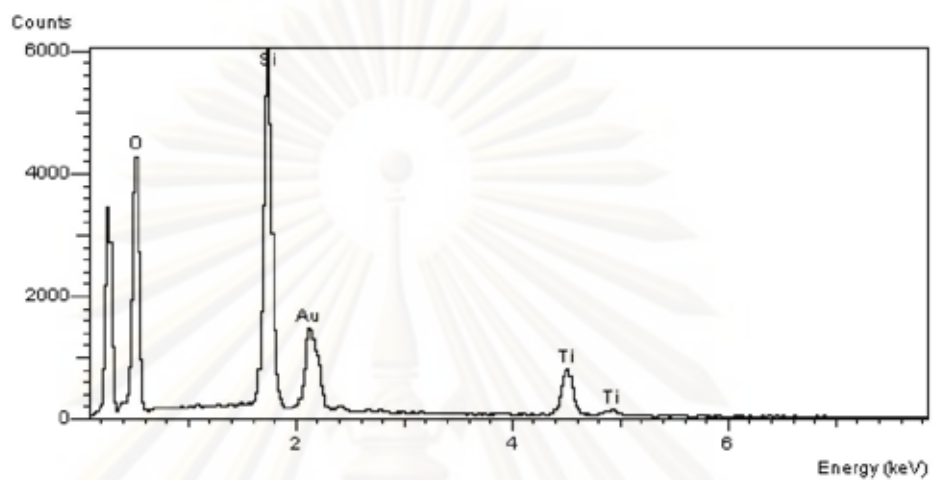
Element	Element(%)	Atomic(%)
O	67.34	80.11
Si	24.65	16.71
Ti	8.01	3.18

Figure 5.10 A typical spectrum of the TiMCM750 microparicle composites from EDX analysis.
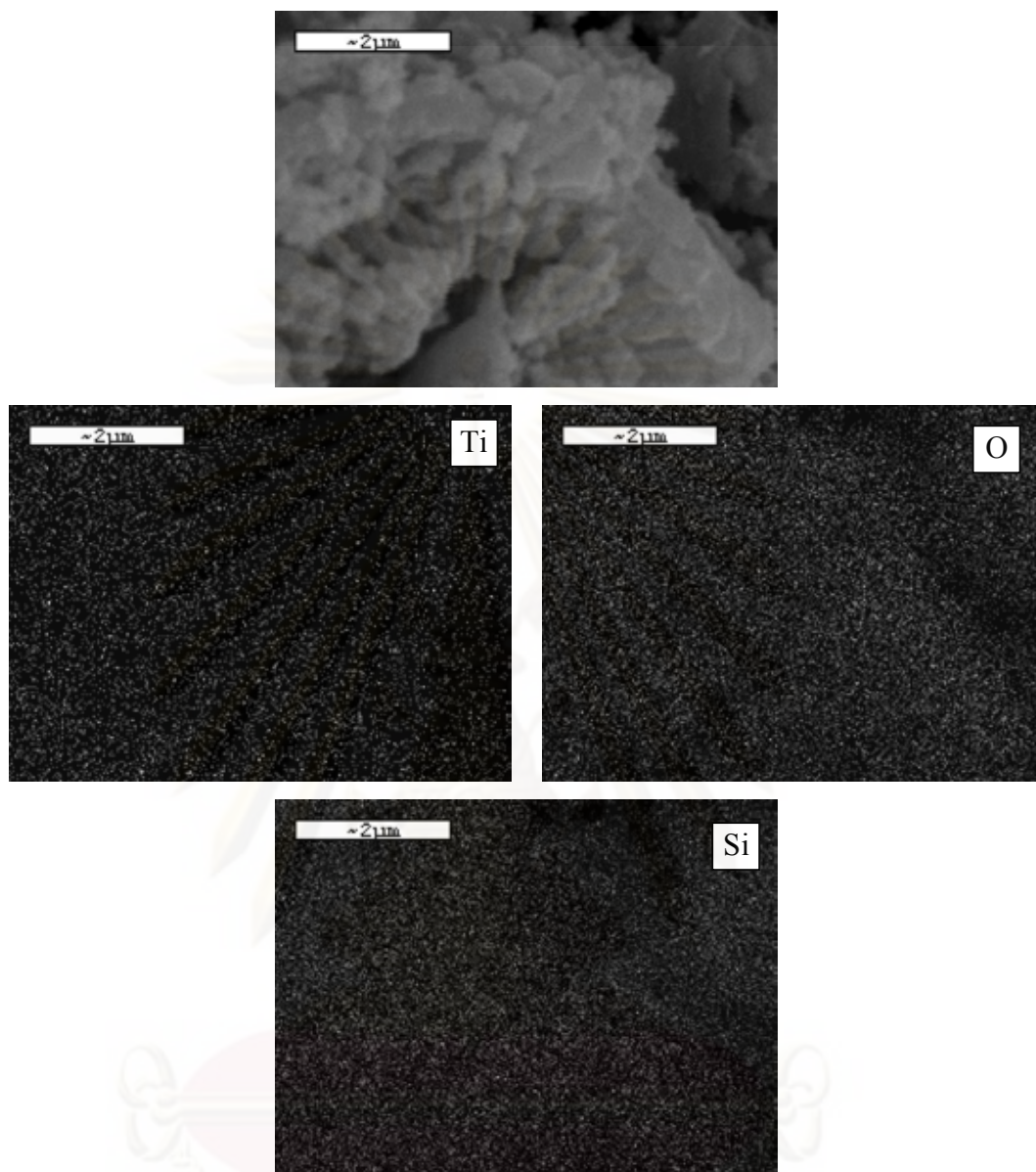
Figure 5.11 EDX mapping of TiMCM750 microparicle composites.

5.2 Characteristic of silica and titania-silica composites-microparticle supported cobalt catalyst.

This section presents the characteristic of silica and titania-silica composites microparticle supported cobalt catalyst by incipient wetness impregnation of cobalt (II) nitrate hexahydrate.

5.2.1 Preparation and characterization of spherical silica (SSP) and titania-spherical silica composites (TiSSP)-supported cobalt catalyst.

5.2.1.1 X-Ray Diffraction
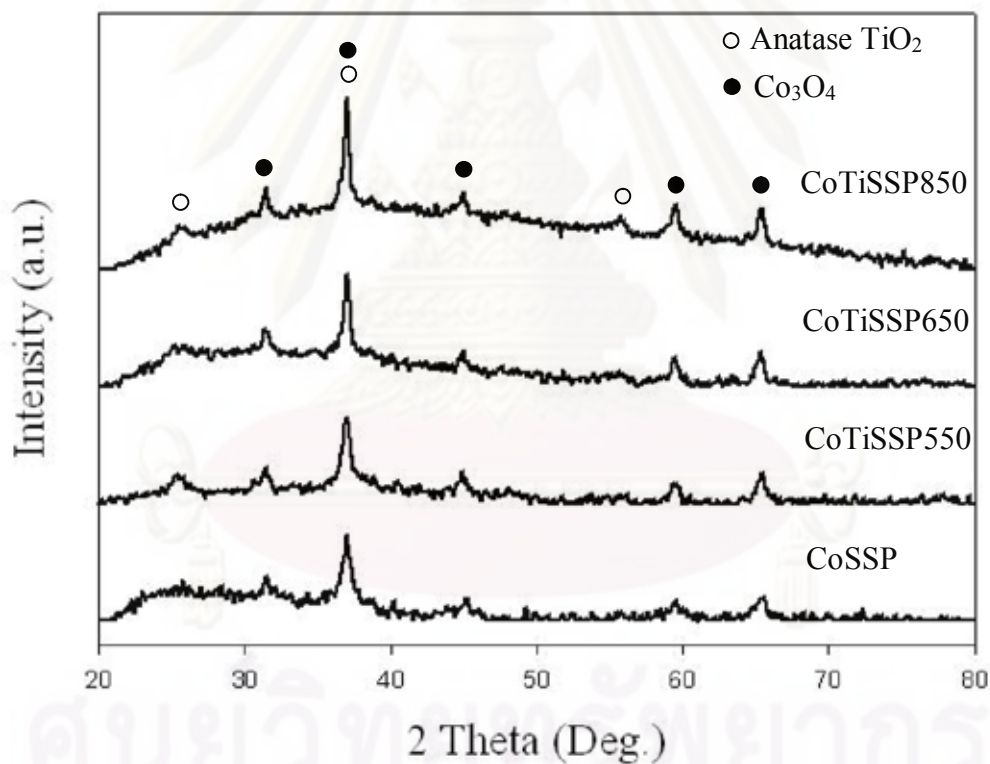
Figure 5.12 XRD patterns of the CoSSP, CoTiSSP550, CoTiSSP650 and CoTiSSP850 catalysts.

The phase identification is carried out on the basis of data from X-ray diffraction. A 20% wt of cobalt was impregnated onto SSP and TiSSP supports. After calcination in air at 500°C for 4 h, all catalysts were tested by XRD. XRD patterns for the calcined Co catalysts on all supports are shown in Figure 5.12. They exhibited almost identical XRD patterns. The XRD peaks of Co_3O_4 were observed at 31°, 37°, 45°, 59°, and 65° (S. Rojanapipatkul and B. Jongsomjit, 2008). Moreover, anatase TiO_2 crystalline form exhibited XRD peaks at 2θ of 25.3° displayed distinctly for all CoTiSSP catalysts.

5.2.1.2 Nitrogen physisorption

The BET surface areas, pore volume and average pore diameter analysis of cobalt was impregnated onto SSP and TiSSP , calcined at 550, 650 and 850°C, were measured by nitrogen physisorption technique as shown in Table 5.4.

Table 5.4 BET surface areas, pore volume and pore diameter of CoSSP, CoTiSSP550, CoTiSSP650 and CoTiSSP850 catalysts.

Support samples	A_{BET} m^2/g	V_p cm^3/g	D_{BJH} nm
SSP	927	0.8135	2.04
TiSSP550	755	0.6476	2.40
TiSSP650	716	0.5671	2.59
TiSSP850	385	0.1587	3.23
CoSSP	637	0.4898	2.26
CoTiSSP550	574	0.4496	2.70
CoTiSSP650	498	0.4109	2.73
CoTiSSP850	380	0.2117	2.82

From the result, it can be observed that the surface areas of CoSSP and all CoTiSSP were less than support particles. This was in accordance with the larger pore sizes of CoSSP, CoTiSSP550 and CoTiSSP650 catalysts than those of pure support particles. In contrast, the pore sizes and pore volume of CoTiSSP850 was smaller than pure support particles.

5.2.1.3 Scanning electron microscopy (SEM) and energy dispersive X-ray spectroscopy (EDX)
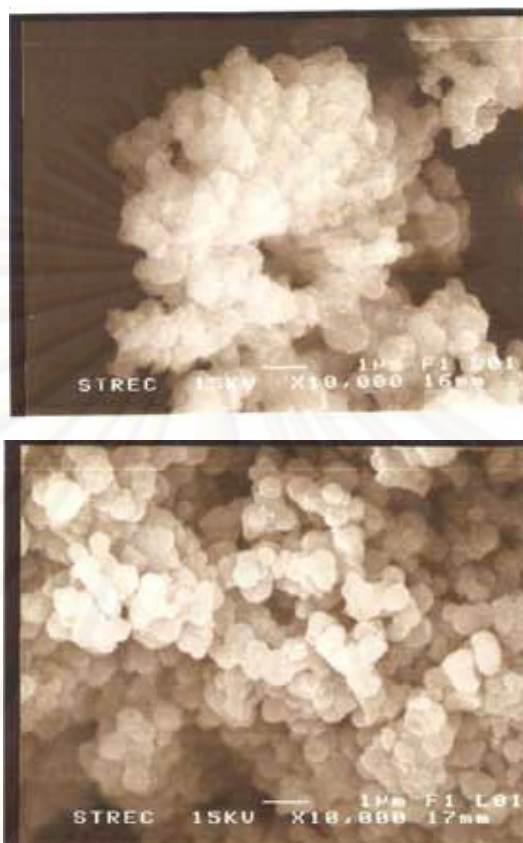
Figure 5.13 SEM micrograph for the CoTiSSP550 and CoTiSSP650 catalysts.

Scanning electron microscopy (SEM) and energy dispersive X-ray spectroscopy (EDX) were also conducted in order to study the morphologies and elemental distribution of the samples, respectively. The SEM micrographs of the CoTiSSP550 and CoTiSSP650 were shown in Figure 5.13. It displays the catalyst particles that was also substantial coagulation in CoTiSSP550. In contrast, the small amount of CoTiSSP650 was coagulated. Figures 5.14 and 5.15 present a typical spectrum and element quantity of the CoSSP and CoTiSSP850 surface from EDX analysis, respectively. The results show that CoSSP exhibited has higher the amount of Co than CoTiSSP850 with regards to at the external surface. Figures 5.16 and 5.17 show the EDX mapping of cobalt distribution on CoSSP and CoTiSSP850 suface. It can be seen that the cobalt oxide species show good distribution on the surface of CoSSP and CoTiSSP850 catalysts.
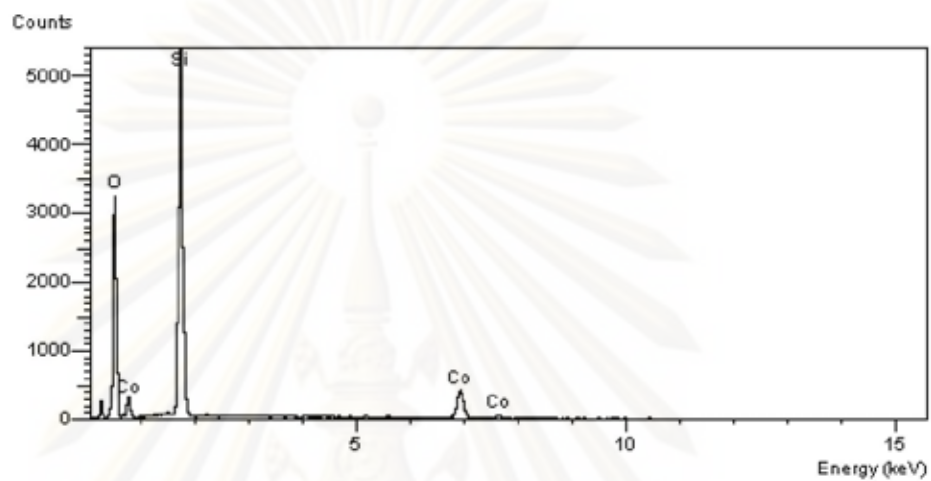
Element	Element(%)	Atomic(%)
Co	8.85	2.96
Si	27.58	19.29
O	63.57	77.75

Figure 5.14 A typical spectrum of the CoSSP catalyst from EDX analysis.
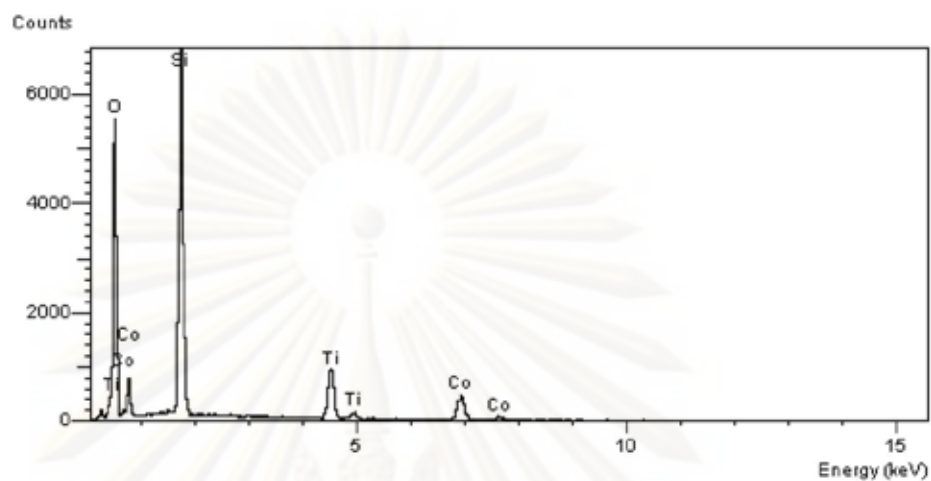
Element	Element(%)	Atomic(%)
Co	7.63	2.55
Ti	6.01	2.72
Si	20.88	14.67
O	64.90	80.05

Figure 5.15 A typical spectrum of the CoTiSSP850 catalyst from EDX analysis.
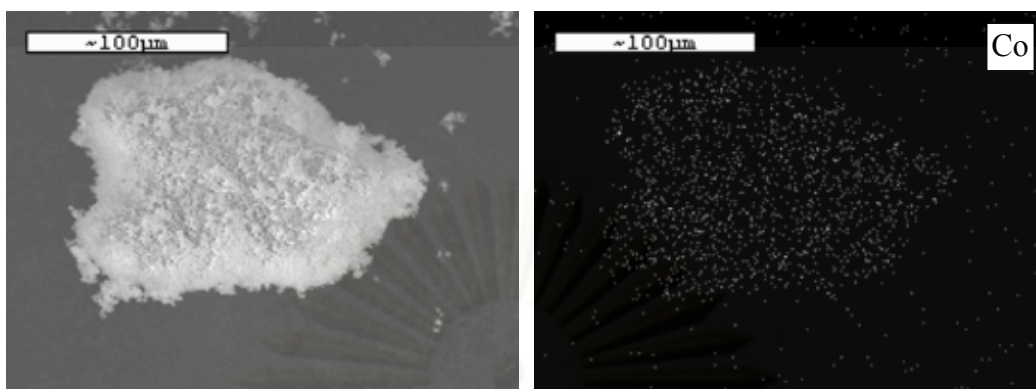
Figure 5.16 EDX mapping of CoSSP catalyst.
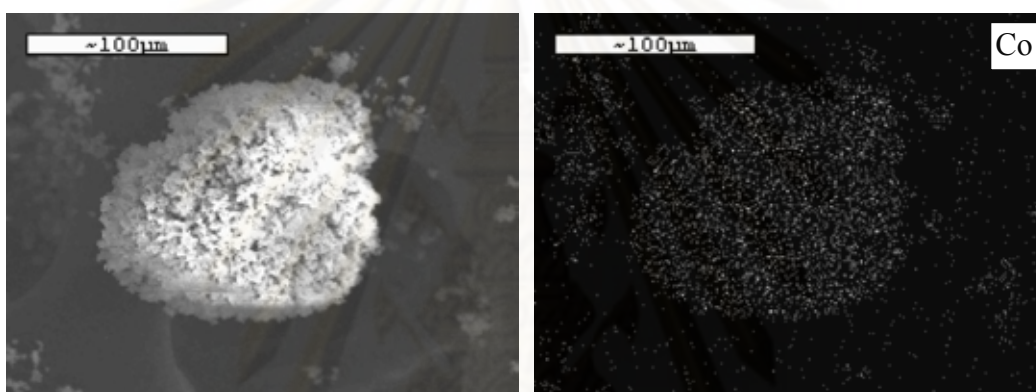
Figure 5.17 EDX mapping of CoTiSSP850 catalyst.

5.2.1.4 Temperature Programmed Reduction (TPR)

TPR was performed in order to determine the reduction behaviors. The TPR profiles of Co supported on SSP and TiSSP supports are shown in Figure 5.18. From these profiles the maximum temperature for each catalyst are given in Table 5.5. Reduction was observed for all catalysts, which can be assigned to the overlap of two step reduction of Co_3O_4 to CoO and then to Co^0. Besides reduction behaviors obtained from TPR results, reducibilities of the catalysts can be measured based on the peak area below TPR curve. From the result, all TiSSP-supported Co catalysts resulted in slightly shift of the maximum reduction temperature to higher temperature with increasing calcination temperature of TiSSP. It indicated that the titania on silica support increased during reduction due to stronger interaction between cobalt and

support. In contrast, the reducibilities and H_2 consumption of all CoTiSSP catalysts were higher than CoSSP.
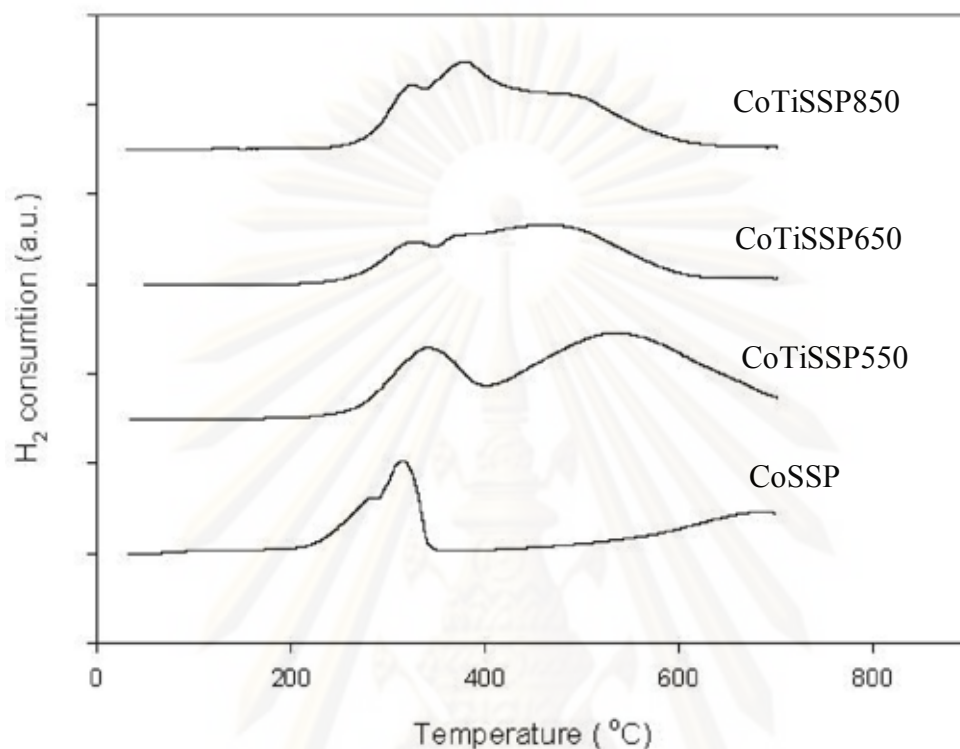
Figure 5.18 TPR patterns of CoSSP, CoTiSSP550, CoTiSSP650 and CoTiSSP850 catalysts.

Table 5.5 Maximum temperatures and H_2 consumption from TPR profiles of SSP and TiSSP supported Co catalysts.

	Temperature (^{o}C)		Total	Reducibility
Catalysts	Maximum 1	Maximum 2	H_2 consumption μmol H_2/g.cat	(%)
CoSSP	274.52	319.44	1,371	30.3
CoTiSSP550	341.86	544.62	2,801	61.9
CoTiSSP650	322.98	366.97	1,709	37.8
CoTiSSP850	319.17	369.62	2,056	45.4

5.2.1.5 CO-chemisorption

Active site of catalysts can be determined by calculation from amount of carbon monoxide adsorption on catalysts. The calculation the active site of catalysts is shown in Appendix B. Absorbed amount of carbon monoxide is directly proportional to the active site, the higher absorbed amount of carbon monoxide means the higher active site. The characterization results of CO chemisorption for the catalyst samples are illustrated in Table 5.6.

Table 5.6 Amount of carbon monoxide adsorbed on catalysts.

Catalysts	Active site, Moleculex10^{-18} per gram	Total CO chemisorption μmol CO/g.cat	% dispersion of Cobalt	CO chemisorption/ BET surface area μmol CO/g.cat/m^2
CoSSP	17.12	28.44	0.84	0.045
CoTiSSP550	2.25	3.74	0.11	0.007
CoTiSSP650	4.84	8.04	0.24	0.016
CoTiSSP850	12.54	20.83	0.61	0.055

From the result, amount of active site and Co dipersion of CoSSP was higher than those of all the CoTiSSP catalysts. Consequently, in order to eliminate the effect of BET from the effect of crystalline size, the results were also reported in term of CO chemisorption per unit surface area. It was found that CO chemisorption/ BET of CoTiSSP550 and CoTiSSP650 was lower than CoSSP. In contrast with those, CO chemisorption/ BET of CoTiSSP850 was higher than CoSSP.

5.2.1.6 Catalytic activity for CO_2-hydrogenation over SSP and TiSSP supported cobalt catalyst.

In order to determine the catalytic behaviors of the Co supported on SSP and TiSSP supports, CO_2 hydrogenation (H_2/CO_2 = 10.36/1) under methanation condition was performed to determine the overall activity and product selectivity of the samples. Before reaction, the catalysts was reduced in-situ in H_2 flow 50 ml/min at 350°C for 3 h in order to obtain metallic phase cobalt. Hydrogenation of CO_2 was carried out at 220 and 270°C. A flow rate of $H_2/CO_2/Ar$ = 19.3344/1.8656/8.8 cm^3/min in a fixed-bed flow reactor was used. The resulted reaction test is shown in Table 5.7 and 5.8, respectively.

Table 5.7 Activity and product selectivity of CoSSP, CoTiSSP550, CoTiSSP650 and CoTiSSP850 catalysts.

Catalysts	Conversion[a]		Rate[c] (x10^2 g CH$_2$/g cat.h)	TOF[d] (x10^3 s^{-1})	Product selectivity[c] (%)	
	Initial[b]	Steady state[c]			CH$_4$	CO
CoSSP	38.16	26.62	16.49	4.23	89.46	10.54
CoTiSSP550	10.59	5.62	2.00	6.58	53.25	46.75
CoTiSSP650	13.84	14.78	8.86	7.82	91.34	8.65
CoTiSSP850	16.94	15.78	9.96	2.89	92.13	7.85

[a] CO_2 hydrogenation was carried out at 220°C, 1 atm, and $H_2/CO_2/Ar$ = 19.3344/1.8656/8.8, F/W= 18 L/g cat.h.

[b] After 5 min of reaction.

[c] After 4 h of reaction.

[d] The TOF calculation was based on CO chemisorption.

Table 5.7 shows the result from hydrogenation of CO_2 that was performed at 220 °C. It indicated that the steady state CO_2 conversions were ranged between 5.62 to 26.62% with corresponding to the reaction rate at 2.00 to 16.49 (x10^2 g CH$_2$/g cat.h) of cobalt supported on SSP and TiSSP catalysts. This also showed that the activities of cobalt catalysts decreased with the presence of titania in the supports. The results were in good agreement with those reported by Jongsomjit et al. (2006).

However, the selectivities to methane of CoTiSSP650 and CoTiSSP850 was higher than CoSSP. The rate vs. time on stream of cobalt supported on SSP and TiSSP catalysts with reaction temperature at 220°C is illustrated in Figure 5.19. The rate of catalysts decreased with the presence of titania. The activities for cobalt catalysts can be attributed to the cobalt dispersion on the catalysts as seen from CO chemisorption results.
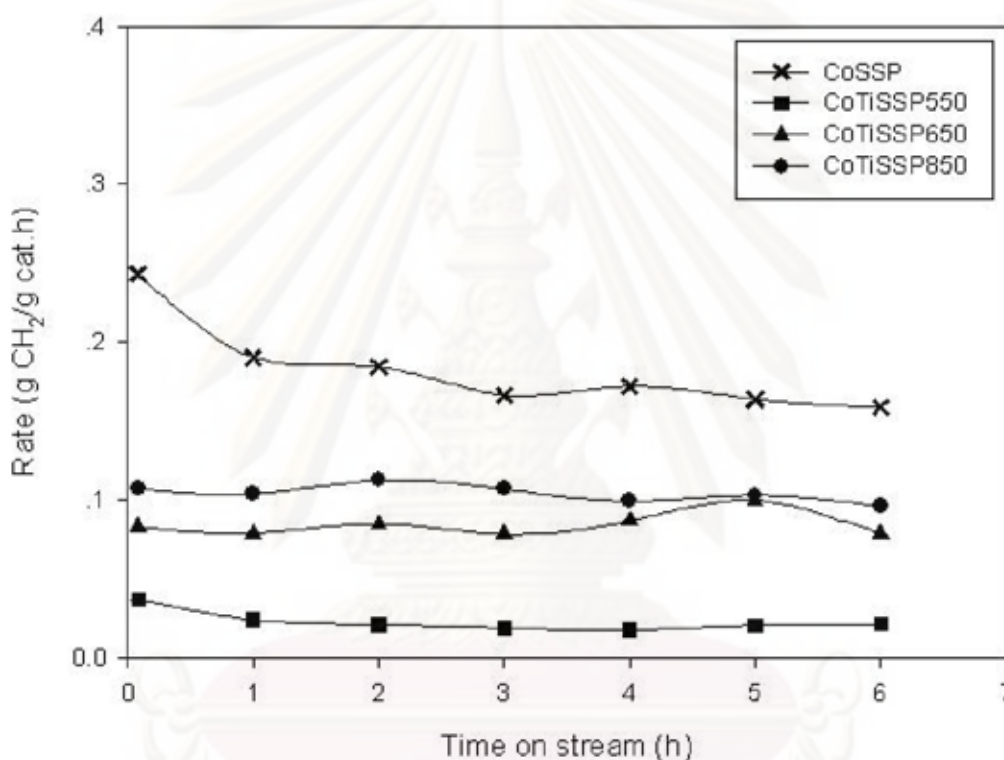
Figure 5.19 Reaction rate at 220°C vs. time on stream of CoSSP, CoTiSSP550, CoTiSSP650 and CoTiSSP850

Table 5.8 Activity and product selectivity of CoSSP, CoTiSSP550, CoTiSSP650 and CoTiSSP850 catalysts.

Catalysts	Conversion [a]		Rate [c] (x10^{-2} g CH$_2$/g cat.h)	TOF [d] (x10^3 s^{-1})	Product selectivity [c] (%)	
	Initial [b]	Steady state [c]			CH$_4$	CO
CoSSP	63.35	49.90	31.11	7.63	90.08	9.92
CoTiSSP550	21.85	23.22	12.44	26.41	80.01	19.99
CoTiSSP650	36.83	36.33	20.64	18.68	86.57	13.43
CoTiSSP850	47.21	41.76	25.61	7.55	89.54	10.46

[a] CO$_2$ hydrogenation was carried out at 270°C, 1 atm, and H$_2$/CO$_2$/Ar = 19.3344/1.8656/8.8, F/W= 18 L/g cat.h

[b] After 5 min of reaction.

[c] After 4 h of reaction.

[d] The TOF calculation was based on CO chemisorption.

Table 5.8 shows the result from hydrogenation of CO$_2$ that was carried out at 270 °C. It indicated that the steady state CO$_2$ conversions were ranged between 23.22 to 49.90% with corresponding to the reaction rate at 12.44 to 31.11 (x10^2 g CH$_2$/g cat.h) of cobalt supported on SSP and TiSSP catalysts. The result was similar with the hydrogenation of CO$_2$ that was performed at 220°C. This also showed that the activities of cobalt catalysts decreased with the presence of titania in the supports. However, the CO$_2$ conversions increased with increasing reaction temperature. For Fischer-Tropsch CO$_2$ hydrogenation, the operating temperature must be rather high because of the equilibrium constraints for the reverse CO shift reaction. This limits the application of temperature in the lower range for Fischer-Tropsch conversion (Riedel et al., 1999). Nevertheless, the selectivities to methane of CoTiSSP was lower than CoSSP at this operating temperature. The rate vs. time on stream of cobalt supported on SSP and TiSSP catalysts with reaction temperature at 270°C is illustrated in Figure 5.20.
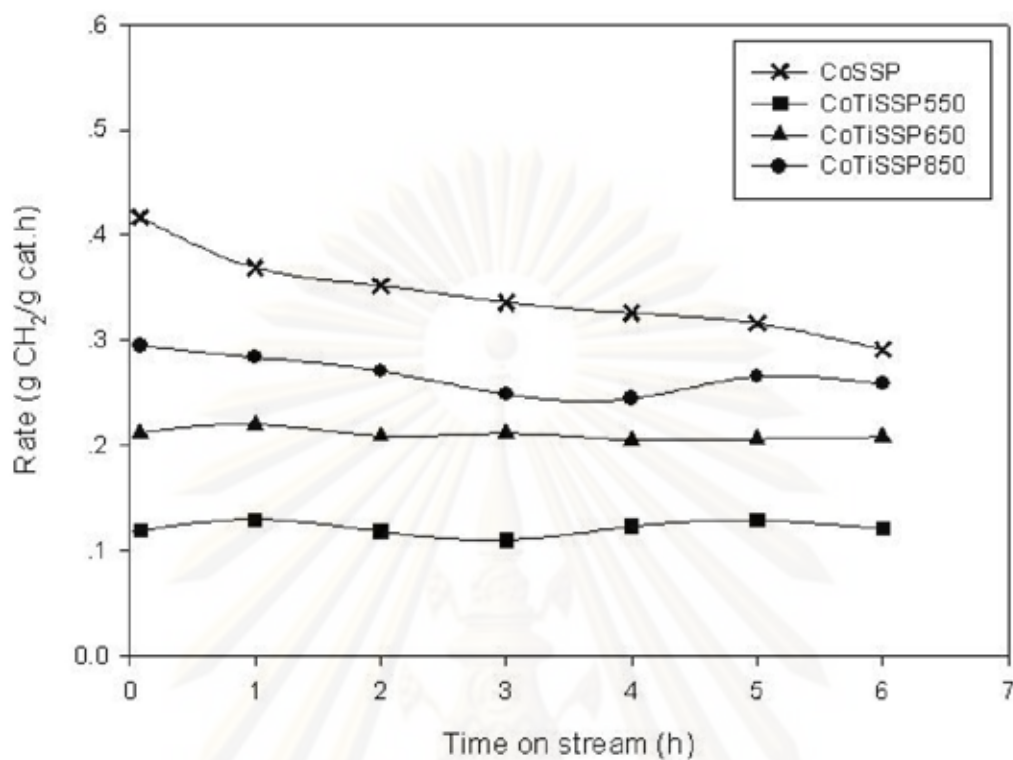
Figure 5.20 Reaction rate at 270°C vs. time on stream of CoSSP, CoTiSSP550, CoTiSSP650 and CoTiSSP850.

5.2.2 Preparation and characterization of MCM-41 and titania-MCM-41 composites (TiMCM)-supported cobalt catalyst.

5.2.2.1 X-Ray Diffraction
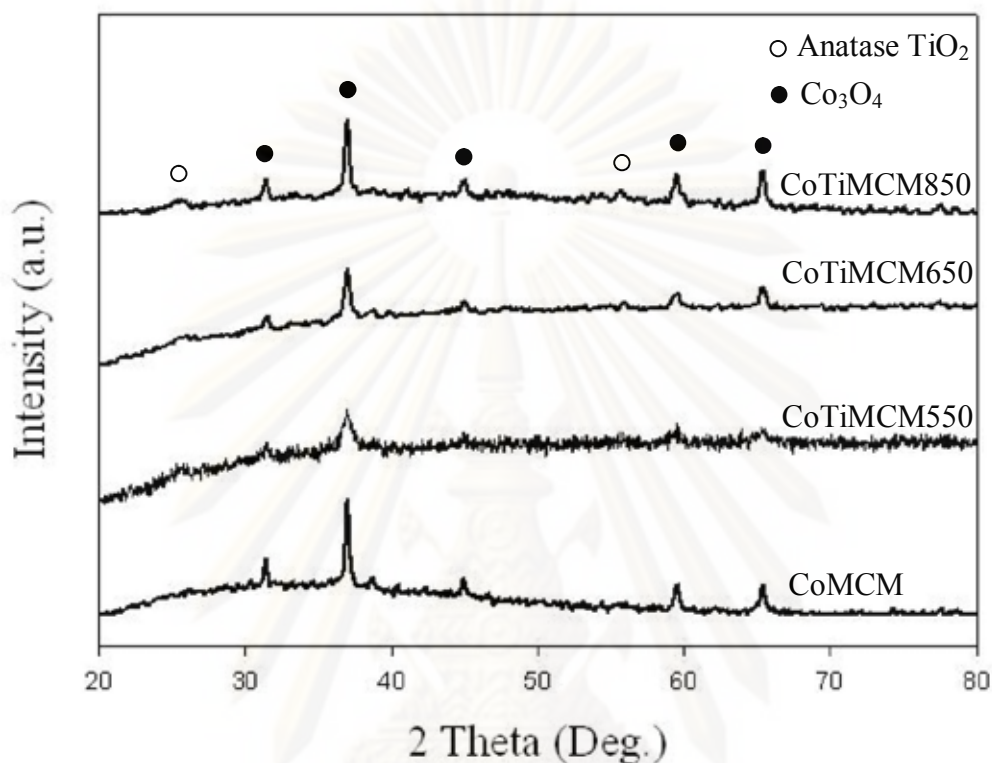
Figure 5.21 XRD patterns of CoMCM, CoMCM550, CoMCM650 and CoTiMCM850 catalysts.

From the results, it can be observed the similar XRD patterns of the cobalt impregnated onto MCM-41 and TiMCM supports. After calcination in air at 500°C for 4 h, all catalysts were tested by XRD. XRD patterns for the calcined Co catalysts on all supports are shown in Figure 5.21. They exhibited almost identical XRD patterns. The XRD peaks of Co_3O_4 were observed at 31°, 37°, 45°, 59°, and 65° (S. Rojanapipatkul and B. Jongsomjit, 2008). Moreover, XRD peaks of all CoTiMCM catalysts exhibited the slight diffraction peak of anatase TiO_2 crystalline at 2θ of 25.3°.

5.2.2.2 Nitrogen physisorption

The BET surface area, pore volume and average pore diameter analysis of cobalt impregnated onto MCM-41 and TiMCM , which calcined at 550, 650 and 850 ^{o}C, were measured by nitrogen physisorption technique are shown in Table 5.9.

Table 5.9 BET surface areas, pore volume and pore diameter of CoMCM, CoMCM550, CoMCM650 and CoTiMCM850 catalysts.

Support samples	A_{BET} m^2/g	V_p cm^3/g	D_{BJH} nm
MCM	1187	1.0287	2.13
TiMCM550	837	0.6219	2.64
TiMCM650	607	0.3486	3.01
TiMCM850	137	0.1371	4.57
CoTiMCM	583	0.2134	2.58
CoTiMCM550	318	0.2955	3.73
CoTiMCM650	447	0.2173	3.07
CoTiMCM850	126	0.1004	4.24

From the result, it can be observed that the surface areas of CoMCM and all CoTiMCM were similar to those of CoTiSSP. The surface areas were less than those of the support particles. This was in accordance with the larger pore sizes of CoMCM, CoTiMCM550 and CoMCM650 catalysts than those of pure support particles, whereas the pore sizes of CoTiMCM850 was smaller than pure support particles.

5.2.2.3 Scanning electron microscopy (SEM) and energy dispersive X-ray spectroscopy (EDX)
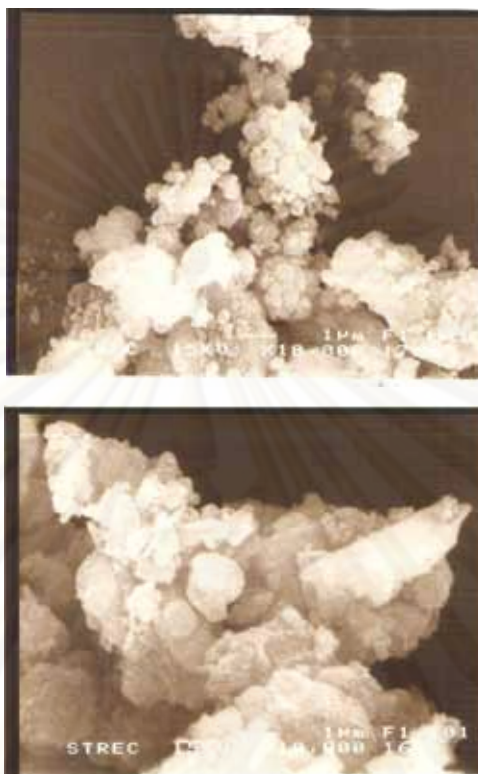
Figure 5.22 SEM micrograph for the CoTiMCM550 and CoTiMCM650 catalysts.

Scanning electron microscopy (SEM) and energy dispersive X-ray spectroscopy (EDX) were also conducted in order to study the morphologies and elemental distribution of the samples, respectively. The SEM micrographs of the CoTiMCM550 and CoTiMCM650 are shown in Figure 5.22. It displays the catalyst particles that are also substantial coagulation in CoTiMCM550 and CoTiMCM650. Figures 5.23 and 5.24 present a typical spectrum and element quantity of the CoMCM and CoTiMCM850 surface from EDX analysis, respectively. The results show that the amount of Co at the external surface of CoMCM was lower than CoTiMCM850. Figures 5.25 and 5.26 show that the EDX mapping of cobalt distribution on CoMCM and CoTiMCM850 suface. It can be seen that the cobalt oxide species show good distribution on the surface of CoMCM and CoTiMCM850 catalysts.
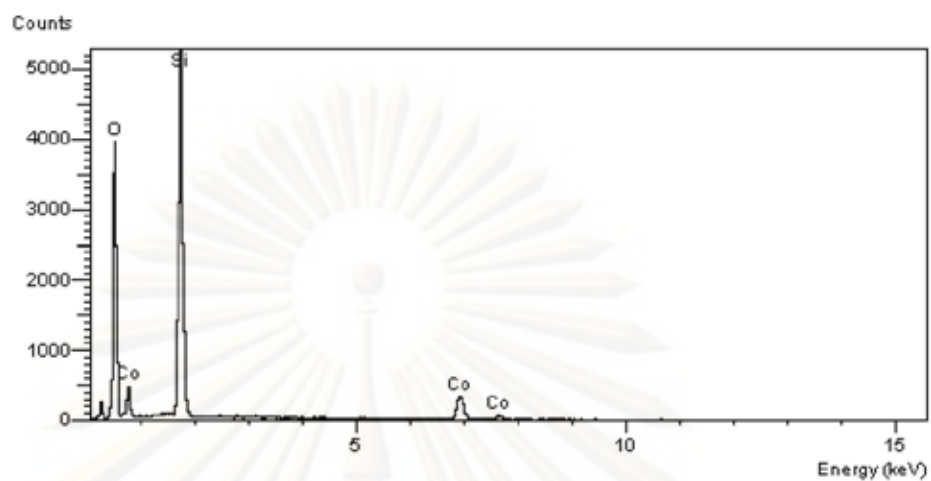
Element	Element(%)	Atomic(%)
Co	11.77	4.02
Si	27.01	19.26
O	61.22	76.72

Figure 5.23 A typical spectrum of the CoMCM catalyst from EDX analysis.
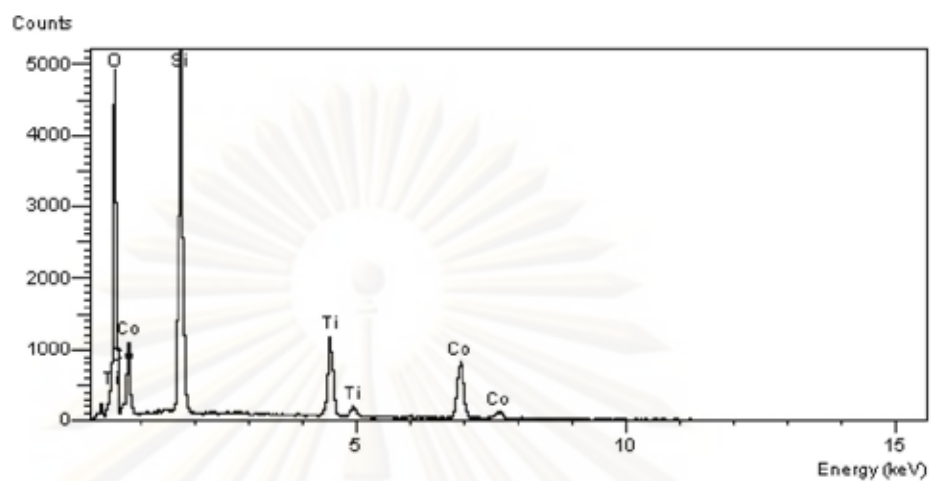
Element	Element(%)	Atomic(%)
Co	12.31	4.36
Ti	9.22	4.03
Si	18.42	13.65
O	60.05	77.96

Figure 5.24 A typical spectrum of the CoTiMCM850 catalyst from EDX analysis.
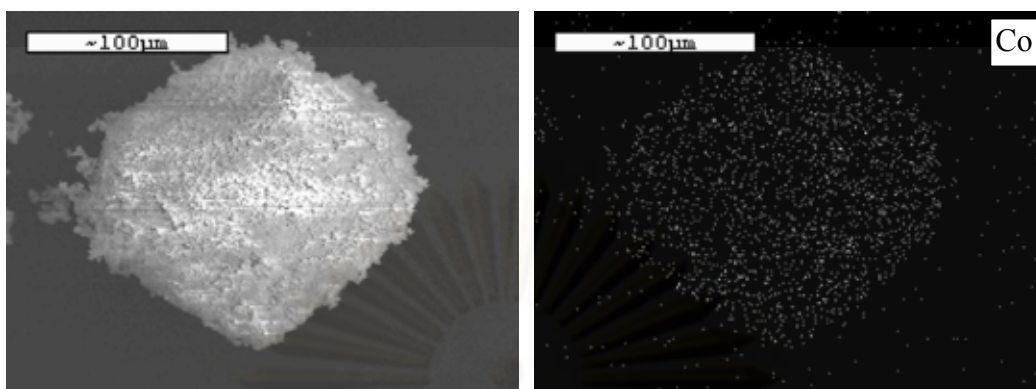
Figure 5.25 EDX mapping of CoMCM catalysts.
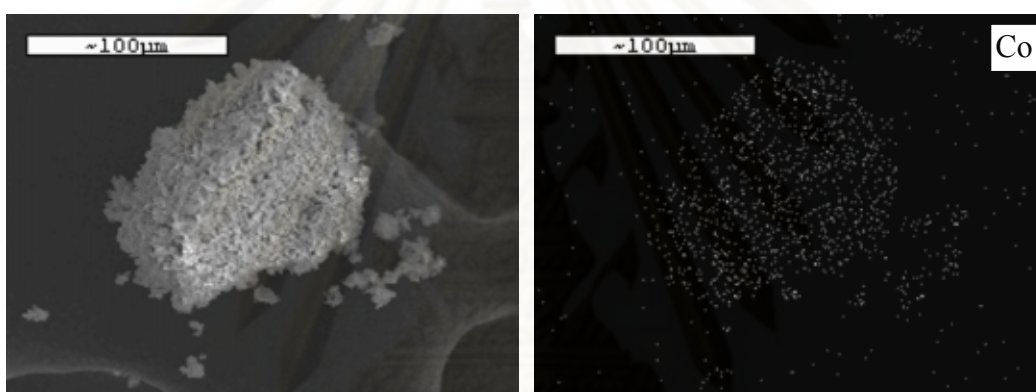
Figure 5.26 EDX mapping of CoTiMCM850 catalysts.

5.2.2.4 Temperature Programmed Reduction (TPR)

The TPR profiles of Co supported on MCM-41 and TiMCM supports are shown in Figure 5.27. From these profiles the maximum temperature for each catalyst are given in Table 5.10. From the result, all TiMCM supported Co catalysts were similar with those CoTiSSP catalysts. It was slightly shifted of the maximum reduction temperature to higher temperature with increasing calcination temperature of TiMCM. Furthermore, the reducibilities and H_2 consumption of all CoTiMCM catalysts were higher than CoMCM.

.
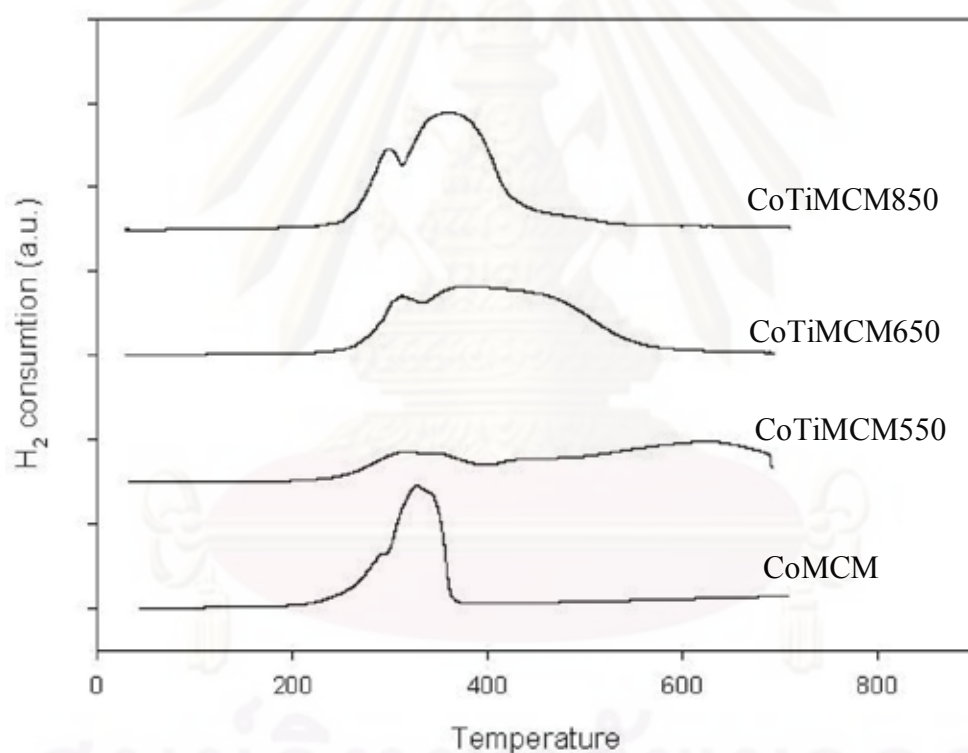
Figure 5.27 TPR patterns of CoMCM, CoMCM550, CoMCM650 and CoTiMCM850 catalysts.

Table 5.10 Maximum temperatures and H_2 consumption from TPR profiles of CoMCM, CoMCM550, CoMCM650 and CoTiMCM850 catalysts.

Catalysts	Temperature (^{o}C)		Total H_2 consumption μmol H_2/g.cat	Reducibility (%)
	Maximum 1	Maximum 2		
CoMCM	287.33	325.43	960.96	21.2
CoTiMCM550	317.61	353.42	1,022.06	22.6
CoTiMCM650	308.78	376.21	1,979.85	43.8
CoTiMCM850	298.28	364.64	2,059.94	45.5

5.2.2.5 CO-chemisorption

Amount of carbon monoxide adsorption on catalysts was performed in order to measure the number of reduced cobalt metal surface atoms. Adsorbed amount of carbon monoxide is directly proportional to the active site. The results of CO chemisorption for the catalyst samples are illustrated in Table 5.11.

Table 5.11 Amount of carbon monoxide adsorbed on catalysts.

Catalysts	Active site, Moleculex10^{-18} per gram	Total CO chemisorption μmol CO/g.cat	% dispersion of Cobalt	CO chemisorption/ BET surface area μmol CO/g.cat/m^2
CoMCM	22.55	37.47	1.10	0.064
CoTiMCM550	6.47	10.75	0.32	0.034
CoTiMCM650	11.73	19.50	0.57	0.044
CoTiMCM850	11.52	19.14	0.56	0.152

From Table 5.11, amount of active site and Co dipersion of CoMCM was similar to CoSSP. It was higher active than those of all the CoTiMCM catalysts. The CO chemisorption per unit surface area of CoTiMCM550 and CoTiMCM650 was lower than CoMCM. In contrast with those, CO chemisorption/ BET of CoTiMCM 850 was higher than CoMCM.

5.2.2.6 Catalytic activity for CO_2-hydrogenation over MCM and TiMCM supported cobalt catalyst.

In order to determine the catalytic behaviors of the Co supported on MCM and TiMCM supports, CO_2 hydrogenation (H_2/CO_2 = 10.36/1) under methanation condition was performed to determine the overall activity and product selectivity of the samples. Hydrogenation of CO_2 was carried out at 220 and 270°C. A flow rate of $H_2/CO_2/Ar$ = 19.3344/1.8656/8.8 cm^3/min in a fixed-bed flow reactor was used. The resulted reaction test is shown in Table 5.12 and 5.13, respectively.

Table 5.12 Activity and product selectivity of CoMCM, CoTiMCM550, CoTiMCM 650 and CoTiMCM850 catalysts.

Catalysts	Conversion[a]		Rate[c] (x10^2 g CH$_2$/g cat.h)	TOF[d] (x10^3 s^{-1})	Product selectivity[c] (%)	
	Initial[b]	Steady state[c]			CH$_4$	CO
CoMCM	35.45	28.48	18.05	2.86	91.44	8.56
CoTiMCM550	4.8	7.58	4.48	3.01	88.93	11.04
CoTiMCM650	24.73	24.69	15.37	5.28	93.56	6.43
CoTiMCM850	35.31	33.99	22.29	6.55	94.89	5.11

[a] CO_2 hydrogenation was carried out at 220°C, 1 atm, and $H_2/CO_2/Ar$ = 19.3344/1.8656/8.8, F/W= 18 L/g cat.h

[b] After 5 min of reaction.

[c] After 4 h of reaction.

[d] The TOF calculation was based on CO chemisorption.

Table 5.12 shows the result from hydrogenation of CO_2 that was performed at 220 °C. It indicated that the steady state CO_2 conversions were ranged between 7.58 to 33.99% with corresponding to the reaction rate at 4.48 to 22.29 (x10^2 g CH$_2$/g cat.h) of cobalt supported on MCM and TiMCM catalysts. It showed that the activities of cobalt supported on MCM and TiMCM were higher than CoSSP and CoTiSSP. However, the selectivities to methane of CoTiMCM650 and CoTiMCM850 were higher than CoMCM. This result was similar to those of CoTiSSP. It was in

accordance with the presence of crystalline titania in the support before impregnation of cobalt nitrate. The rate vs. time on stream of cobalt supported on MCM and TiMCM catalysts with reaction temperature at 220°C is illustrated in Figure 5.28. The rate of catalysts decreased with the presence of titania. The activities for cobalt supported on MCM and TiMCM catalysts can not be attributed to the cobalt dispersion on the catalysts as seen from CO chemisorption results. Recent studies have shown that methanation turnover rates are also independent of Co dispersion on supported catalysts and of surface orientation on Co single crystals (Johnson et al., 1991).

Figure 5.28 Reaction rate at 220°C vs. time on stream of CoMCM, CoTiMCM550, CoTiMCM650 and CoTiMCM850 catalysts.

Table 5.13 Activity and product selectivity of CoMCM, CoTiMCM550, CoTiMCM 650 and CoTiMCM850 catalysts.

Catalysts	Conversion[a]		Rate[c] (x10^2 g CH$_2$/g cat.h)	TOF[d] (x10^3 s^{-1})	Product selectivity[c] (%)	
	Initial[b]	Steady state[c]			CH$_4$	CO
CoMCM	63.07	57.23	36.79	5.65	92.74	7.26
CoTiMCM550	15.31	17.87	9.92	7.19	83.56	16.49
CoTiMCM650	53.01	47.50	29.08	9.88	91.99	8.01
CoTiMCM850	53.99	51.17	33.47	9.98	94.64	5.36

[a] CO$_2$ hydrogenation was carried out at 270°C, 1 atm, and H$_2$/CO$_2$/Ar = 19.3344/1.8656/8.8, GSHV= 11400 h^{-1}.

[b] After 5 min of reaction.

[c] After 4 h of reaction.

[d] The TOF calculation was based on CO chemisorption.

Table 5.13 shows the result from hydrogenation of CO$_2$ was carried out at 270 °C. It indicated that the steady state CO$_2$ conversions were ranged between 17.87 to 57.23% with corresponding to the reaction rate at 9.92 to 36.79 (x10^2 g CH$_2$/g cat.h) of cobalt supported on MCM and TiMCM catalysts. The result was similar with the hydrogenation of CO$_2$ of CoSSP and CoTiSSP that was performed at 220 and 270°C. This also showed that the activities of cobalt supported on MCM was highest. However, the CO$_2$ conversions increased with increasing reaction temperature. Nevertheless, the selectivities to methane of CoTiMCM650 and CoTiMCM850 less decreased with increased operating temperature. The rate vs. time on stream of cobalt supported on MCM and TiMCM catalysts with reaction temperature at 270°C is illustrated in Figure 5.29.
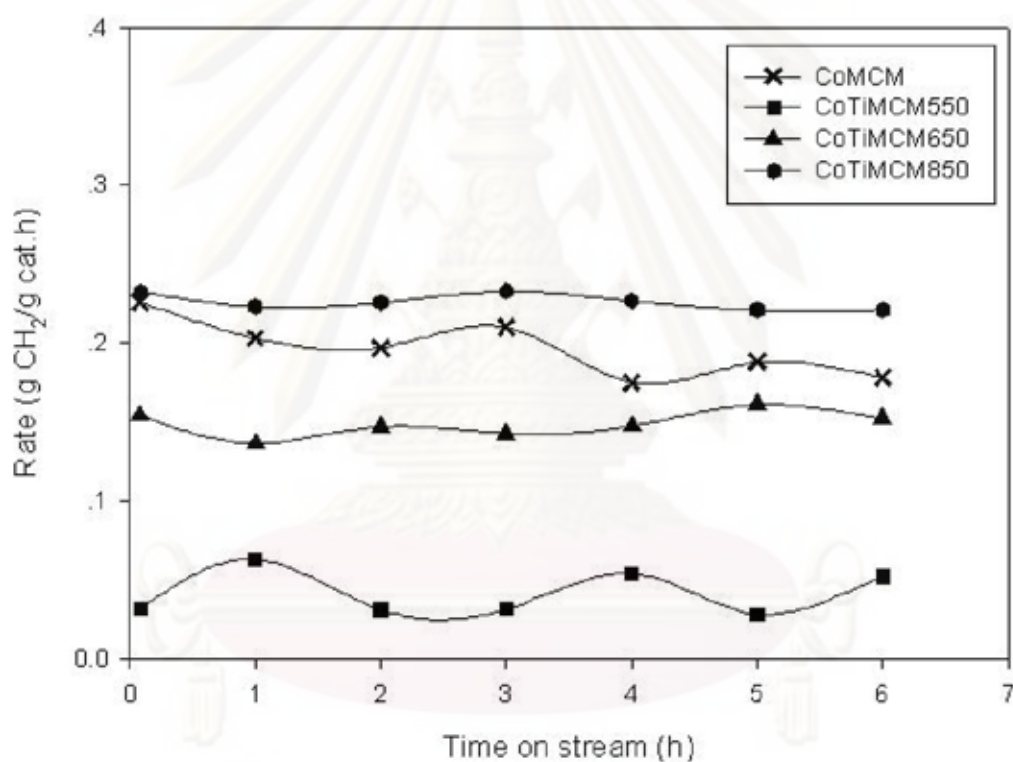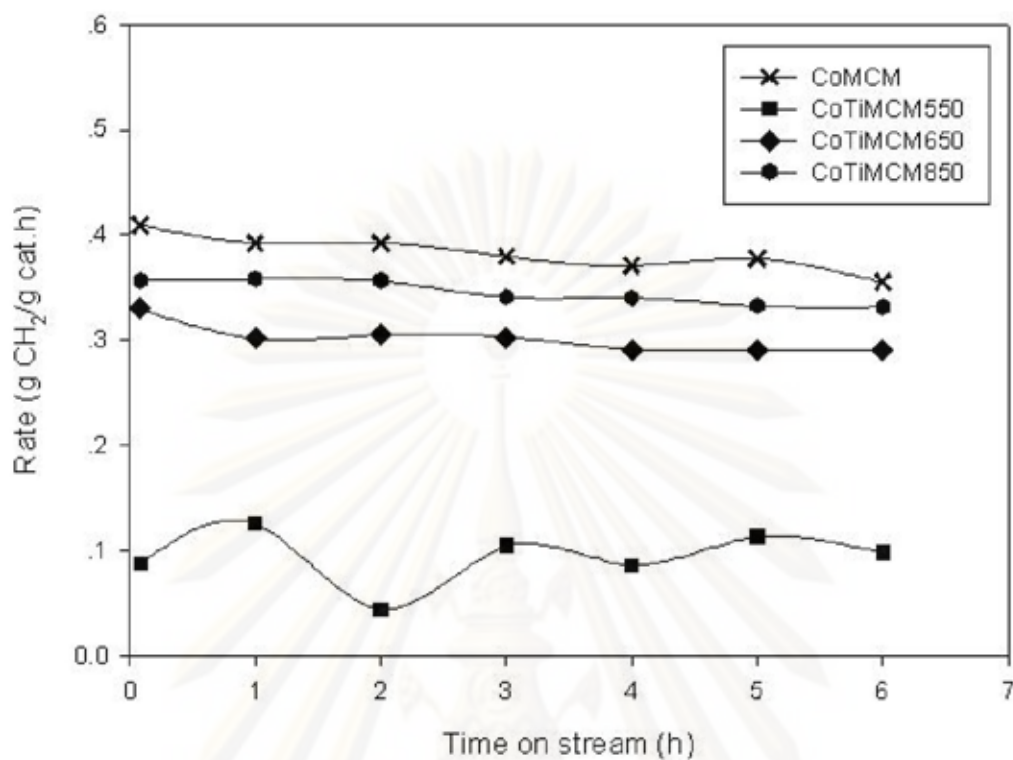
Figure 5.29 Reaction rate at 270 °C vs. time on stream of CoMCM, CoTiMCM550, CoTiMCM650 and CoTiMCM850 catalysts.

5.3 Characteristic of silica and titania-silica composites microparticle supported nickel catalyst.

This section presents the characteristic of silica and titania-silica composites microparticle supported nickel catalyst by incipient wetness impregnation of nickel (II) nitrate hexahydrate.

5.3.1 Preparation and characterization of spherical silica (SSP) and titania-spherical silica composites (TiSSP)-supported nickel catalyst.

5.3.1.1 X-Ray Diffraction
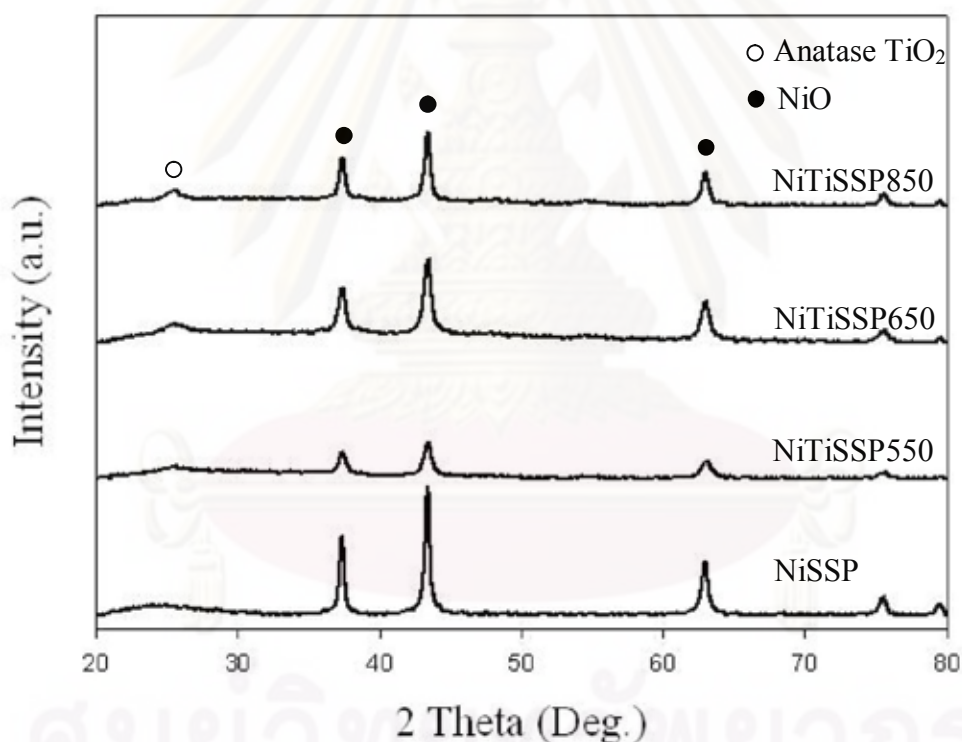
Figure 5.30 XRD patterns of NiSSP, NiTiSSP550, NiTiSSP650 and NiTiSSP850 catalysts.

XRD analysis was carried out for catalysts calcined at 500°C, with 20% wt of nickel impregnated onto SSP and TiSSP supports. XRD patterns for the nickel catalysts on all supports are shown in Figure 5.30. The diffractograms displayed diffraction typical of NiO crystals, which were observed at 37.3°, 43.3°,

62.8° and 75.5° (Grzechowiak et al., 2008). The small diffraction patterns of anatase TiO_2 crystaline form at 2θ of 25.3°, which was observed in all NiTiSSP catalysts.

5.3.1.2 Nitrogen physisorption

The BET surface areas, pore volume and average pore diameter analysis of nickel impregnated onto SSP and TiSSP calcined at 550, 650 and 850°C, were measured by nitrogen physisorption technique are shown in Table 5.14.

Table 5.14 BET surface areas, pore volume and pore diameter of NiSSP, NiTiSSP550, NiTiSSP650 and NiTiSSP850 catalysts.

Support samples	A_{BET} m^2/g	V_p cm^3/g	D_{BJH} nm
SSP	927	0.8135	2.04
TiSSP550	755	0.6476	2.40
TiSSP650	716	0.5671	2.59
TiSSP850	385	0.1587	3.23
NiSSP	620	0.5296	2.20
NiTiSSP550	559	0.4584	2.60
NiTiSSP650	602	0.3512	2.71
NiTiSSP850	201	0.0925	4.02

Nitrogen physisorption of the catalyst samples showed that the surface areas of NiSSP and all NiTiSSP were less than support particles. This was in accordance with the larger pore sizes of Ni catalysts than those of pure support particles. When compared the surface areas of all NiTiSSP catalysts, it can be observed that the surface areas of NiTiSSP650 was the highest for all NiTiSSP catalysts.This is probably due to the less coagulation of NiTiSSP650 particles.

5.3.1.3 Scanning electron microscopy (SEM) and energy dispersive X-ray spectroscopy (EDX)

Figure 5.31 SEM micrograph for the NiTiSSP550 and NiTiSSP650 catalysts.

Scanning electron microscopy (SEM) and energy dispersive X-ray spectroscopy (EDX) were also conducted in order to study the morphologies and elemental distribution of the samples, respectively. The SEM micrographs of the NiTiSSP550 and NiTiSSP650 were shown in Figure 5.31. It reveals the surface of NiTiSSP650 was more smooth than NiTiSSP550. Figures 5.32 and 5.33 presents a typical spectrum and element quantity of the NiSSP and NiTiSSP850 surface from EDX analysis, respectively. The results show that NiSSP has lower the amount of Ni than NiTiSSP850 with regards to at the external surface. Figures 5.34 and 5.35 show that the EDX mapping of nickel distribution on NiSSP and NiTiSSP850 suface. It indicates that the nickel oxide species on the surface of NiSSP and NiTiSSP850 catalysts show good distribution.
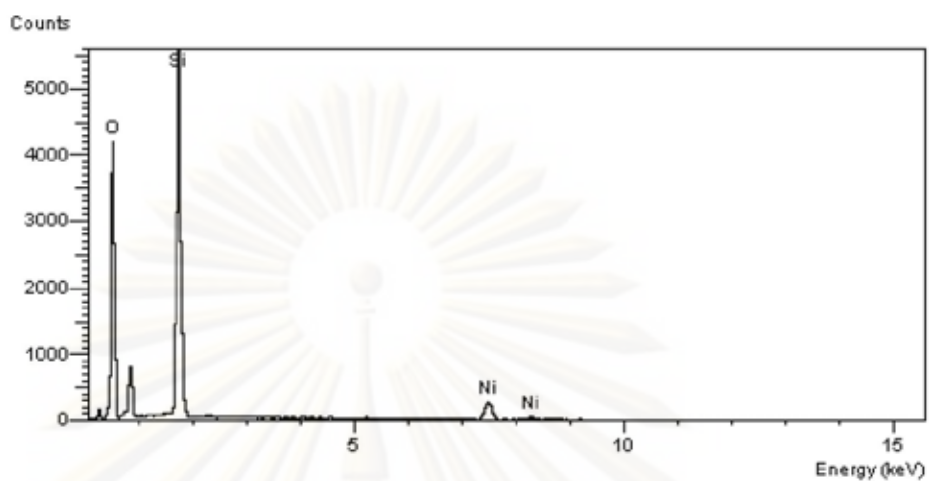
Element	Element(%)	Atomic(%)
Ni	8.91	3.00
Si	27.55	19.29
O	63.54	77.71

Figure 5.32 A typical spectrum of the NiSSP catalyst from EDX analysis.
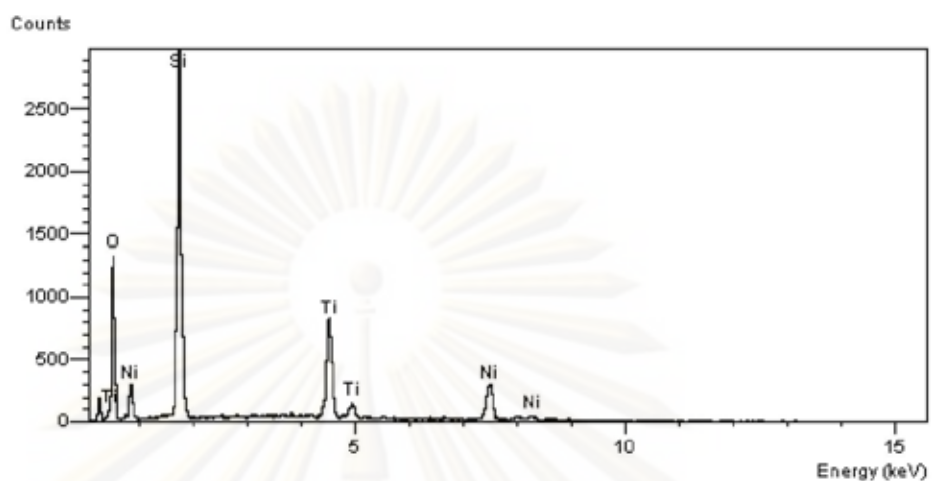
Element	Element(%)	Atomic(%)
Ni	12.09	4.41
Ti	9.94	4.47
Si	22.58	17.20
O	55.40	73.92

Figure 5.33 A typical spectrum of the NiTiSSP850 catalyst from EDX analysis.
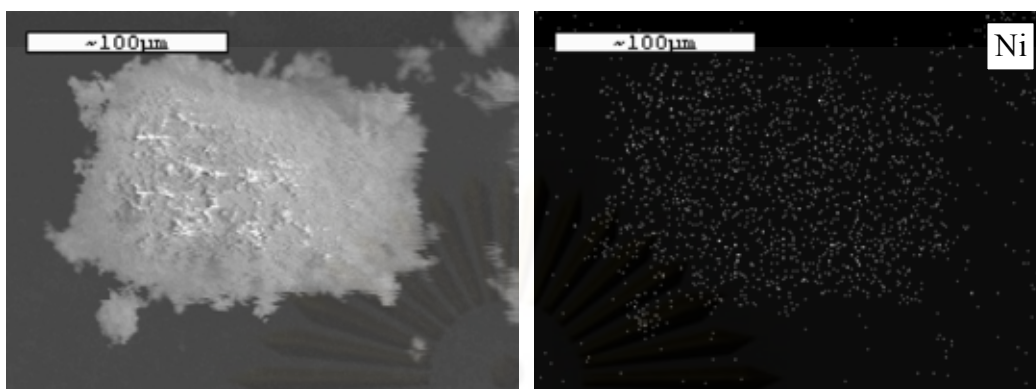
Figure 5.34 EDX mapping of NiSSP catalyst.
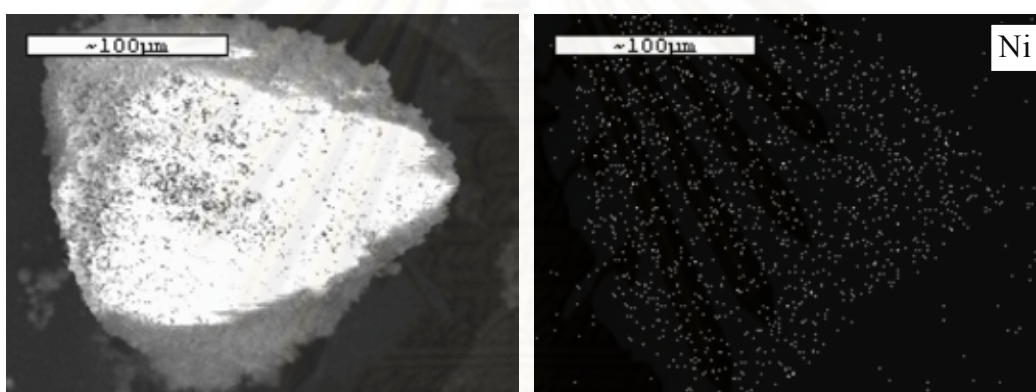
Figure 5.35 EDX mapping of NiTiSSP850 catalysts.

5.3.1.4 Temperature Programmed Reduction (TPR)

TPR patterns of nickel supported on SSP and TiSSP support are shown in Figure.5.36. From these profiles the maximum temperature for each catalyst are given in Table 5.15. The reduction profiles of all nickel catalysts contain two distinct maximum temperature at low temperature one ranging from 360 to 390ºC, which have weak interaction with support. Furthermore, a high temperature one within the range from 500 to 550ºC, which nickel-support interaction is stronger. The two distinct of reduction indicate that metal-support interactions are varied. From the result, the nickel-support interaction was shifted into stronger interaction in NiTiSSP550 and NiTiSSP650. This was in accordance with the peak area increasing of the second maximum reduction temperature. In contrast, the reducibilities and H_2 consumption of NiTiSSP550 and NiTiSSP650 catalysts were higher than NiSSP.
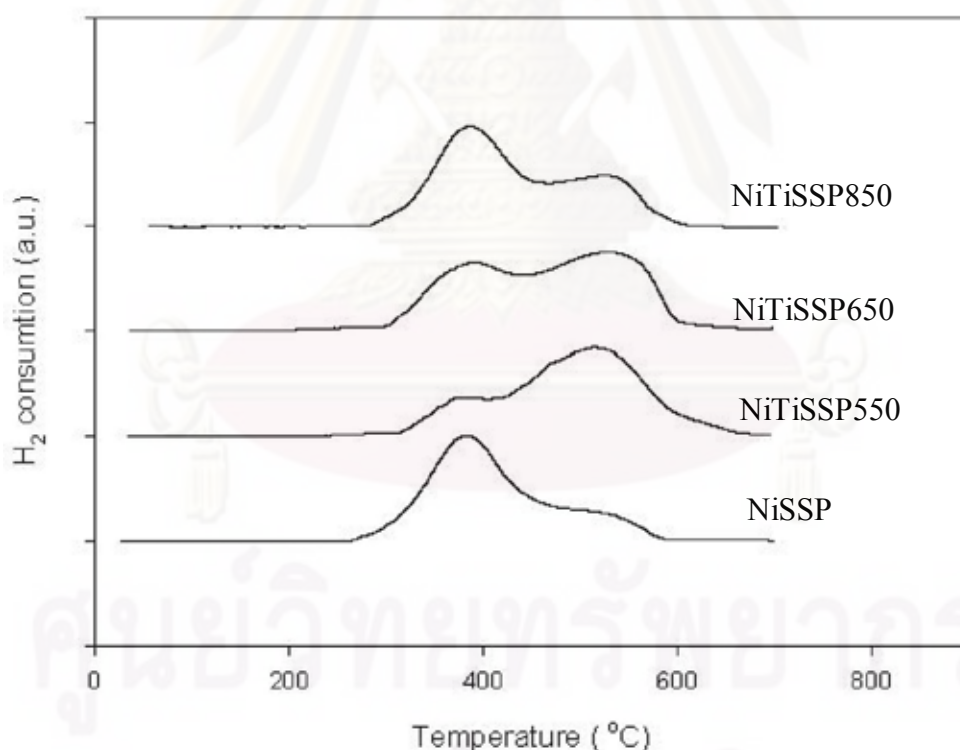
Figure 5.36 TPR patterns of NiSSP, NiTiSSP550, NiTiSSP650 and NiTiSSP850 catalysts.

Table 5.15 Maximum temperatures and H_2 consumption from TPR profiles of NiSSP, NiTiSSP550, NiTiSSP650 and NiTiSSP850 catalysts.

Catalysts	Temperature (^{o}C)		Total H_2 consumption μmol H_2/g.cat	Reducibility (%)
	Maximum 1	Maximum 2		
NiSSP	380.30	504.66	1,455	42.9
NiTiSSP550	372.64	510.89	1,652	48.7
NiTiSSP650	374.99	544.69	1,659	48.7
NiTiSSP850	384.33	530.12	1,457	42.9

5.3.1.5 CO-chemisorption

The amount of carbon monoxide adsorption on catalysts was performed in order to determine the number of active site on the catalysts surface. The results of CO chemisorption for the nickel catalyst samples are illustrated in Table 5.16.

Table 5.16 Show amount of carbon monoxide adsorbed on catalysts.

Catalysts	Active site, Moleculex10^{-18} per gram	Total CO chemisorption μmol CO/g.cat	% dispersion of nickel	CO chemisorption/ BET surface area μmol CO/g.cat/m^2
NiSSP	22.91	38.06	1.12	0.061
NiTiSSP550	10.73	17.82	0.53	0.032
NiTiSSP650	16.43	27.29	0.80	0.045
NiTiSSP850	3.53	5.86	0.17	0.029

From the results, amount of active site and Ni dispersion of NiSSP was higher than those of all the NiTiSSP catalysts. Moreover, The CO chemisorption per unit surface area of NiSSP was higher than those of all the NiTiSSP catalysts, too. Comparison of the active site and Ni dispersion in all NiTiSSP catalysts, it can be observed that active site and Ni dispersion of NiTiSSP650 was the highest.

5.3.1.6 Catalytic activity for CO_2-hydrogenation over SSP and TiSSP supported nickel catalyst.

In order to determine the catalytic behaviors of the Ni supported on SSP and TiSSP supports, CO_2 hydrogenation (H_2/CO_2 = 10.36/1) under methanation condition was performed to determine the overall activity and product selectivity of the samples. Hydrogenation of CO_2 was carried out at 220 and 270°C. A flow rate of $H_2/CO_2/Ar$ = 19.3344/1.8656/8.8 cm^3/min in a fixed-bed flow reactor was used. The resulted reaction test is shown in Table 5.17 and 5.18, respectively.

Table 5.17 Activity and product selectivity of NiSSP, NiTiSSP550, NiTiSSP650 and NiTiSSP850 catalysts.

Catalysts	Conversion [a]		Rate [c] (x10^2 g CH_2/g cat.h)	TOF [d] (x10^3 s^{-1})	Product selectivity [c] (%)	
	Initial [b]	Steady state [c]			CH_4	CO
NiSSP	9.63	5.83	4.05	0.68	100	0.00
NiTiSSP550	20.53	5.20	3.48	1.30	100	0.00
NiTiSSP650	16.43	10.13	7.00	1.69	100	0.00
NiTiSSP850	18.86	17.37	11.53	12.67	100	0.00

[a] CO_2 hydrogenation was carried out at 220°C, 1 atm, and $H_2/CO_2/Ar$ = 19.3344/1.8656/8.8, F/W= 18 L/g cat.h.

[b] After 5 min of reaction.

[c] After 4 h of reaction.

[d] The TOF calculation was based on CO chemisorption.

Table 5.17 shows the result from hydrogenation of CO_2 that was performed at 220 °C. It indicated that the steady state CO_2 conversions were ranged between 5.20 to 17.37% with corresponding to the reaction rate at 3.48 to 11.53 (x10^2 g CH_2/g cat.h) of nickel supported on SSP and TiSSP catalysts. It showed that the activities of nickel supported on SSP and TiSSP were lower than CoSSP and CoTiSSP. However, the selectivities to methane of all nickel catalysts were dramatically complete. This result presents that the conversion of NiTiSSP650 and NiTiSSP850 were higher than NiSSP. It was in accordance with the presence of crystalline titania in the support

before impregnation of nickel nitrate. The rate vs. time on stream of nickel supported on SSP and TiSSP catalysts with reaction temperature at 220°C is illustrated in Figure 5.28. The rate of catalysts increased with the presence of crystalline titania. The activities for nickel supported on SSP and TiSSP catalysts can not be attributed to the nickel dispersion on the catalysts as seen from CO chemisorption results.
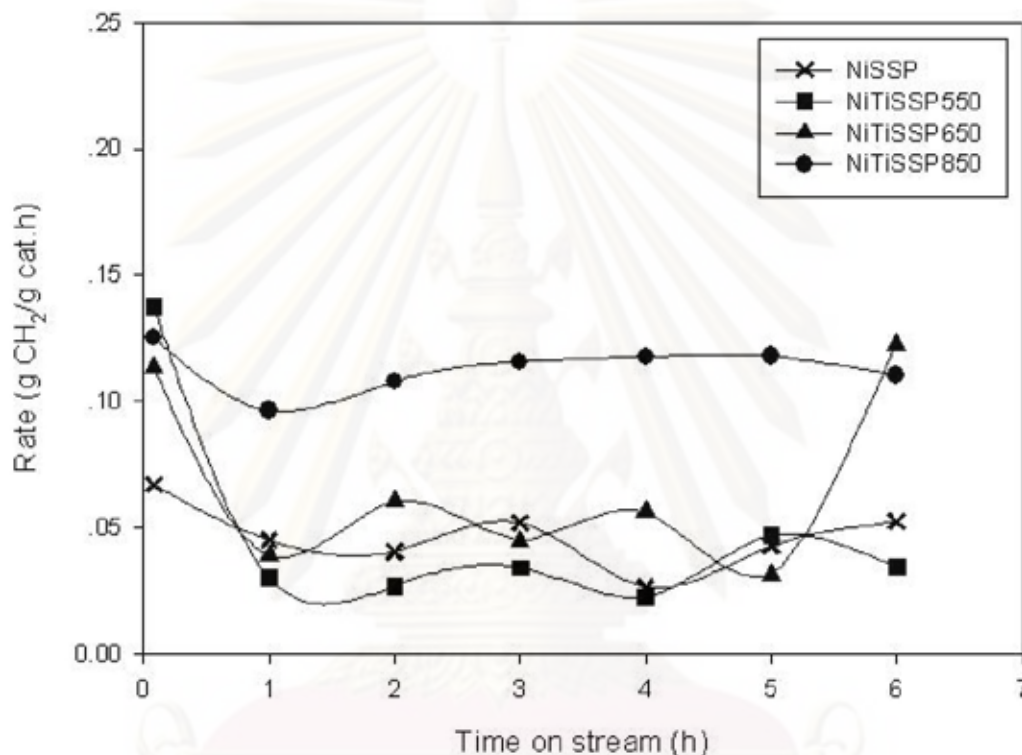

Figure 5.37 Reaction rate at 220°C vs. time on stream of NiSSP, NiTiSSP550, NiTiSSP650 and NiTiSSP850 catalysts.

Table 5.18 Activity and product selectivity of NiSSP, NiTiSSP550, NiTiSSP650 and NiTiSSP850 catalysts.

Catalysts	Conversion[a]		Rate[c] (x10^{-2} g CH$_2$/g cat.h)	TOF[d] (x10^3 s^{-1})	Product selectivity[c] (%)	
	Initial[b]	Steady state[c]			CH$_4$	CO
NiSSP	45.04	37.47	25.78	4.35	99.03	0.97
NiTiSSP550	22.73	32.58	21.79	7.91	100	0.00
NiTiSSP650	75.86	82.77	57.21	13.19	100	0.00
NiTiSSP850	77.46	76.71	50.92	54.91	100	0.00

[a] CO$_2$ hydrogenation was carried out at 270°C, 1 atm, and H$_2$/CO$_2$/Ar = 19.3344/1.8656/8.8, F/W= 18 L/g cat.h

[b] After 5 min of reaction.

[c] After 4 h of reaction.

[d] The TOF calculation was based on CO chemisorption.

Table 5.18 shows the result from hydrogenation of CO$_2$ that was carried out at 270 °C. It indicated that the steady state CO$_2$ conversions were ranged between 32.58 to 82.77% with corresponding to the reaction rate at 21.79 to 57.21 (x10^2 g CH$_2$/g cat.h) of nickel supported on SSP and TiSSP catalysts. The result was similar to the cobalt catalysts. This also showed that the CO$_2$ conversions increased with increasing reaction temperature. This was in accordance with Fischer-Tropsch CO$_2$ hydrogenation operating temperature must be rather high because of the equilibrium constraints for the reverse CO shift reaction. This limits the application of temperature in the lower range for Fischer-Tropsch conversion (Riedel et al., 1999). Moreover, Chang et al. (2003) reports that 500°C was suitable for hydrogenation of CO$_2$ with maximum yield and selectivity of methane in Ni/RHA-Al$_2$O$_3$. In contrast with Co catalysts, the activities of nickel supported on SSP and TiSSP were larger than all of cobalt catalysts at this reaction temperature. the selectivities to methane of all NiTiSSP remained dramatically complete at this reaction temperature. This also showed that the activities of nickel catalysts remained complete with the presence of titania in the supports. The rate vs. time on stream of nickel supported on SSP and TiSSP catalysts with reaction temperature at 270°C is illustrated in Figure 5.38.
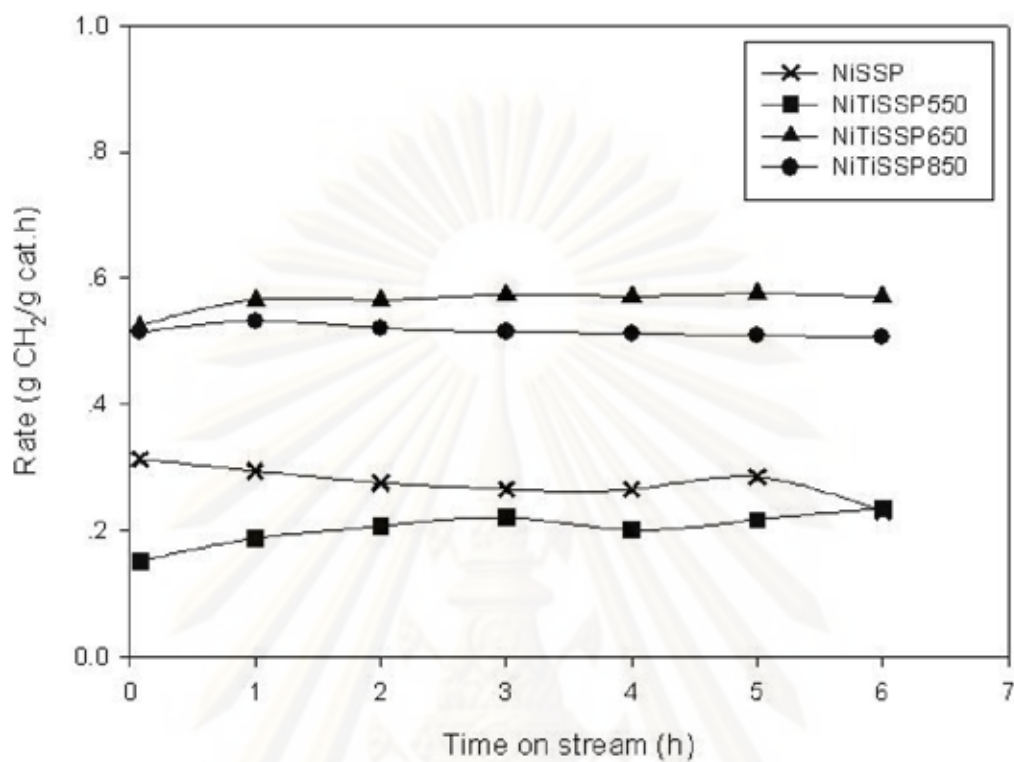
Figure 5.38 Reaction rate at 270°C vs. time on stream of NiSSP, NiTiSSP550, NiTiSSP650 and NiTiSSP850 catalysts.

5.3.2 Preparation and characterization of MCM-41 and titania-MCM-41 composites (TiMCM)-supported nickel catalyst.

5.3.2.1 X-Ray Diffraction
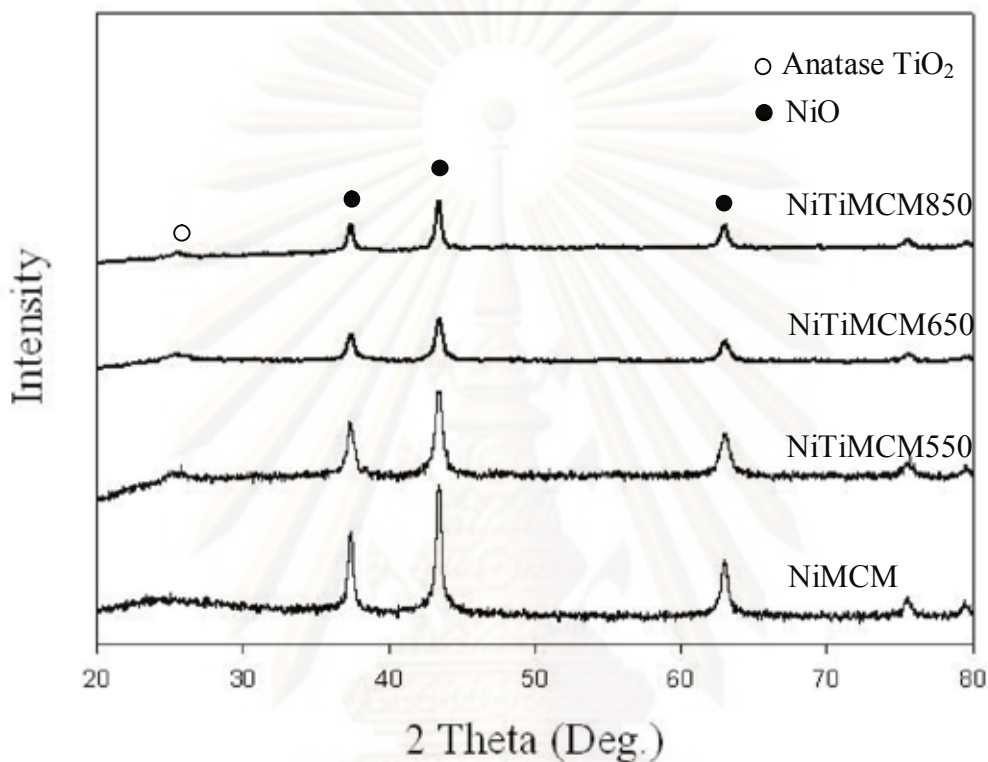
Figure 5.39 XRD patterns of the NiMCM, NiTiMCM550, NiTiMCM650 and NiTiMCM850 catalysts.

XRD patterns of the nickel impregnated onto MCM-41 and TiMCM supports and calcined at 500°C for 4 h. XRD patterns for the nickel catalysts on all supports are shown in Figure 5.39. The typical XRD peaks of NiO crystals were observed at 37.3°, 43.3°, 62.8° and 75.5° (Grzechowiak et al., 2008). The slight diffraction peak of anatase TiO_2 crystaline form were observed at 2θ of 25.3° in all NiTiSSP catalysts.

5.3.2.2 Nitrogen physisorption

The BET surface areas, pore volume and average pore diameter analysis of nickel impregnated onto MCM-41 and TiMCM, which calcined at 550, 650 and 850 ^{o}C, were measured by nitrogen physisorption technique are shown in Table 5.19.

Table 5.19 BET surface areas, pore volume and pore diameter of NiMCM, NiTiMCM550, NiTiMCM650 and NiTiMCM850 catalysts.

Support samples	A_{BET} m^2/g	V_p cm^3/g	D_{BJH} nm
MCM	1187	1.0287	2.13
TiMCM550	837	0.6219	2.64
TiMCM650	607	0.3486	3.01
TiMCM850	137	0.1371	4.57
NiMCM	805	0.4160	2.44
NiTiMCM550	428	0.3154	3.25
NiTiMCM650	440	0.1970	3.30
NiTiMCM850	51	0.0985	7.18

The results are similar to those of NiSSP and all NiTiSSP catalysts. The surface areas of NiMCM and all NiTiMCM were less than pure support particles. This was in accordance with the larger pore sizes of Ni catalysts than those of pure support particles. The comparison in the surface areas of all NiTiMCM catalysts showed that the surface areas of NiTiMCM650 was the highest for all NiTiMCM catalysts. This is probably due to the less coagulation of NiTiMCM650 particles.

5.3.2.3 Scanning electron microscopy (SEM) and Energy dispersive X-ray spectroscopy (EDX)
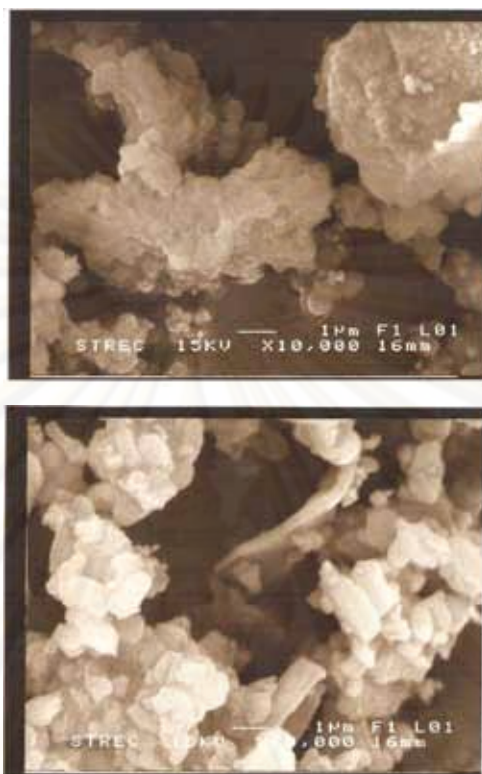
Figure 5.40 SEM micrograph for the NiTiMCM550 and NiTiMCM650 catalysts.

Scanning electron microscopy (SEM) and energy dispersive X ray spectroscopy (EDX) were powerful tool in order to study the morphologies and elemental distribution of the samples, respectively. The SEM micrographs of the NiTiMCM550 and NiTiMCM650 were shown in Figure 5.40. It exhibited the catalyst particles that was also extreme coagulation in NiTiMCM550. Figures 5.41 and 5.42 present a typical spectrum and element quantity of the NiMCM and NiTiMCM850 surface from EDX analysis, respectively. The results show that NiMCM displayed has lower the amount of Ni than NiTiMCM850 with regards to at the external surface. Figures 5.43 and 5.44 shows that the EDX mapping of nickel distribution on NiMCM and NiTiMCM850 suface. It shows good nickel distribution on the surface of NiMCM and NiTiMCM850 catalysts.
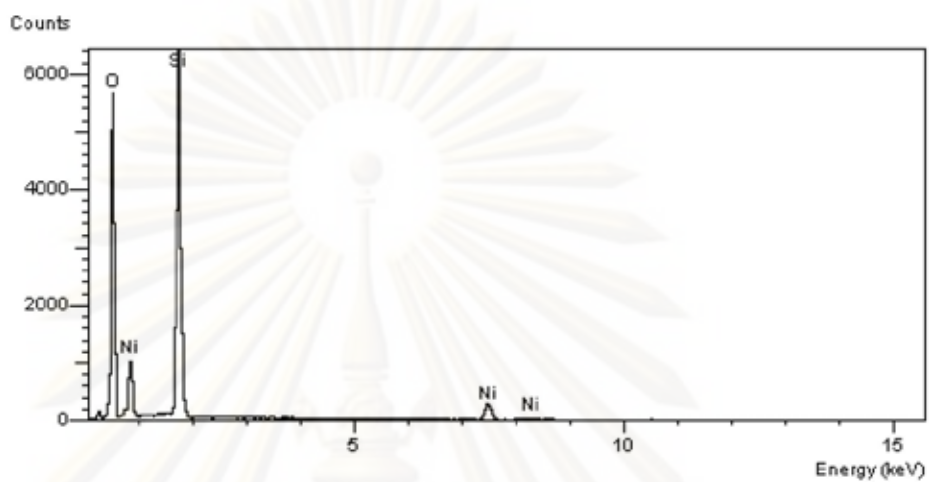
Element	Element(%)	Atomic(%)
Ni	6.42	2.11
Si	28.65	19.63
O	64.93	78.23

Figure 5.41 A typical spectrum of the NiMCM microparicle composites from EDX analysis.
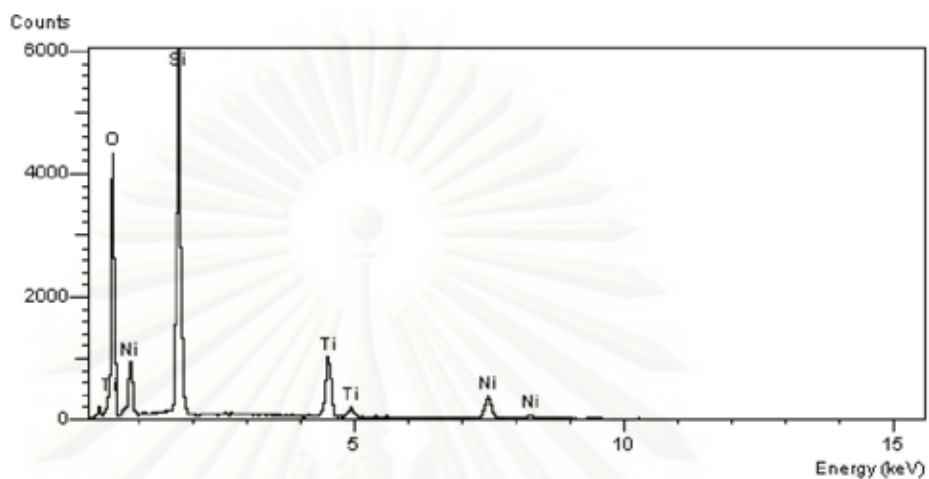
Element	Element(%)	Atomic(%)
Ni	10.19	3.64
Ti	8.63	3.72
Si	21.51	15.79
O	59.67	76.85

Figure 5.42 A typical spectrum of the NiTiMCM850 microparicle composites from EDX analysis.
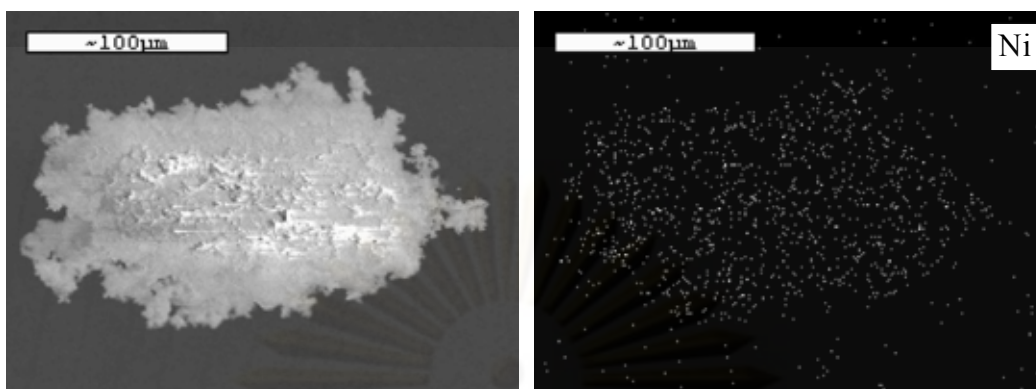
Figure 5.43 EDX mapping of NiMCM microparicle composites.
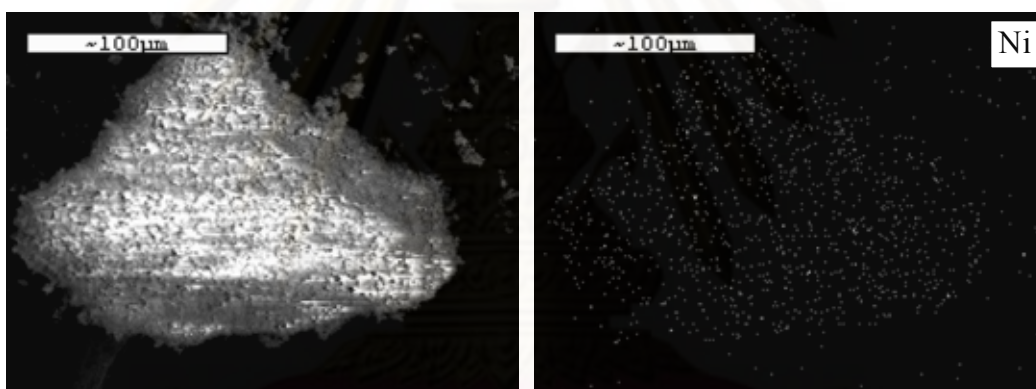
Figure 5.44 EDX mapping of NiTiMCM850 microparicle composites.

5.2.1.5 Temperature Programmed Reduction (TPR)

TPR patterns of nickel supported on MCM-41 and TiMCM support are shown in Figure.5.45. From these profiles the maximum temperature for each catalyst are given in Table 5.20. The reduction profiles of all nickel catalysts contain two distinct maximum temperature. The amount of nickel oxide species, which have weak interaction with support, of NiMCM is larger than those of all NiTiMCM. From the result, the nickel-support interaction was shifted into stronger interaction in all NiTiSSP. This was in accordance with the peak area increasing of the second maximum reduction temperature. In contrast, the reducibilities and H_2 consumption of all NiTiMCM catalysts were higher than NiMCM.
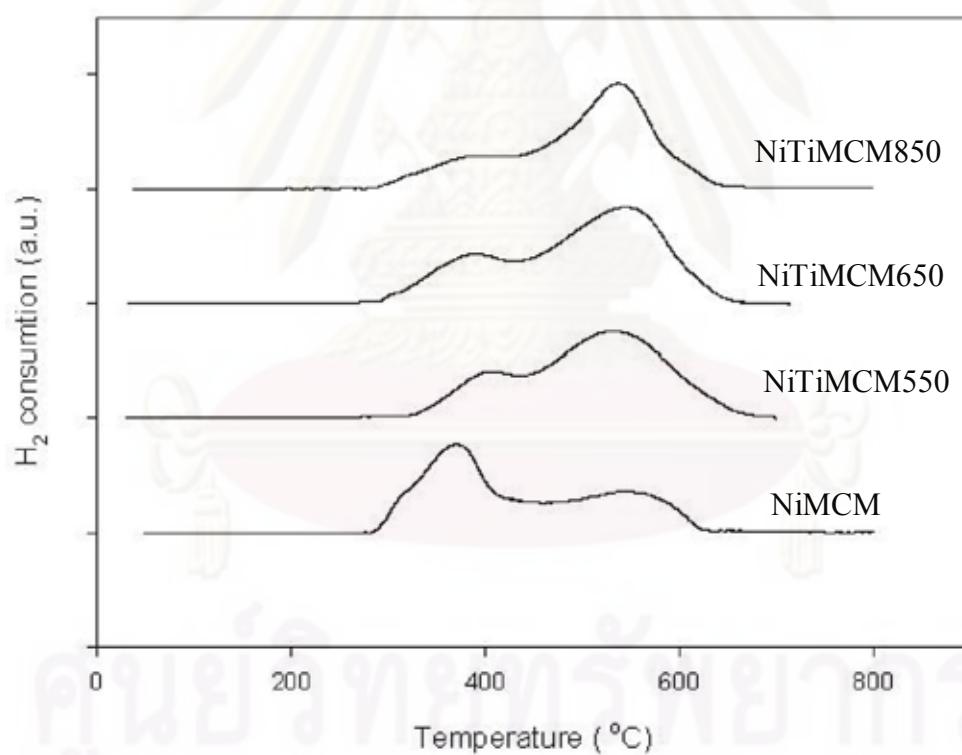
Figure 5.45 TPR patterns of NiMCM, NiTiMCM550, NiTiMCM650 and NiTiMCM850.

Table 5.20 Maximum temperatures and H_2 consumption from TPR profiles of NiMCM, NiTiMCM550, NiTiMCM650 and NiTiMCM850.

Catalysts	Temperature (^{o}C)		Total H_2 consumption µmol H_2/g.cat	Reducibility (%)
	Maximum 1	Maximum 2		
NiMCM	365.40	559.74	1,189	35.0
NiTiMCM550	397.32	533.68	1,567	46.2
NiTiMCM650	379.76	547.48	1,566	46.2
NiTiMCM850	391.21	538.47	1,295	38.2

5.2.1.4 CO-chemisorption

The amount of carbon monoxide adsorption on catalysts was performed inorder to determine the number of active site on the catalysts surface. The results of CO chemisorption for the nickel catalyst samples are illustrated in Table 5.21.

Table 5.21 showed amount of carbon monoxide adsorbed on catalysts.

Catalysts	Active site, Molecule*10^-18 per gram	Total CO chemisorption µmol CO/g.cat	% dispersion of Nickel	CO chemisorption/ BET surface area µmol CO/g.cat/m^2
NiMCM	20.97	34.83	1.03	0.043
NiMCM550	16.82	27.95	0.82	0.065
NiMCM650	6.39	10.61	0.31	0.024
NiMCM850	13.88	23.05	0.68	0.452

From the results, amount of active site and Ni dispersion of NiMCM was higher than those of all the NiTiMCM catalysts. In contrast, The CO chemisorption per unit surface area of NiTiMCM850 was highest. Comparison of the active site and Ni dispersion in all NiTiMCM catalysts, it can be observed that active site and Ni dispersion of NiTiSSP550 was the highest.

5.3.1.6 Catalytic activity for CO_2-hydrogenation over MCM and TiMCM supported nickel catalyst.

In order to determine the catalytic behaviors of the Ni supported on MCM and TiMCM supports, CO_2 hydrogenation (H_2/CO_2 = 10.36/1) under methanation condition was performed to determine the overall activity and product selectivity of the samples. Hydrogenation of CO_2 was carried out at 220 and 270°C. A flow rate of $H_2/CO_2/Ar$ = 19.3344/1.8656/8.8 cm^3/min in a fixed-bed flow reactor was used. The resulted reaction test is shown in Table 5.17 and 5.18, respectively.

Table 5.22 Activity and product selectivity of NiMCM, NiTiMCM550, NiTiMCM650 and NiTiMCM850.

Catalysts	Conversion[a]		Rate[c] (x10^{-2} g CH$_2$/g cat.h)	TOF[d] (x10^3 s^{-1})	Product selectivity[c] (%)	
	Initial[b]	Steady state[c]			CH$_4$	CO
NiMCM	17.59	16.41	11.52	2.04	100	0.00
NiTiMCM550	5.08	8.27	5.65	1.35	100	0.00
NiTiMCM650	24.89	19.72	13.37	8.58	100	0.00
NiTiMCM850	25.88	18.59	12.75	3.63	100	0.00

[a] CO_2 hydrogenation was carried out at 220°C, 1 atm, and $H_2/CO_2/Ar$ = 19.3344/1.8656/8.8, F/W= 18 L/g cat.h

[b] After 5 min of reaction.

[c] After 4 h of reaction.

[d] The TOF calculation was based on CO chemisorption.

Table 5.22 shows the result from hydrogenation of CO_2 that was performed at 220 °C. It indicated that the steady state CO_2 conversions were ranged between 8.27 to 19.72% with corresponding to the reaction rate at 5.65 to 13.37 (x10^2 g CH$_2$/g cat.h) of nickel supported on MCM and TiMCM catalysts. It showed that the activities of nickel supported on MCM and TiMCM were similar with NiSSP and all NiTiSSP. However, the selectivities to methane of all nickel catalysts remained dramatically complete. In recently studies, CO_2 methanation, coprecipitated catalysts

show higher methanion activity and lower CO production level for all nickel loading
(Erhan et al., 1997). This result presents that the conversion of NiTiMCM650 and
NiTiMCM 850 were higher than NiMCM. It was in accordance with similar reason of
NiSSP and all NiTiSSP. The rate vs. time on stream of nickel supported on MCM
and TiMCM catalysts with reaction temperature at 220°C is illustrated in Figure 5.46.

Figure 5.46 Reaction rate at 220°C vs. time on stream of NiMCM, NiTiMCM550,
NiTiMCM650 and NiTiMCM850.

Table 5.23 Activity and product selectivity of NiMCM, NiTiMCM550, NiTiMCM650 and NiTiMCM850.

Catalysts	Conversion[a]		Rate[c] (x10^{-2} g CH$_2$/g cat.h)	TOF[d] (x10^3 s^{-1})	Product selectivity[c] (%)	
	Initial[b]	Steady state[c]			CH$_4$	CO
NiMCM	73.10	64.72	44.96	8.19	98.93	1.07
NiTiMCM550	21.88	30.47	20.83	5.07	100	0.00
NiTiMCM650	70.40	71.83	48.69	29.98	100	0.00
NiTiMCM850	73.04	74.60	51.15	13.97	100	0.00

[a] CO$_2$ hydrogenation was carried out at 270°C, 1 atm, and H$_2$/CO$_2$/Ar = 19.3344/1.8656/8.8, F/W= 18 L/g cat.h

[b] After 5 min of reaction.

[c] After 4 h of reaction.

[d] The TOF calculation was based on CO chemisorption.

Table 5.23 shows the result from hydrogenation of CO$_2$ that was carried out at 270 °C. It indicated that the steady state CO$_2$ conversions were ranged between 30.47 to 74.60% with corresponding to the reaction rate at 20.83 to 51.15 (x10^2 g CH$_2$/g cat.h) of nickel supported on MCM and TiMCM catalysts. The result was similarly with cobalt catalysts. This also showed that the CO$_2$ conversions increased with increasing operated temperature. In contrast with Co catalysts, the activities of nickel supported on MCM and TiMCM were larger than all of cobalt catalysts at this operated temperature. the selectivities to methane of all NiTiMCM remained dramatically complete at this operating temperature. This also showed that the activities of nickel catalysts remained complete with the presence of titania in the supports. However, the decreasing in selectivities to methane of NiMCM was larger than NiSSP. The rate vs. time on stream of nickel supported on MCM and TiMCM catalysts with reaction temperature at 270°C is illustrated in Figure 5.46.
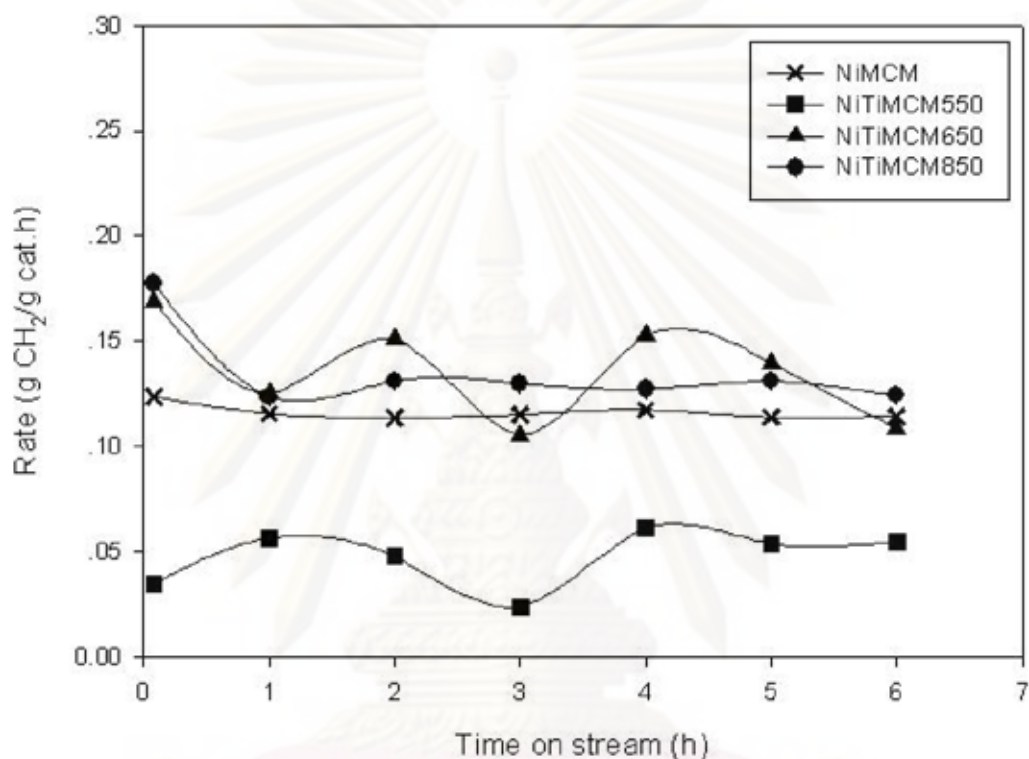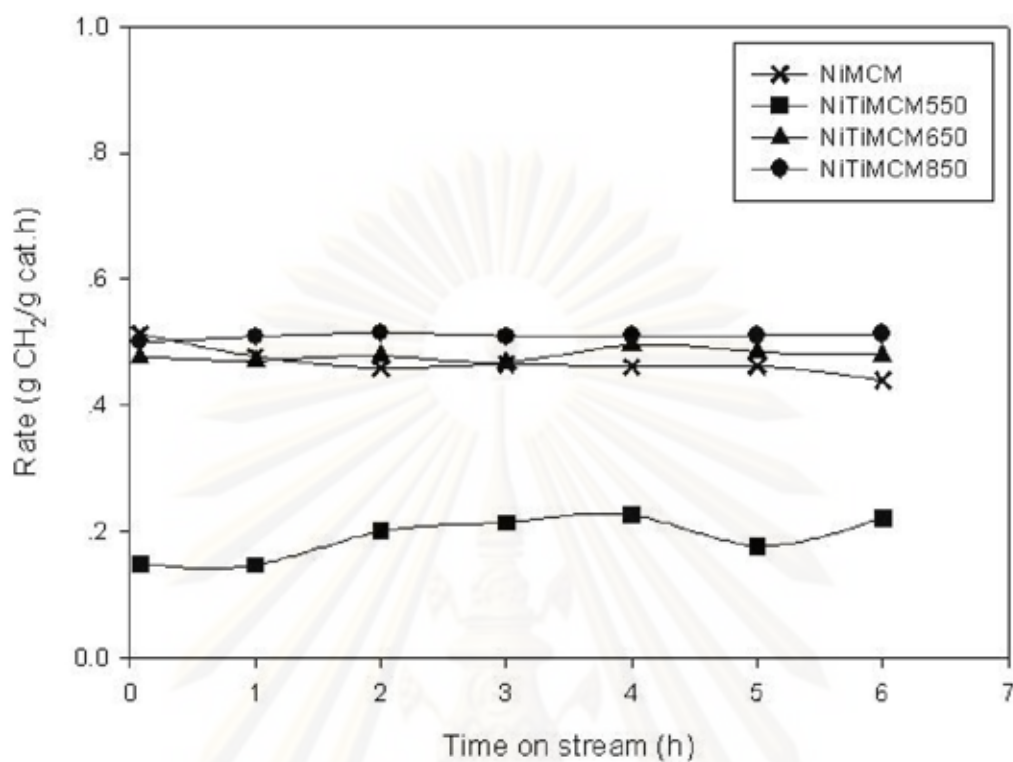
Figure 5.46 Reaction rate at 270°C vs. time on stream of NiMCM, NiTiMCM550, NiTiMCM650 and NiTiMCM850.
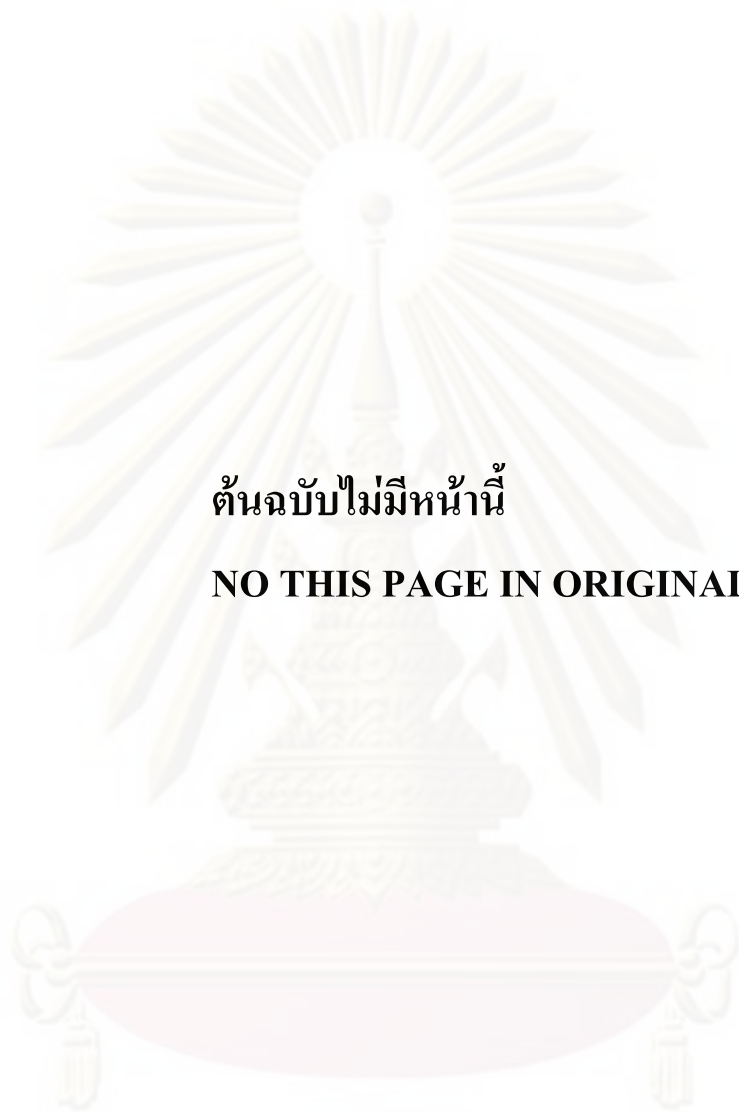
ต้นฉบับไม่มีหน้านี้

NO THIS PAGE IN ORIGINAL

6.2 Recommendations

1. The CO_2 hydrogenation that was performed at higher temperature should be futher studied.

2. Introduce TEM (Transmission Electron Microscope) technique to investigate the titania, cobalt and nickel crystalline size.

3. Besides Co and Ni metal, other metals such as Fe , Cu and etc should be further investigated with TiO_2-SiO_2 microparticle composites on the supports.
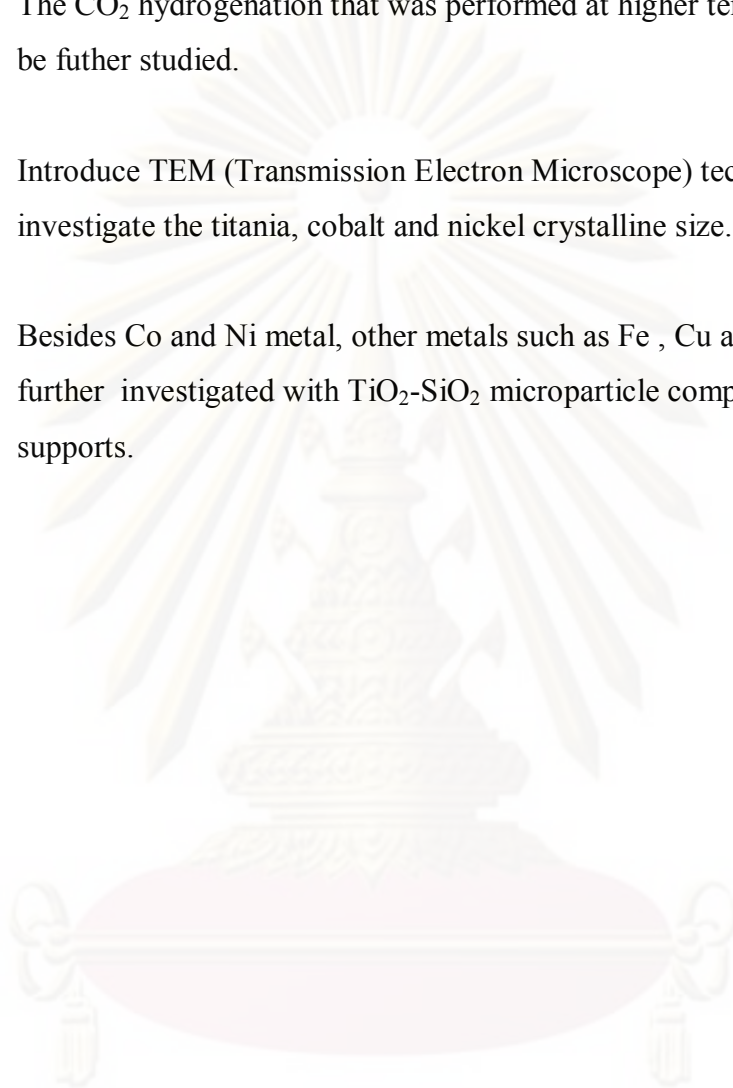
REFERENCES

Adesina, A. A. Hydrocarbon synthesis via Fischer-Tropsch reaction: travails and triumphs. Appl. Cat. A 138 (1996): 345-367.

Aksoylu, A.E., Onsan, Z.H. Hydrogenation of carbon oxides using coprecipitated and impregnated Ni/Al_2O_3 catalysts. Applied Catalysis A. 164 (1997): 1-11.

Anderson, C., Bard, A.J. An improved photocatalyst of TiO/SiO prepared by a sol-gel synthesis. Journal of Physical Chemistry 99 (1995): 9882-9885.

Arakawa, H. Dubois, J.L., Sayama, K. Selective conversion of CO_2 to methanol by catalytic hydrogenation over promoted copper catalyst. Energy Convers 33 (1992): 521-528.

Castner D.G., Blacard R.L., Somorjai G.A. CO hydrogenation over clean and oxidized rhodium foil and single crystal catalysts. Correlations of catalyst activity, selectivity, and surface composition. J.Catal. 66 (1980): 257.

Carp, O., Huisman, C. L., and Reller, A. Photoinduced reactivity of titanium dioxide. Prog. Solid State Chem. 32 (2004): 33-177.

Chang, F.W., Tsay, M.T., Liang, S.P. Hydrogenation of CO_2 over nickel catalysts supported on rice husk ash prepared by ion exchange. Applied CatalysisA 209 (2001): 217–227.

Chang, F.W., Kuo, M.S., Tsay, M.T., Hsieh, M.C. Hydrogenation of CO_2 over nickel catalysts on rice husk ash-alumina prepared by incipient wetness impregnation. Applied Catalysis A 247 (2003): 309–320.

Chen, C.S., Lin, J.H., Wu, J.H., Chiang, C.Y. Growth of carbon nano fibers synthesized from CO_2 hydrogenation on a $K/Ni/Al_2O_3$ catalyst. Catalysis Communications (2009)

Choudhury, M.B.I., Ahmed, S., Shalabi, M.A., Inui, T. Preferential methanation of CO in a syngas involving CO at lower temperature range. Applied Catalysis A: General 314 (2006): 47-53.

Chun, H., Yizhong, W., Hongxiao, T. Preparation and characterization of surface bond-conjugated TiO/SiO and photocatalysis for azo dyes. Applied Catalysis B: Environmental 30 (2001): 277-285.

Chung, H.T., Cheong, D.S., Kim, C.S. Role of nanoparticle in PNN-PZT/Ag nanocomposite. Materials Letters, 59 (2005): 920-924

Dagle, R.A., Wang, Y., Xia, G.G., Strohm, J.J., Holladay, J., Palo, D.R. Selective CO methanation catalysts for fuel processing applications. Applied Catalysis A: General, 326 (2007): 213-218.

Dry, M.E. Practical and theoretical aspects of the catalytic Fischer-Tropsch process. Appl. Cat. A 138 (1996): 319-334

Eidenmeyer, M., Grasser, S., Köhler, K., Anwander, R. Microporous Mesoporous Mater. 3276 (2001): 44-45.

Ernst, K.H., Campbell, C.T., Moretti, G. Kinetics of the reverse water-gas shift reaction over Cu(110) J.Catal.134 (1992): 66.

Fu, W., Yang, H., Li, M., Li, M., Yang, N., Zou, G. Anatase TiO nanolayer coating on cobalt ferrite nanoparticles for magnetic photocatalyst. Materials Letters 59 (2005): 3530-3534.

Fu, X.A. and Qutubuddin, S. Synthesis of titania-coated silica nanoparticles using ono –ionic water-in-oil. Colloids Surf. A 178 (2001): 151

Fujitani, T., Nakamura, I., Uchijima, T., Nakamura, J.The kinetics and mechanism of methanol synthesis by hydrogenation of CO over a Zn-deposited Cu(111) surface. Surf. Sci. 383 (1997): 285-298.

Grzechowiak, J.R., Szyszka, I., Masalska, A. Effect of TiO_2 content and method of titania–silica preparation on the nature of oxidic nickel phases and their activity in aromatic hydrogenation. Catalysis Today 137 (2008): 433–438.

Hinchiranan, S., Zhang, Y., Nagamori, S., Vitidsant, T., Tsubaki, N. TiO_2 promoted Co/SiO_2 catalysts for Fischer–Tropsch synthesis. Fuel Processing Technology 89 (2008): 455 – 459.

Iglesia, E. Design, synthesis, and use of cobalt-based Fischer-Tropsch synthesis catalysts. Appl. Cat. A 161 (1997): 59-78.

Johnson, B.G., Bartholomew, C.H., Goodman, D.W. The role of surface structure and dispersion in CO hydrogenation on cobalt. Journal of Catalysis 128 (1991): 231.

Jongsomjit, B., Ngamposri, S., Praserthdam., P. Catalytic Activity During Copolymerization of Ethylene and 1-Hexene via Mixed TiO_2/SiO_2 supported MAO with rac-Et[Ind]$_2$ZrCl$_2$ Metallocene Catalyst. journal of Molecules 10 (2005): 603-609.

Jongsomjit, B., Wongsalee, T., Praserthdam, P. Catalytic behaviors of mixed TiO_2-SiO_2 supported cobalt Fischer-Tropsch catalysts for carbon monoxide hydrogenation. journal of Material Chem. And Physics. 97 (2006): 343-350.

Kusama, H., Bando, K.K., Okabe, K., Arakawa, H. Effect of precursors on structure of Rh nanoparticles on SiO_2 support: *in-situ* EXAFS observation during CO_2 hydrogenation. Appl. Catal.A 207 (2001): 85-94.

Lackner, K. S. A guide to CO sequestration**.** Science 300 (2003): 1677-1678.

Lahtinen, J., Anraku, T., Somorjai, G.A. C, CO and CO2 hydrogenation on cobalt foil model catalysts : evidence for the need of CoO reduction. Catal. Let. 25 (1994): 241-255.

Lehninger, A.L. Biochemistry. Worth Publishers. Inc. NewYork, 1970

Medina, J.C., Butala, S.J., Bartholomew, C.H., Lee, M.L. Iron-catalyzed CO_2 hydrogenation as a mechanism for coalbed gas formation. Fuel 79 (2000): 89–93.

Messina, P.V., Morini, M.A., Sierra, M.B., Schulz, P.C. Mesoporous silica-titania composed materials. Journal of Colloid and Interface Science 300 (2006): 270–278.

Mills, G.A. and Steffgren, F.W. Catal. Rev. 8 (1973) 159.

Mohamed, R.M. Characterization and catalytic properties of nano-sized Pt metal catalyst on TiO_2-SiO_2 synthesized by photo-assisted deposition and impregnation methods. journal of materials processing technology 209 (2009): 577–583.

Mrowiec, B.J. Porosity of titania-silica aerogels prepared with ammonium fluoride**.** Polish Journal of Chemistry 74 (2000): 539-548.

Nerlov, J., Chorkendorff, I. Promotion through gas phase induced surface segregation: Methanol synthesis from CO, CO and H over Ni/Cu(100). Catal.Lett. 54 (1998): 171.

Ogawa, M. Nanoporous silica films containing aluminum and titanium. Colloid and Polymer Science 281 (2003): 665-672.

Ohno, T., Tagawa, S., Itoh, H., Suzuki, H., Matsuda, T. Size effect of TiO_2-SiO_2 nano-hybrid particle. Materials Chemistry and Physics 113 (2009): 119–123.

Okabe, K., Li, X., Wei, M., Arakawa, H. Fischer–Tropsch synthesis over Co–SiO_2 catalysts prepared by the sol–gel method. Catalysis Today 89 (2004): 431–438.

Panagiotopoulou, P., Kondarides, D.I., Verykios, X.E. Selective methane tion of CO over supported noble metal catalysts : Effects of the nature of the metallic phase on catalytic performance. Applied Catalysis A. 344 (2008): 45–54.

Peebles, D.E., Goodman, D.W. and White, J.M. Methanation of carbon dioxide on nickel(100) and the effects of surface modifiers. J. Phys. Chem. 87 (1983): 4378.

Rasmussen, P.B.;Kazuta, M., Chorkendorff, I. Synthesis of methanol from a mixture of H_2 and CO_2 on Cu(100). Surf.Sci. 318 (1994): 267.

Riedel, R., Michael, C. , Hans, S., Georg S., Sang-Sung, N., Ki-Won J., Myoung-Jae C., Gurram K., Kyu-Wan L. Comparative study of Fischer–Tropsch synthesis with H_2/CO and H_2/CO_2 syngasusing Fe-and Co-based catalysts. Applied catalysis A (1999): 201-213.

Rojanapipatkul, S. and Jongsomjit, B. Synthesis of cobalt on cobalt-aluminate via solvothermal method and its catalytic properties for carbon monoxide hydrogenation. Catal. Com. 10 (2008): 232-236.

Ruetten, S.A., Thomas, J.K. Photoinduced electron transfer at solid surfaces: The TiO -SiO system. Photochemical and Photobiological Sciences, 2 (2003): 1018-1022.

Ruiz, A.G. and Ramos, I.R. Hydrogenation of CO2 on carbon-supported nickel and cobalt. React. Kinet. Catal. Lett. 23 (1985): 93-99.

Somorjai, G.A. Introduction to Surface Chemistry and Catalysis, Wiley, NewYork, 1994

Song, C. Global challenges and strategies for control, conversion and utilization of CO for sustainable development involving energy, catalysis, adsorption and chemical processing. Catal. Today 115 (2006): 2-32.

Storsaeter, S., Totdal, B., Walmsley, J.C., Tanem, B.S., Holmen, A. Characterization of alumina-, silica-, and titania-supported cobalt Fischer–Tropsch catalysts. J. of Catal. 236 (2005): 139-152.

Suo, Z., Kou, Y., Niu, J., Zhang, W., Wang, H. Characterization of TiO_2-, ZrO_2- and Al_2O_3-supported iron catalysts as used for CO2 hydrogenation Appl. Catal. A 148 (1997): 301-313.

Takanabe, K., Nagaoka, K., Nariai., K., Aika, K. Titania-supported cobalt and nickel bimetallic catalysts for carbon dioxide reforming of methane. Journal of Catalysis 232 (2005): 268–275.

Takenaka, S., Shimizu, T., Otsuka, K. Complete removal of carbon monoxide in hydrogen-rich gas stream through methanation over supported metal catalysts. International Journal of Hydrogen Energy 29 (2004): 1065–1073.

Xiao, F.-S., Han, Y., Yu, Y., Meng, X., Yang, M., Wu, S. Hydro thermally stable ordered mesoporous titanosilicates with highly active catalytic sites. Journal of the American Chemical Society 124 (2002): 888-889.

Xu, G., Chen, X., Zhang, Z.G. Temperature-staged methanation: An alternative method to purify hydrogen-rich fuel gas for PEFC. Chemical Engineering Journal 121 (2006): 97-107.

Yoshihara, J., Parker, S.C., Schafer, A., Campbell, C.T. Methanol synthesis and reverse water-gas shift kinetics over clean polycrystalline copper. J.Catal. Lett. 34 (1995): 313.

Zhao, L., Yu, J., Cheng, B. Preparation and characterization of SiO_2/TiO_2 composite microsphere with microporous SiO_2 core/mesoporous TiO_2 shell. Journal of Solid State Chemistry 178 (2005): 1818–1824.

Zhao, Z., Yung, M.M., Ozkan, U.S. Effect of support on the preferential oxidation of CO over cobalt catalysts. Catalysis Communications 9 (2008): 1465–1471.

APPENDICES

APPENDIX A

CALCULATION FOR CATALYST PREPARATION

Calulation of TiO$_2$- SiO$_2$ composites supports

Preparation of titania-silica composites supports support with 25% ratios of Titania (TiO$_2$) to support by sol gel method are shown as follows:

Reagent: - Titanium isopropoxide 97% (TiPOT)

Molecular weight = 284.26 g/mol

Titania (TiO$_2$), formula weight = 79.867 g/mol

- Support : - SiO$_2$

- For 25%wt of Titania (TiO$_2$) is shown as follow:

Based on 75 g of silica (SiO$_2$) used, the composition of the catalyst will be as follows:

TiO$_2$ = 25 g

79.867 g of TiO$_2$ required 284.26 g of TiPOT

25.00 g of TiO$_2$ required $25.00 \times \dfrac{284.26}{79.867}$ g of TiPOT

= 88.979 g of TiPOT

TiPOT 97 g   provide 97% Titanium isopropoxide solution 100 g

TiPOT 88.979 g provide 97% Titanium isopropoxide solution $\dfrac{88.979}{0.97}$

= 91.731 g

Calculation of cobalt loading

Preparations of 20%wtCo/SiO$_2$ by the incipient wetness impregnation method are shown as follows:

Reagent: - Cobalt (II) nitrate hexahydrate (Co(NO$_3$)$_2$·6H$_2$O)

      Molecular weight   =   291.03 g/mol

     Cobalt (Co), Atomic weight = 58.933 g/mol

    - Support: - spherical silica particle

              - MCM-41

              - titania-silica composite supports

Based on 1.00 g of catalyst used, the composition of the catalyst will be as follows:

    Cobalt   =   0.20 g

    SiO$_2$ =   1.00 – 0.20   =   0.80 g

Cobalt 0.20 g was prepared from Cobalt (II) nitrate hexahydrate

Cobalt (II) nitrate hexahydrate required   = $\dfrac{0.20}{58.933}$ x 291.03

                                      =   0.9877 g

Since the pore volume of MCM-41 support is 1.0287 ml/g. Thus, the total volume of impregnation solution which must be used is 0.82296 ml for MCM-41 by the requirement of incipient wetness impregnation method, the de-ionized water is added until equal pore volume for dissolve cobalt (II) nitrate hexahydrate.

Calculation of nickel loading

Preparations of 20%wtCo/Al_2O_3 by the incipient wetness impregnation method are shown as follows:

Reagent: -Nickel (II) nitrate hexahydrate ($Ni(NO_3)_2 \cdot 6H_2O$)

         Molecular weight   =   290.79 g/mol

        Nickel (Ni), Atomic weight = 58.693 g/mol

       - Support: - spherical silica particle

                   - MCM-41

                   - titania-silica composite supports

Based on 1.00 g of catalyst used, the composition of the catalyst will be as follows:

Nickel	=	0.20 g		
SiO_2	=	1.00 – 0.20	=	0.80 g

Nickel 0.20 g was prepared from Nickel (II) nitrate hexahydrate

Nickel (II) nitrate hexahydrate required $= \dfrac{0.20}{58.693} \times 290.79$

$\qquad\qquad\qquad\qquad\qquad\qquad\qquad\qquad\quad = 0.9909$ g

Since the pore volume of MCM-41 support is 1.0287 ml/g. Thus, the total volume of impregnation solution which must be used is 0.82296 ml for MCM-41 by the requirement of incipient wetness impregnation method, the de-ionized water is added until equal pore volume for dissolve nickel (II) nitrate hexahydrate.

APPENDIX B

CALCULATION FOR TOTAL CO CHEMISORPTION AND DISPERSION

Calculation of the total CO chemisorption and metal dispersion of the catalyst, a stoischiometry of CO/Co = 1, is assumed. The calculation procedure is as follows:

Let the weight of catalyst used	=	W	g
Integral area of CO peak after adsorption	=	A	unit
Integral area of 100 μl of standard H_2 peak	=	B	unit
Amounts of CO adsorbed on catalyst	=	B-A	unit
Concentration of Co	=	C	%wt
Volume of H_2 adsorbed on catalyst	=	$100 \times [(B-A)/B]$	μl
Volume of 1 mole of CO at 30 °C	=	24.86×10^6	μl

Mole of CO adsorbed on catalyst $= [(B-A)/B] \times [100/24.86]$ μmole

Total CO chemisorption =

$$[(B-A)/B] \times [100/29.93] \times [1/W] \quad \text{μmole}/g_{catalyst}$$

$$= \quad N \quad \text{μmole}/g_{catalyst}$$

$$\%Co\,dispersion = \frac{\text{The amount of cobalt equivalent to CO adsorption after reduction} \times 100}{\text{Total amount of cobalt active sites expected to exist after reduction}}$$

Molecular weight of cobalt $=$ 58.93

Metal dispersion (%) $= \dfrac{1 \times CO_{tot} \times 100}{\text{No. μmole Co}_{tot}}$

$$= \frac{1 \times N \times 100}{No.\,\mu mole\,Co_{tot}}$$

$$= \frac{1 \times N \times 58.93 \times 100 \times 100}{[C \times 10^6]}$$

$$= \frac{0.59 \times N}{C}$$

APPENDIX C

CALCULATION FOR REDUCIBILITY

For supported cobalt catalyst, it can be assumed that the major species of calcined Co catalysts is Co_3O_4. H_2 consumption to reduce Co_3O_4 is calculated as follows:
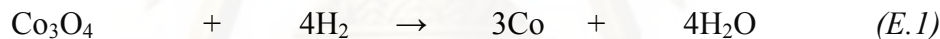
Molecular weight of Co　　=　　58.93

Molecular weight of Co_3O_4　　=　　240.79

Calculation of the calibration of H_2 consumption using cobalt oxide (Co_3O_4)

Let the weight of Co_3O_4 used　　=　　0.1 g

=　　4.153×10^{-4} mole

From equation of Co_3O_4 reduction;

$$Co_3O_4 \quad + \quad 4H_2 \quad \rightarrow \quad 3Co \quad + \quad 4H_2O \qquad (E.1)$$

Mole of hydrogen consumption　　=　　4 Mole of Co_3O_4 consumption

=　　$4 \times 4.153 \times 10^{-4}$

=　　1.661×10^{-3} mole

Integral area of hydrogen used to reduce Co_3O_4 0.1 g = 115.63 unit

At 100 % reducibility, the amount of hydrogen consumption is 1.661×10^{-3} mole related to the integral area of Co_3O_4 after reduction 115.63 unit.

Calculation of reducibility of supported cobalt catalyst

$$\% \, Reducibility = \frac{Amount \, of \, H_2 \, uptake \, to \, reduce \, 1 \, g \, of \, catalyst \times 100}{Amount \, of \, theoretical \, H_2 \, uptake \, to \, reduce \, Co_3O_4 \, to \, Co^0 \, for \, 1 \, g \, of \, catalyst}$$

Integral area of the calcined catalyst $\qquad$ = $\qquad$ X $\qquad$ unit

The amount of H_2 consumption $\qquad$ =

$$\left[2 \times 1.661 \times 10^{-3} \times (X)/115.63\right] \text{mole}$$

Let the weight of calcined catalyst used $\qquad$ = $\qquad$ W $\qquad$ g

Concentration of Co $\qquad$ = $\qquad$ Y $\qquad$ %wt

Mole of Co $\qquad$ = $\qquad$ $\left[(W \times Y/100)/58.93\right]$ mole

Mole of Co_3O_4 $\qquad$ = $\qquad$ $\left[(W \times Y/100)/(3 \times 58.93)\right]$ mole

Amount of theoretical $\qquad$ = $\qquad$ $\left[(W \times Y/100) \times 4/(3 \times 58.93)\right]$ mole

Reducibility (%) of supported Co catalyst $\qquad$ =

$$\frac{\left[2 \times 1.661 \times 10^{-3} \times (X)/115.63\right] \times 100}{\left[(W \times Y/100) \times 4/(3 \times 58.93)\right]}$$

Example for 20Co/ Z

Integral area of the calcined catalyst $\qquad$ = $\qquad$ *6.016 unit*

The amount of H_2 consumption $\qquad$ = $\left[2 \times 1.661 \times 10^{-3} \times (X)/115.63\right] mole$

Let the weight of calcined catalyst used $\qquad$ = $\qquad$ *0.1 g*

Concentration of Co $\qquad$ = $\qquad$ *20 %wt*

Mole of Co $\qquad$ = $\qquad$ $\left[(0.1 \times 20/100)/58.93\right]$ *mole*

Mole of Co_3O_4 $\qquad$ = $\qquad$ $\left[(0.1 \times 20/100)/(3 \times 58.93)\right]$ *mole*

Amount of theoretical $\qquad$ = $\qquad$ $\left[(0.1 \times 20/100) \times 4/(3 \times 58.93)\right] mole$

Reducibility (%) of supported Co catalyst $\qquad$ =

$$\frac{\left[2 \times 1.661 \times 10^{-3} \times (6.016)/115.63\right] \times 100}{\left[(0.1 \times 20/100) \times 4/(3 \times 58.93)\right]}$$

$\qquad$ = $\qquad$ 34.6 %

For supported nickel catalyst, it can be assumed that the major species of calcined Ni catalysts is NiO. H_2 consumption to reduce NiO is calculated as follows:
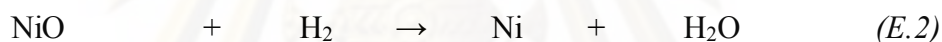
$$\text{Molecular weight of Ni} = 58.69$$

$$\text{Molecular weight of NiO} = 74.69$$

Calculation of the calibration of H_2 consumption using cobalt oxide (NiO)

$$\text{Let the weight of NiO used} = 0.1 \text{ g}$$

$$= 1.339 \times 10^{-3} \text{ mole}$$

From equation of Co_3O_4 reduction;

$$NiO \quad + \quad H_2 \quad \rightarrow \quad Ni \quad + \quad H_2O \qquad (E.2)$$

$$\text{Mole of hydrogen consumption} = \text{Mole of NiO consumption}$$

$$= 1.339 \times 10^{-3} \text{ mole}$$

Integral area of hydrogen used to reduce NiO 0.1 g = 93.21 unit

At 100 % reducibility, the amount of hydrogen consumption is 1.339×10^{-3} mole related to the integral area of NiO after reduction 93.21 unit.

Calculation of reducibility of supported cobalt catalyst

$$\% \, Reducibility = \frac{Amount \; of \; H_2 \; uptake \; to \; reduce \, 1 \, g \; of \; catalyst \times 100}{Amount \; of \; theoretical \; H_2 \; uptake \; to \; reduce \; NiO \; to \; Ni^0 \; for \; 1 \, g \; of \; catalyst}$$

$$\text{Integral area of the calcined catalyst} = X \quad \text{unit}$$

$$\text{The amount of } H_2 \text{ consumption} = \left[2 \times 1.339 \times 10^{-3} \times (X)/93.21 \right] \text{mole}$$

Let the weight of calcined catalyst used   =   W   g
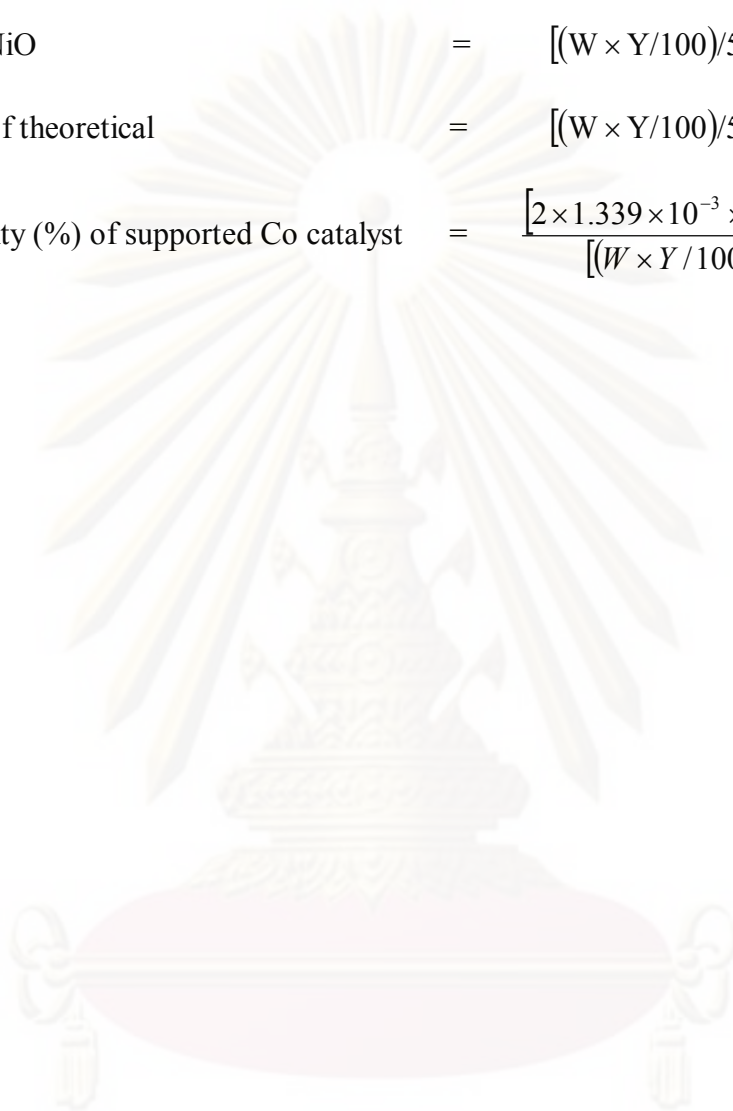
Concentration of Ni   =   Y   %wt

Mole of Ni   = $[(W \times Y/100)/58.69]$ mole

Mole of NiO   = $[(W \times Y/100)/58.69]$ mole

Amount of theoretical   = $[(W \times Y/100)/58.69]$ mole

Reducibility (%) of supported Co catalyst   = $\dfrac{[2 \times 1.339 \times 10^{-3} \times (X)/93.21] \times 100}{[(W \times Y/100) \times 1/(58.69)]}$

APPENDIX D

CALIBRATION CURVES

This appendix showed the calibration curves for calculation of composition of reactant and products in CO hydrogenation reaction. The reactant is CO and the main product is methane. The other products are linear hydrocarbons of heavier molecular weight that are C_2-C_4 such as ethane, ethylene, propane, propylene and butane.

The thermal conductivity detector, gas chromatography Shimadzu model 8A was used to analyze the concentration of CO by using Molecular sieve 5A column.

The thermal conductivity detector (TCD), gas chromatography Shimadzu model 8A was used to analyze the concentration of CO_2 by using porapack-Q column.

The VZ10 column are used with a gas chromatography equipped with a flame ionization detector, Shimadzu model 14B, to analyze the concentration of products including of methane, ethane, ethylene, propane, propylene and butane. Conditions uses in both GC are illustrated in Table C.1.

Mole of reagent in y-axis and area reported by gas chromatography in x-axis are exhibited in the curves. The calibration curves of CO, methane, ethane, ethylene, propane, propylene and butane are illustrated in the following figures.

Table D.1 Conditions use in Shimadzu modal GC-8A and GC-14B.

Parameters	Condition	
	Shimadzu GC-8A	Shimadzu GC-14B
Width	5	5
Slope	50	50
Drift	0	0
Min. area	10	10
T.DBL	0	0
Stop time	50	60
Atten	0	0
Speed	2	2
Method	41	41
Format	1	1
SPL.WT	100	100
IS.WT	1	1

$$y = 3E\text{-}11x^2 + 5E\text{-}05x$$
$$R^2 = 0.9982$$
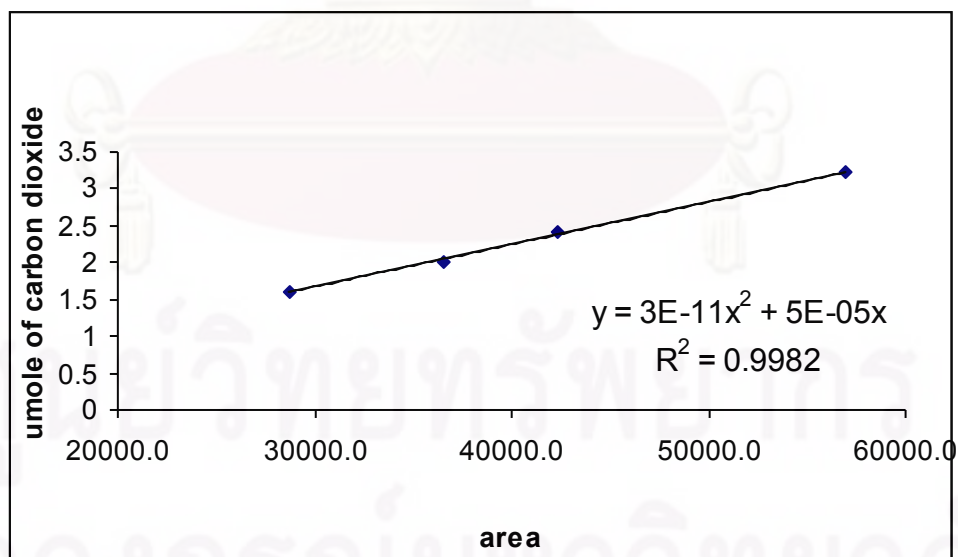
Figure D.1 The calibration curve of carbon dioxide.
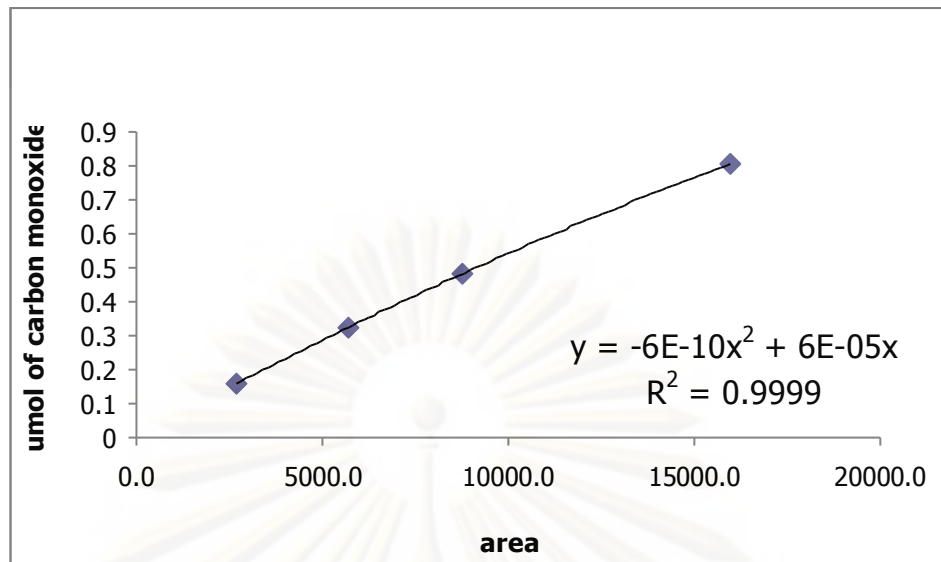
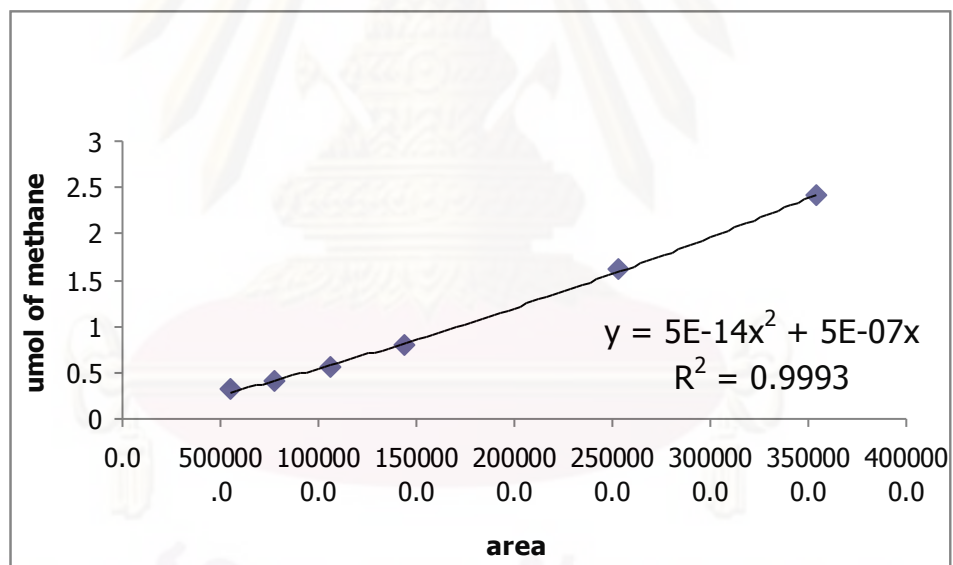**Figure D.2** The calibration curve of carbon monoxide.
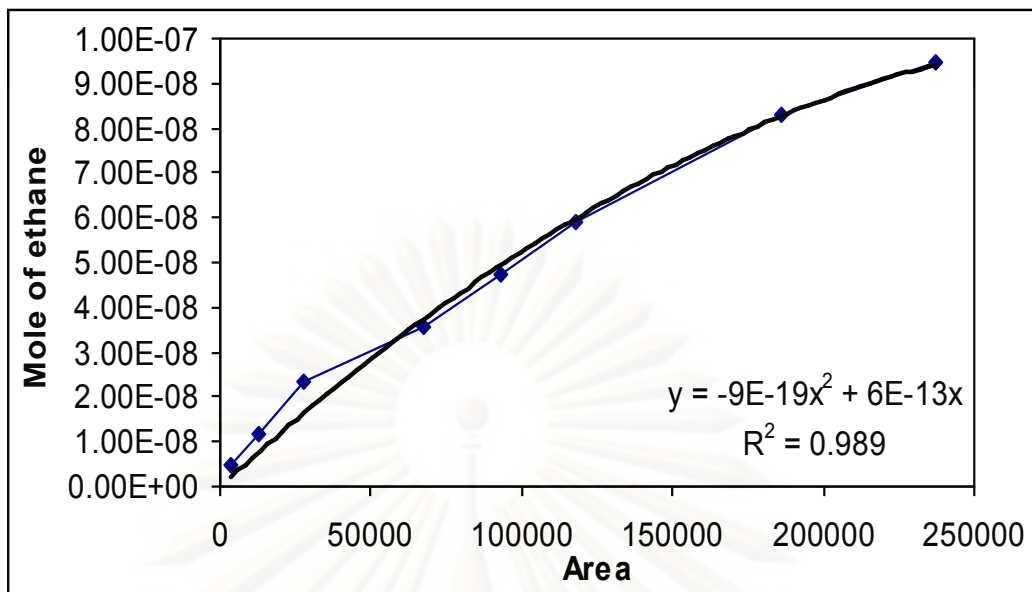

Figure D.3 The calibration curve of methane.

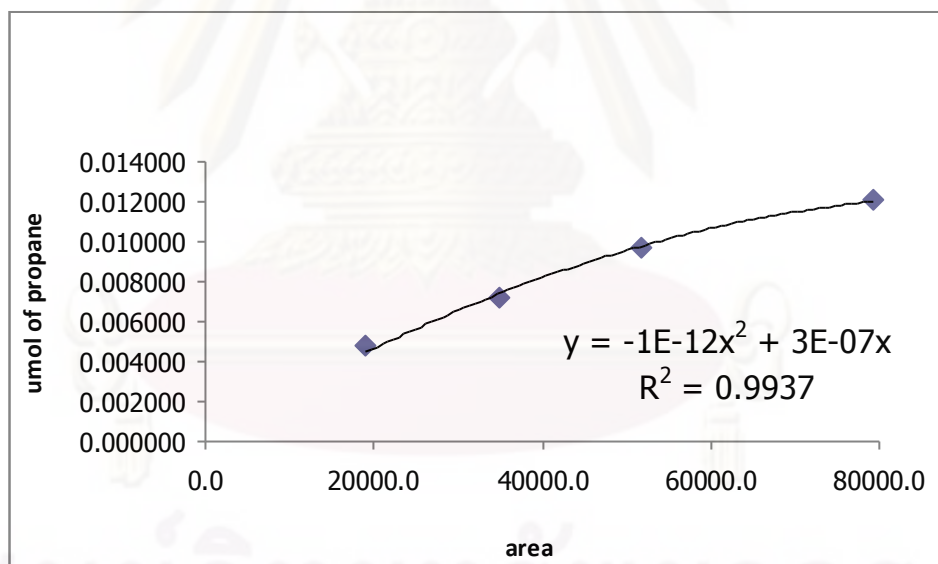**Figure D.4** The calibration curve of ethane.

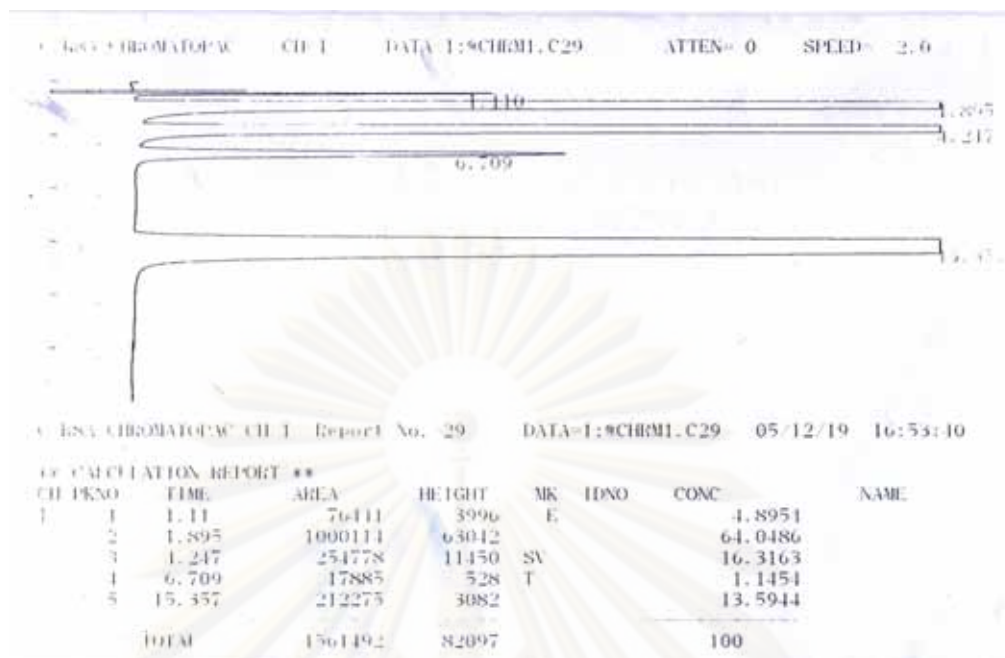**Figure D.5** The calibration curve of propane.

Figure D.6 The chromatograms of catalyst sample from thermal conductivity detector, gas chromatography Shimadzu model 8A (Molecular sieve 5A column).
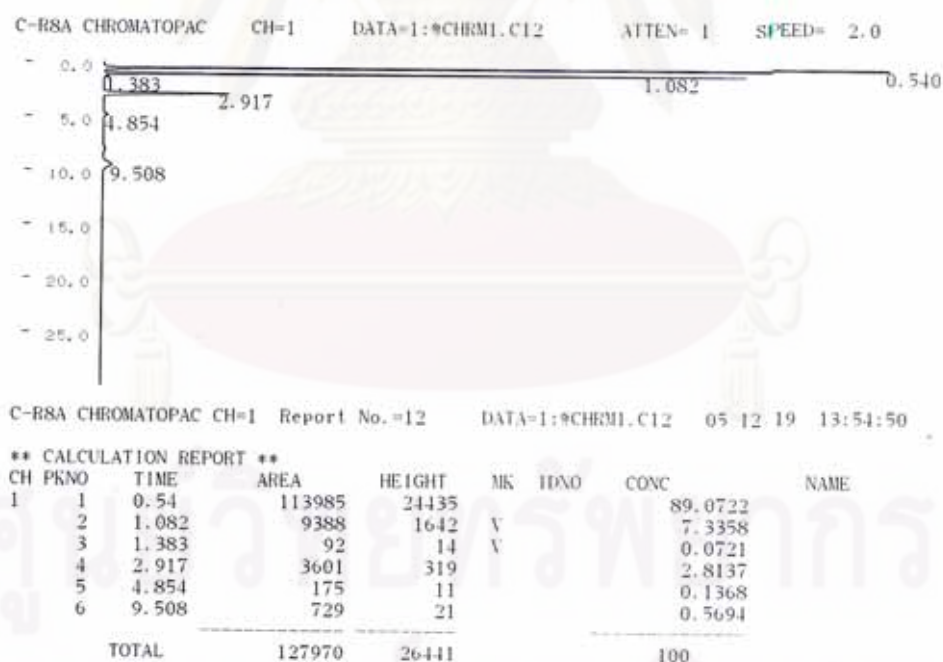

Figure D.7 The chromatograms of catalyst sample from flame ionization detector, gas chromatography Shimadzu model 14B (VZ10 column).

APPENDIX E

CALCULATION OF CO_2 CONVERSION, REACTION RATE AND SELECTIVITY

The catalyst performance for the CO_2 hydrogenation was evaluated in term of activity for CO_2 conversion, reaction rate and selectivity.

CO_2 conversion is defined as moles of CO_2 converted with respect to CO_2 in feed:

$$CO_2 \text{ conversion (\%)} = \frac{100 \times [mole\ of\ CO_2\ in\ feed - mole\ of\ CO_2\ in\ product]}{mole\ of\ CO_2\ in\ feed} \quad \text{(i)}$$

Reaction rate was calculated from CO_2 conversion that is as follows:

Let the weight of catalyst used	=		W	g
Flow rate of CO_2	=		2	cc/min
Reaction time	=		60	min
Weight of CH_2	=		14	g
Volume of 1 mole of gas at 1 atm	=		22400	cc
Selectivity to CH_4	=		S	

$$\text{Reaction rate (g } CH_2/\text{g of catalyst.h)} = \frac{(\%\ conversion\ of\ CO_2\ /100) \times 60 \times 14 \times 2}{W \times 22400} \times S \quad \text{(ii)}$$

Selectivity of product is defined as mole of product (B) formed with respect to mole of CO_2 converted:

$$\text{Selectivity of B (\%)} = 100 \times [mole\ of\ B\ formed\ /\ mole\ of\ total\ products] \quad \text{(iii)}$$

Where B is product, mole of B can be measured employing the calibration curve of products such as methane, ethane, ethylene, propane, propylene and butane

$$\text{mole of } CH_4 = \text{(area of } CH_4 \text{ peak from integrator plot on GC-14B)} \times 8 \times 10^{12} \quad \text{(iv)}$$

VITA

Mr Jakrapan Janlamool was born on October 30th, 1983 in Pichit province, Thailand. He finished high school from Pichit Pittayakom School in 2002. He received the bachelor's degree of General science and Biochemistry from Faculty of Science, Kasetsart University in 2006 and 2007, respectively. He continued his master's study at Department of Chemical Engineering, Faculty of Engineering, Chulalongkorn University in June, 2007.

LIST OF PUBLICATIONS

- **Proceeding**

1. Jakrapan Janlamool and Bunjerd Jongsomjit, "Characteristics of TiO_2-SiO_2 microparticle composites using different types of SiO_2 particle." Pure and Applied Chemistry International Conference, Ubon Ratchathani Thailand, 21-23 January., 2010.

2. Jakrapan Janlamool and Bunjerd Jongsomjit, "Preparation and characterization of TiO_2-SiO_2 microparticle composites using spherical silica and MCM41 particle." Proceeding of the 3rd Technology and Innovation for Sustainable Development International Conference, Nong Khai Thailand, March., 2010.